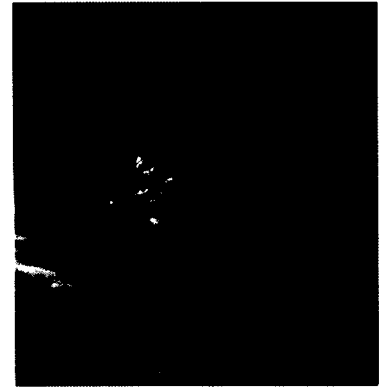
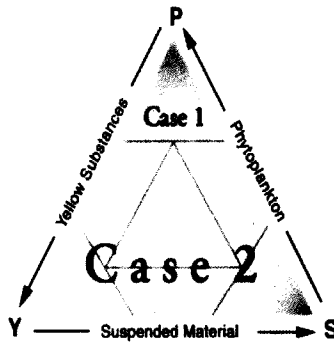


Analysis of optical properties and retrieval of water constituents from waters of different optical domains through a visible satellite sensor



Thesis submitted to Goa University for the degree of
Doctor of Philosophy in Marine Sciences

By

Aneesh A. Lotliker, M. Sc.

Research Supervisor
Prof. Harilal B. Menon

Department of Marine Sciences

Goa University
Taleigao Plateau,
Goa 403206



April 2008

578.77
LOT/Ane
T-441

441

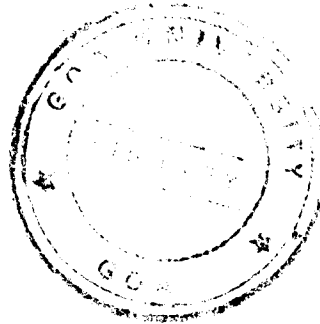
In a day if you find yourself with no obstacles then you be
sure that you're on the wrong path

Swami Vivekanand

dedicated to my parents

DECLARATION

As required under the University Ordinance 0.19.8 (vi), I hereby declare that the present thesis entitled 'Analysis of optical properties and the retrieval of water constituents from the waters of different optical domains through a visible satellite sensor' is my original work carried out in the Department of Marine Sciences, Goa University, and the same has not been submitted in part or in full elsewhere for any other degree or diploma. To the best of my knowledge, the present research is the first comprehensive work of its kind from the area studied.



Place: Goa University

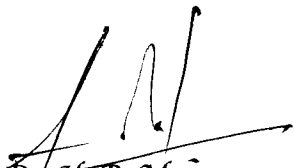
Aneesh A. Lotliker
Aneesh A. Lotliker

Date: 12 January 2009

CERTIFICATE

This is to certify that the thesis entitled 'Analysis of optical properties and the retrieval of water constituents from the waters of different optical domains through a visible satellite sensor' submitted by Aneesh A. Lotliker for the award of the degree of Doctor of Philosophy in Marine Sciences is based on his original studies carried out by him under my supervision. The thesis or any part thereof has not been previously submitted for any degree or diploma in any Universities or Institutions.

Place: Goa University
Date: 12/11/2009



Dr. H. B. Meñon,

Research Guide & Reader,

Department of Marine Sciences,

Goa University, Taleigao Plateau,

Goa 403206

All the corrections indicated by the referees have been incorporated at appropriate places in thesis.

R. Ramakrishna Reddy
12/11/09

Acknowledgements

The thesis marks the end of a long and eventful journey for which there are many people that I would like to acknowledge for their support along the way. It is a pleasant aspect that I have now the opportunity to express my gratitude for all of them.

My first debts of gratitude go to Prof. H. B. Menon, who undertook to act as my research guide despite his many other academic and professional commitments. He patiently provided the vision, encouragement and advice necessary for me to proceed through the doctoral program and complete my thesis. His ability to identify the discontinuities in my writing continuously challenged my thinking and encouraged me to keep pushing the boundaries of my work.

I wish to thank Head, Department of Marine Sciences for the encouragement and the facilities made available for this work.

I am also thankful to Prof. H. B. Menon, Co-ordinator, Remote Sensing Lab, Goa University, for facilities provided to process satellite data.

I am thankful to the Dean, faculty of Life Sciences and Environment, for his kind help and co-operation.

I am also thankful to Dr. S. Upadhyay, Dr. Aftab Can, Dr. Rivonkar and Dr. V. M. Matta, faculty members of Department of Marine Sciences, for their encouragement.

Special thanks to Dr. S.S.C. Sheno, Scientist, National Institute of Oceanography, Goa, members of my Faculty Research Council who monitored my work.

I am thankful to Dr. Shailesh Nayak, Secretary, Ministry of Earth Sciences (MoES) for his timely help and encouragement.

I would like to thank Director, National Institute of Oceanography, Goa for providing me with necessary library facilities.

I also wish to thank research scholars at Goa University who continuously helped me in field exercises and provided moral support and encouragement, in particular Nutan Sangekar, Racheal Chacko, Deepti Dessai, K. Tomchou Singh, Amita Caisuker, Vishal Bhandare and Harrylon Lobo.

Thanks to the non-teaching staff of Goa University for their timely help and co-operation in technical and administrative work: Narayan, Achut, Amonkar, Sanjana, Sadanand, Ashok, Vandana and Baby.

This dissertation would not have been possible without the emotional and social support from my friends: Shantanu, Mandar and Mohamed.

I gratefully acknowledge Dr. Prakash Chauhan, Dr. R. M. Dwivedi, Dr. Arvind Sahay and Dr. Yeshwant Pradhan from Space Application Center, Ahmedabad and Dr. M. Mohan, Space Physical Laboratory, VSSC, Trivandrum to enhance my knowledge on the calibration, operation of radiometer along with processing of data and image processing software.

Thanks to Dr. T. Nallatambi and Shri. R. S. Robin for the help rendered during the field work.

I continued the writing process when I joined Indian Center for Ocean Information Services (INCOIS), Hyderabad. In INCOIS I met a bunch of wonderful and special people who shared scholarly engagement with me, encouraged my work, and took care of me while I was writing. For all-

around the clock support I thank the group Head, Dr. T. Srinivasa Kumar and Director, INCOIS. Thank you both. You gave me a 'community' and a 'home'.

This research has been supported and funded by various organizations in various stages of this thesis: Indian Space Research Organization (ISRO) financed the beginning years of this thesis and Council of Scientific and Industrial Research (CSIR) the last ones.

Above all I would like to acknowledge the tremendous sacrifices that my parents made to ensure that I had an excellent education. Their unwavering faith and confidence in my abilities and in me is what has shaped me to be the person I am today. For this and much more, I am forever in their debt. It is to them that I dedicate this thesis.

I want to acknowledge my wife Joereen for her love, support, encouragement and understanding.

The chain of my gratitude would be definitely incomplete if I would forget to thank the "The Prime Mover". My deepest and sincere gratitude for inspiring and guiding this humble being.

Aneesh A. Lotliker

Abbreviations

AOP	Apparent optical properties
AOT	Aerosol optical thickness
ARMEX	Arabian Sea Monsoon Experiment
AWS	Automatic weather station
CDOM	Coloured dissolved organic matter
CFC	Chlorofluorocarbon
CRV	Coastal Research Vessel
CTD	Conductivity – temperature – depth
CZCS	Coastal Zone Colour Scanner
DCM	Deep chlorophyll maxima
DN	Digital numbers
DOM	Dissolved organic matter
EMR	Electromagnetic radiation
GCP	Ground controlled points
GPS	Global Positioning System
IOP	Inherent optical properties
IRS	Indian Remote Sensing Satellite
ISRO	Indian Space Research Organization
MLD	Mixed layer depth
NIR	Near infrared
NRSA	National Remote Sensing Agency
OAS	Optically active substances
OCM	Ocean Colour Monitor
OD	Optical density
ORV	Ocean Research Vessel
PAR	Photosynthetically active radiation
PNF	PAR – natural fluorescence
PSLV	Polar Satellite Launching Vehicle 4
RT	Radiative transfer

SK	Sagar Kanya
SMSR	Satlantic Multichannel Surface Reference
SPMR	Satlantic Profiling Multichannel Radiometer
TISM	Total inorganic suspended matter
UV	Ultraviolet
VSF	Volume scattering function
a	Total absorption coefficient
a_w	Absorption coefficient of water molecule
a^*_c	Specific absorption coefficient of chlorophyll_a
a^*_s	Specific absorption coefficient of total inorganic suspended matter
a_{CDOM}	Absorption coefficient of coloured dissolved organic matter
b_b	Total backscattering coefficient
b	Total scattering coefficient
b_w	Scattering coefficient of water molecule
b_c	Scattering coefficient of chlorophyll_a
b_s	Scattering coefficient of total inorganic suspended matter
c	Total attenuation coefficient
C_c	Chlorophyll_a concentration
C_s	Concentration of total inorganic suspended matter
$a_{CDOM440}$	Absorption coefficient of coloured dissolved organic matter at wavelength 440 nm
s	Slope coefficient
k_u	Upwelling diffuse attenuation coefficient
k_d	Diffuse attenuation coefficient of downwelling irradiance
k_d (PAR)	Diffuse attenuation coefficient of Photosynthetically available radiation
F_s	Solar irradiance at the top of atmosphere
L_T	Total radiance received by a satellite sensor
L_a	Radiance received by a sensor onboard satellite from aerosol
L_r	Radiance received by a sensor onboard satellite from air molecule
L_g	Sunlint radiance

L_w	Water leaving radiance
E_s	Downwelling irradiance at sea surface
E_d	Downwelling radiance
L_u	Upwelling radiance
E_u	Upwelling irradiance
R_{rs}	Remote sensing reflectance
R	Subsurface reflectance
T	Direct transmission coefficient
T_d	Diffuse transmission coefficient
Q	Bi-directional reflectance coefficient
α	Angstrom wavelength exponent
β	Turbidity factor
θ_s	Sun zenith angle
θ_v	Satellite zenith angle
ω_0	Single scattering albedo
μ_a	Slope of the curve between absorption coefficient and downwelling diffuse attenuation coefficient
μ_b	Slope of the curve between sum of absorption and backscattering coefficient and downwelling diffuse attenuation coefficient
h	Plank's constant
λ	Wavelength

List of figures

- Fig. 2.1.1 (a) Map of study area showing hydrographic stations covered during cruise SK 186, SK 193, SK 214 and in Lakshadweep waters.
- Fig. 2.1.1 (b) Map of study area showing hydrographic stations covered onboard CRV Sagar Purvi (CF01; CG01 – CG21), CRV Sagar Paschimi (CD01 – CD05; CE01 – CE03) and onboard trawler in Mandovi – Zuari estuarine system (E01 – E22) of Goa.
- Fig. 3.2.1 Vertical profiles of mean temperature ($^{\circ}\text{C}$), fluorescence ($\mu\text{-g}^{-1}$) and PAR (%) in open ocean (O), coastal (C) and estuarine (E) waters. The vertical distribution of PAR is presented on a logarithmic scale.
- Fig. 3.2.2 Variability of downwelling irradiance (E_d) at 490 nm at different depths at stations corresponding to a) open ocean (O), b) coastal (C) and c) estuarine (E) waters.
- Fig. 3.3.1 Regression between a) DCM and downwelling diffuse attenuation coefficient (k_d) at 490 nm and b) downwelling diffuse attenuation coefficient of PAR (k_d (PAR)) and downwelling diffuse attenuation coefficient (k_d) at 490 nm.
- Fig. 3.3.2 Spectral variation of total absorption coefficient (a) corresponding to stations in open ocean (O), coastal (C) and estuarine (E) waters. The thick line indicates the mean and the thin line above and below the thick lines indicates the standard deviation.
- Fig. 3.3.3 Spectral variation of total backscattering coefficient (b_b) corresponding to stations in open ocean (O), coastal (C) and estuarine (E) waters. The thick line indicates the mean and the thin line above and below the thick lines indicates the standard deviation.

- Fig. 3.3.4 Spectral variation of remote sensing reflectance (R_{rs}) corresponding to stations in open ocean (O), coastal (C) and estuarine (E) waters. The thick line indicates the mean and the thin line above and below the thick lines indicates the standard deviation.
- Fig. 4.2.1 Spectral variability of absorption coefficient due to pure water (a_w), specific absorption coefficient due to chlorophyll_a (a^*_c), TISM (a^*_s) and absorption coefficient due to a_{CDOM} at a selected stations from open ocean (O), coastal (C) and estuarine (E) waters.
- Fig. 4.3.1 Spectral variability of percent irradiance, entering the water column, absorbed by pure water (W), chlorophyll_a (C), TISM (S) and CDOM (Y) in a) open ocean (O), b) coastal (C) and c) estuarine (E) waters.
- Fig. 4.4.1.1 Spectral variability of mean specific absorption coefficient due to chlorophyll (a^*_c) in open ocean (O) waters. The vertical bars indicate the standard deviation.
- Fig. 4.4.1.2 Spectral variability of mean specific absorption coefficient due to chlorophyll (a^*_c) in coastal (C) waters. The vertical bars indicate the standard deviation.
- Fig. 4.4.1.3 Spectral variability of mean specific absorption coefficient due to chlorophyll_a (a^*_c) in estuarine (E) waters during (a) pre-monsoon in (i) middle and (ii) lower estuary and (b) post-monsoon in (i) middle and lower estuary. The vertical bars indicate the standard deviation.
- Fig. 4.4.2.1 Spectral variability of mean specific absorption coefficient due to TISM (a^*_s) in open ocean (O) waters. The vertical bars indicate the standard deviation.

- Fig. 4.4.2.2 Spectral variability of mean specific absorption coefficient due to TISM (a^*_s) in coastal (C) waters. The vertical bars indicate the standard deviation.
- Fig. 4.4.2.3 Spectral variability of mean specific absorption coefficient due to TISM (a^*_s) in estuarine (E) waters during (a) pre-monsoon in (i) middle and (ii) lower estuary and (b) post-monsoon in (i) middle and lower estuary. The vertical bars indicate the standard deviation.
- Fig. 4.4.3.1 Spectral variability of mean absorption coefficient due to CDOM (a_{CDOM}) in coastal (C) waters. The vertical bars indicate the standard deviation.
- Fig. 4.4.3.2 Spectral variability of mean absorption coefficient due CDOM (a_{CDOM}) in estuarine (E) waters during (a) pre-monsoon in (i) middle and (ii) lower estuary and (b) post-monsoon in (i) middle and lower estuary. The vertical bars indicate the standard deviation.
- Fig. 4.5.1 Variability of mean chlorophyll_a and TISM in open ocean (O) waters. The vertical bars indicate the standard deviation.
- Fig. 4.5.2 Variability of mean chlorophyll_a, TISM and $a_{CDOM440}$ in coastal (C) waters. The vertical bars indicate the standard deviation.
- Fig. 4.5.3 Variability of mean (a) chlorophyll_a in middle and lower zone during pre-monsoon and post-monsoon season, (b) TISM in middle and lower zone during pre-monsoon and post-monsoon season and (c) $a_{CDOM440}$ in middle and lower zone during pre-monsoon and post-monsoon season in estuarine (E) waters. The vertical bars indicate the standard deviation.
- Fig. 4.6.1 Variability of slope coefficient with $a_{CDOM440}$ in (a) coastal (C) and (b) estuarine (E) waters.
- Fig. 5.1.2.1 Spectral variation of computed hyperspectral water leaving radiance (L_w) at stations CA04, E07 and CA01.

- Fig. 5.1.3.1 Correlation between absorption coefficient (a) generated through water sample analysis (computed) and that derived through radiometric measurements (measured) for wavelengths a) 412 nm, b) 443 nm, c) 490 nm, d) 510 nm, e) 555 nm and f) 670 nm.
- Fig. 5.1.3.2 Correlation between measured and computed water leaving radiance (L_w) at stations CA04, E07 and CA01.
- Fig. 5.2.1.1 Ternary plots illustrating the relative contribution of chlorophyll_a (a_c), TISM (a_s) and a_{CDOM} to absorption for stations in open ocean (O – waters), coastal (C – waters) and estuarine (E – waters) waters at wavelengths 412, 443, 490, 510, 555 and 670 nm. The labels correspond to maximum fraction.
- Fig. 5.2.2.1 Regression between a) chlorophyll_a concentration and the ratio of water leaving radiance at 670 and 555 nm, b) TISM (sediment) concentration and the ratio of water leaving radiance (L_w) between 490 and 670 nm and c) $a_{CDOM440}$ and the ratio of water leaving radiance (L_w) between 412 and 670 nm.
- Fig. 5.2.2.2 Regression between a) chlorophyll_a concentration and remote sensing reflectance (R_{rs}) at 670 and 510 nm, b) TISM (sediment) concentration and the ratio of remote sensing reflectance (R_{rs}) at 490 and 670 nm, c) $a_{CDOM440}$ and the ratio of remote sensing reflectance (R_{rs}) at 412 and 670 nm in inshore waters and d) $a_{CDOM440}$ and the ratio of remote sensing reflectance (R_{rs}) at 412 and 670 nm in offshore waters.
- Fig. 6.2.1 Sampling frequency of AOT measurements over open ocean (O), coastal (C) and estuarine (E) waters.
- Fig. 6.2.2 Spectral variation of mean AOT over open ocean (O), coastal (C) and estuarine (E) waters. The vertical bars indicate standard deviation.

- Fig. 6.2.3 Variability of mean AOT at 500 nm, Angstrom wavelength exponent (α) and turbidity factor (β) over open ocean (O), coastal (C) and estuarine (E) waters. The vertical bars indicate standard deviation.
- Fig. 6.3.1 Correlation between satellite derived and in situ Angstrom wavelength exponent (α). The dotted lines were plotted at 95% confidence level. The error bars indicates standard deviation for the data in respective grid.
- Fig. 6.3.2 Correlation between satellite derived and in situ aerosol radiance (L_a) at 490 nm. The dotted lines indicate 95% confidence level. The error bars indicates standard deviation for the data in respective grid.
- Fig. 7.2.1 Synoptic distribution of chlorophyll_a in Mandovi and Zuari estuaries of Goa, West coast of India on 12th January, 12th February, 18th March, 13th April, 11th May, 17th September, 09th October, 11th November and 09th December 2005.
- Fig. 7.2.2 Synoptic distribution of TISM in Mandovi and Zuari estuaries of Goa, West coast of India on 12th January, 12th February, 18th March, 13th April, 11th May, 17th September, 09th October, 11th November and 09th December 2005.
- Fig. 7.2.3 Synoptic distribution of $a_{CDOM440}$ in Mandovi and Zuari estuaries of Goa, West coast of India on 12th January, 12th February, 18th March, 13th April, 11th May, 17th September, 09th October, 11th November and 09th December 2005.
- Fig. 7.2.1.1 Correlation between in situ and satellite derived chlorophyll_a, TISM and $a_{CDOM440}$ in estuarine waters. The dotted lines represent 95% confidence level.

Fig. 7.3.1 Synoptic distribution of a) chlorophyll_a during (i) 08th January 2003 and (ii) 10th December 2004, b) TISM during (i) 08th January 2003 and (ii) 10th December 2004, c) $a_{CDOM440}$ during 08th January 2003.

Fig. 7.3.1.1 Correlation between in situ and satellite derived chlorophyll_a using standard algorithm (O'Reilly, 1998) and new algorithm.

Fig. 7.3.1.2 Correlation between in situ and satellite derived TISM using standard algorithm (Tassan, 1994) and new algorithm.

Fig. 7.3.1.3 Correlation between in situ and satellite derived $a_{CDOM440}$ using new algorithm.

Fig. 8.1.1 Flowchart showing the summary of the thesis.

List of tables

- Table 2.2.1 Table showing number of stations sampled, instruments used and data generated during different cruises. The notations are as follows: (W) – water samples, (R) – Radiometer, (C) – Conductivity-Temperature-Depth (CTD), (P) – PAR-Natural Fluorescence profiler, (S) – sunphotometer, (IOP) – Inherent optical properties, (AOP) – Apparent optical properties, (AOT) – Aerosol optical thickness, (T) – Temperature, (SL) – Salinity.
- Table 3.3.1 Mean and standard deviation of downwelling diffuse attenuation coefficient at wavelengths 412, 443 (blue), 490 (blue-green), 510, 555 (green) and 670 (red) nm and diffuse attenuation coefficient of PAR (k_d (PAR)) in open ocean (O), coastal (C) and estuarine (E) waters.
- Table 3.3.2 Slope of the scatter plot of a v/s k_d and $a + bb$ v/s k_d at 412, 443, 490, 510, 555 and 670 nm in open ocean (O), coastal (C) and estuarine (E) waters. The mean coefficient of regression (r) is given in the bottom row.
- Table 4.6.1 Table showing the Correlation coefficient (R^2) between chlorophyll_a, TISM and $a_{CDOM440}$ in coastal (C) waters.
- Table 4.6.2 Table showing the Correlation coefficient (R^2) between chlorophyll_a, TISM and $a_{CDOM440}$ in estuarine (E) waters during pre-monsoon and post-monsoon season in middle and lower zones.
- Table 5.1.1.1 Mean and standard deviation of bi-directional reflectance coefficient, expressed by Q-factor, at wavelengths 412, 443, 490, 510, 555 and 670 nm in open ocean (O), coastal (C) and estuarine (E) waters.
- Table 7.1.1 Table showing the constant factor used to convert digital numbers (DN) to the unit of radiance at bands corresponding to that of Ocean Colour Monitor (OCM).

Contents

	Pages
Chapter 1 Introduction	(1 – 9)
1.1 Background	----- (1)
1.2 Objectives	----- (8)
1.3 Layout of the thesis	----- (8)
Chapter 2 Study area, in situ observations and OCM Characteristics	(10 – 18)
2.1 Study area	----- (10)
2.2 In situ observation and satellite data	----- (14)
2.3 Ocean Colour Monitor characteristics	----- (17)
Chapter 3 Light field in the water column	(19 – 34)
3.1 Radiometric measurement	----- (20)
3.2 Hydrographic and optical zonation of water column	----- (22)
3.3 Inherent optical properties, apparent optical properties and water colour	----- (25)
Chapter 4 Bio – optical properties through water sample analysis	(35 – 61)
4.1 Generation of optical properties	----- (36)
4.2 Optically active substances in different optical domains	----- (39)
4.3 Interaction of downwelling irradiance with optically active substances	----- (41)
4.4 Inherent optical properties in different optical domains	----- (43)
4.4.1 Spectral variability of specific absorption coefficient of chlorophyll_a	----- (44)
4.4.2 Spectral variability of specific absorption coefficient of total inorganic suspended matter	----- (48)

4.4.3	Spectral variability of specific absorption coefficient of coloured dissolved organic matter	----- (52)
4.5	Spatial variability of optically active substances in different optical domains	----- (54)
4.6	Sources and sinks of optically active substances in different optical domains	----- (58)
Chapter 5 Development of Algorithms		(62 – 77)
5.1	Hyperspectral water leaving radiance	----- (63)
5.1.1	Theory	----- (63)
5.1.2	Effect of optically active substances on hyperspectral water leaving radiance	----- (66)
5.1.3	Sensitivity analysis of measured and computed absorption coefficient and water leaving radiance	----- (68)
5.2	Identification of wavelengths to derive optically active substances	----- (70)
5.2.1	Qualitative approach	----- (71)
5.2.2	Quantitative approach	----- (74)
Chapter 6 Atmospheric correction		(78 – 87)
6.1	Atmospheric path radiance	----- (79)
6.2	Aerosol characterization in atmospheres of different optical domains	----- (81)
6.3	Satellite retrieval of atmospheric optical properties	----- (85)
Chapter 7 Retrieval of optically active substances from Ocean Colour Monitor		(88 – 99)
7.1	Satellite data processing	----- (88)
7.2	Synoptic distribution of optically active substances in estuarine waters	----- (89)
7.2.1	Validation of satellite derived optically active substances in estuarine waters	----- (93)

7.3	Synoptic distribution of optically active substances in northeastern Arabian Sea	----- (94)
7.3.1	Validation of satellite derived optically active substances in northeastern Arabian Sea	----- (97)
Chapter 8 Summary and Conclusion		(100 – 102)
8.1	Summary	----- (100)
8.2	Conclusion	----- (101)
Bibliography		(103 – 120)

Annexure I Publications

Chapter 1

Introduction

1.1	Background-----	(1)
1.2	Objectives-----	(8)
1.3	Layout of the thesis-----	(8)

1.1 Background

Ocean covers approximately 71 % of earth's surface. It contains about 25% of the total planetary vegetation; with much of this restricted to coastal region (Jeffrey and Mantoura, 1997). It is also highly dynamic in spatial and temporal scales. The most developed areas of the globe are concentrated within the coastal zones. The rapid modernization and its effect on the environment is the main concern to the scientific community which is also a major threat to the biological richness of ocean especially in the coastal areas. Therefore, there is a pressing need for a long-term monitoring of such areas on spatial and temporal scales. Although many research activities have been carried out in the world ocean, the understanding of the ocean dynamics still stands incomplete due to the limited observations from ships, buoys and from fixed coastal stations. The advent of satellites provided consistent, repetitive and wide-area synoptic coverage which in turn radically changed the nature of oceanographic observations in recent years (Abbott and Zion 1985, Gregg et al., 2005).

The use of "optical remote sensing" (ocean colour) has proven to be one of the best suited approaches in understanding dynamics of many ocean ecosystems in open and coastal ocean waters. The physical basis for the detection of ocean colour from space rests on the fact that the sea acts as a monochromator, absorbing and reflecting certain amount of light received from space (Alberotanza, 1989). The ocean colour analysis also refers to a method of determining health of the ocean by measuring oceanic biological activity through optical means. Phytoplankton pigment, chlorophyll_a, major light absorbing component, absorbs blue and red light (resulting in the oceans blue-green

colour) is considered as a good indicator of the health of the ocean and its level of productivity. This also acts as an indicator of the equilibrium of CO₂ concentration between atmosphere and ocean. The other components of colour change in seawater are dissolved organic matter (DOM) and suspended particulate matter. The optical component of DOM known as coloured dissolved organic matter (CDOM) is derived from both terrestrial and oceanic sources (Coble, 1996). Terrestrial CDOM consists of dissolved humic and fulvic acid, which are primarily derived from land-based runoff containing decaying vegetation. In the open ocean, CDOM produced when the phytoplankton are degraded by grazing (Carder et al., 1999). The inorganic particulates consist of sand and dust created by erosion of continental rocks and soils. These enter the ocean through river runoff or by deposition of wind-blown dust on the ocean surface or by wave or current suspension of bottom sediments (Mobley, 1994). Both CDOM and particulates absorb strongly in the blue, yielding yellow to brown colour to the water (Hoepffner and Sathyendranath, 1993).

The ability of optical sensor to map the spatial and temporal patterns of ocean colour over regional and global scales has provided important insights into the fundamental properties and processes in the aquatic medium. The first ocean color sensor, onboard a satellite, launched by NASA in November 1978, was Coastal Zone Color Scanner (CZCS) (Hovis, 1980). Since then, the global archive of ocean color has given rise to numerous works by describing the phytoplankton distribution or using these data in various modeling studies related to primary productivity. Later many missions were launched such as IRS-P3-MOS, Sea WiFS, OCTS, MODIS and MERIS. In order to meet the specific and increasing demands of data in ocean research, intensive efforts were

made by Indian Space Research Organization (ISRO) for developing and launching state-of-art satellites. The first in the series of ocean satellites, Indian Remote Sensing Satellite (IRS) – P4 – Ocean Colour Monitor (OCM) (Oceansat-1), was launched successfully, on 26 May 1999, using the indigenously built Polar Satellite Launch Vehicle (PSLV).

There are mainly three broad scientific applications of ocean-colour data (IOCCG, 1999). The first concerns the ocean carbon cycle and the role of the ocean in climate change. The primary application of ocean colour data, in the larger scale, is the estimation of the role of the phytoplankton in global fluxes of carbon and other biogeochemically important compounds (Platt and Sathyendranath, 1988; Morel, 1991). The marine phytoplanktons carry out photosynthesis by utilizing sun energy to provide the organic matter necessary to sustain the marine food chain. In this process, they remove inorganic carbon and other important plant nutrients from the upper layers and release oxygen. Photosynthesis by phytoplankton, therefore, is a key process in controlling the biogeochemical cycle of carbon, nitrogen and oxygen in the ocean on a global scale. Another byproduct of phytoplankton photosynthesis, which has potential geochemical implications, is dimethylsulfide released from marine phytoplankton into the atmosphere which may be a major source of cloud condensation nuclei (Charlson et al., 1987).

Due to the high spatial and temporal variability of marine phytoplankton concentrations, the magnitude and variability of primary production are poorly known on a global scale. Model studies show that global productivity calculations are very sensitive to the input of surface chlorophyll_a fields (Platt and Sathyendranath, 1988; Behrenfeld and Falkowski, 1997; Field et al., 1998) and thus satellite ocean-colour data are very

important for accurate calculations of the mean and time-varying components of the global distribution of ocean primary production (Field et al., 1998).

The second application of ocean colour is to provide a synoptic, observational link between the development of the ocean ecosystem and physics of the mixed layer. Diffuse attenuation coefficient of downwelling irradiance (k_d) is a key parameter in physical models of the upper ocean which determines stratification through heating and its homogenization through turbulence. The optically active substances (OAS) such as chlorophyll_a, total inorganic suspended matter (TISM) and CDOM absorb solar radiation, precisely in the shorter wavelength of visible part (400-700 nm) of electromagnetic radiation (EMR). Thus plays an important role in ocean heat budget studies. Ocean-colour data were used in upper ocean heat flux calculations in Arabian Sea (Sathyendranath et al., 1991) and in the Equatorial Pacific (Lewis et al., 1990). This new approach makes significant difference to the computed heat flux as well as the vertical distribution of heat in the upper ocean.

The third application of ocean colour is in the domain of coastal zone protection and the management of marine resources. Increased concerns about the rapid changes of the coastal areas have highlighted the necessity for the developments of integrated systems for research and operational use in monitoring the resources and processes in coastal waters. There is conformity that earth observation data, specifically ocean colour, could play a key role in providing real time information on water-quality parameters (e.g. harmful algal blooms and eutrophication). This complements to conventional sampling techniques to resolve specific environmental problems in the coastal zones at sufficient space-time resolutions.

The importance of the coastal and estuarine waters in terms of productivity has been well recognized (Ansari et al., 2003). These areas are also prone to pollution and sedimentation due to anthropogenic activities resulted from increasing human settlement. Apart from this, transient nature of the hydrographic features makes these waters a highly dynamic ecosystem. In addition, estuaries of Asiatic continent are affected by monsoonal freshwater discharge. Hence the circulation in estuaries is governed by tide during non-monsoon period whereas tide and freshwater discharge control the circulation during monsoon. The varying hydrography has a significant impact on the bio-optical properties of estuarine and coastal waters. As OAS play a significant role in determining water quality to coastal zone, understanding the sources and sinks of the OAS is a better approach in coastal zone management. The phytoplankton pigment, chlorophyll_a, determines productivity whereas the quantification of CDOM and TISM could be a good indicator of coastal pollution.

As a potential indicator of perennial source of CO₂, studies on CDOM have gained momentum in the recent past (Menon et al., 2006b). It is now well recognized that the man made chlorofluorocarbon (CFC) causes destruction of ozone in the stratosphere leading to intrusion of ultraviolet (UV) radiation which is harmful to aquatic ecosystems (Williamson et al., 1996; Zepp et al., 1998; Neale and Kieber, 2000). As CDOM absorbs strongly in UV region, it forms a principal component in restricting penetration of these radiation which is potentially harmful to aquatic plants and organisms. Thus, the amount of CDOM in surface waters can have a substantial impact on the levels of damaging radiation received by aquatic organisms. Moreover, in the coastal and estuarine regions, the effect of light absorption by CDOM can extend well over the visible part (400-700

nm) of EMR (Menon et al., 2005). In such a condition, the amount of light available for phytoplankton may reduce thus it can decrease primary productivity. Therefore, CDOM can play a substantial role in biogeochemistry of the natural waters through its influence on the aquatic light field (Vodacek et al., 1995; Conde et al., 2000).

The estuarine regions are highly influenced by discharge of sediment through river runoff. The excess sedimentation in suspension can affect the behavior, health and habitat of fishes (Watts et al., 2003). The excessive sedimentation along the port and its settlement in the fairway channel is of major concern to the port authority. As far as optics is concerned, sediment strongly absorbs and also scatters in the shorter wavelengths. Thus, it forms a key parameter in determining water turbidity in the estuarine and coastal waters. Hence quantification of this parameter is taken as an important tool in coastal zone management.

The retrieval of OAS through a visible satellite sensor requires a suitable algorithm, for which knowledge of bio-optical properties in the environment is very important. These bio-optical properties can be classified into inherent optical properties (IOP) and apparent optical properties (AOP). Absorption (a) and scattering (b) by OAS are termed as IOP. As IOP are solely the properties of the media, they are fundamental in understanding the optical characteristics of the marine environment. Apart from IOP, AOP, such as reflectance and diffuse attenuation coefficient, also describe the optical behavior of water bodies in a particular light field. In the optical arena, waters have been classified, based on the optical constituents, into case I and case II. The case I waters are one in which phytoplankton and their accessory pigments play a dominant role in determining the optical properties. In case II waters, in addition to phytoplankton, TISM

and CDOM determine the optical properties of the water column (Morel and Prieur, 1977). There is a well defined algorithm to retrieve OAS, through remote sensing technique, from case I (open ocean) waters. But in Case II (estuarine and coastal) waters, due to the non-linearity in the optical property, site-specific algorithm needs to be developed. The differential patterns in the absorption and scattering coefficient of OAS in case II waters make it optically complex. Thus understanding the relationship between the reflectance, absorption and backscattering is essential for developing the algorithm to use remote sensing as a monitoring tool in case II waters (Bowers et al., 2004; Menon et al., 2005).

An algorithm alone doesn't suffice the retrieval of OAS from the optical sensor. The effects of atmospheric constituents also need to be incorporated while analyzing optical sensor data. Around 80 – 85 % of the radiance received by a pixel of a sensor, onboard satellite, is from atmosphere. Therefore, to quantify the information received from the water column, it is mandatory to eliminate the atmospheric radiance from the total radiance (Moulin et al., 2001). The radiance due to air molecules (Rayleigh radiance) could be modeled accurately with the knowledge of air pressure and sun zenith angle (Doerffer, 1992). The main difficulty in atmospheric correction is the precise synoptic information of radiance due to aerosol loading in the atmosphere which is variable in both time and space. These suspended particles in the atmosphere follow the motion of the air within a certain broad limit and show a great diversity in their volume and size (Krishnamurthy et al., 1997). The key parameter in understanding the aerosol radiance is aerosol optical thickness (AOT), the spectral variation of which follows angstrom formulae (Angstrom, 1961, 1964). Angstrom wavelength exponent (α) is an

indicator of aerosol size distribution parameter whereas turbidity factor (β) indicates the atmospheric turbidity due to aerosol.

Thus the study is proposed to understand the complexity of interaction of EMR with OAS, of case I and case II waters, and to retrieve the same using a visible satellite sensor, IRS – P4 – OCM, after giving a proper atmospheric correction. The objectives of the present study are

1.2 Objectives

1. To generate inherent and apparent optical properties (IOP and AOP) of the water column of different optical domains and to derive inherent optical properties from apparent optical properties.
2. Development of a suitable site specific algorithm for case II waters to retrieve optically active water constituents through a visible satellite sensor (Ocean Colour Monitor).
3. To give a proper atmospheric correction to the remotely sensed data by analyzing the effect of atmospheric turbidity and aerosol size distribution on radiative transfer.

1.3 Layout of the thesis

The entire thesis is presented in eight chapters. Chapter 1 is introduction. Chapter 2 deals with the description of the study area, the specific protocols to be followed for making optical measurements, different instruments used and characteristics of Ocean Colour monitor. Chapter 3 provides detail methodology adopted in deriving optical

properties through radiometric measurements. The IOP and AOP in three different optical domains, derived through radiometric measurements, were discussed in detail. Chapter 4 describes the generation of bio-optical properties through water sample analysis. The protocols adopted for sampling, analysis and derivation of optical properties of each OAS have been described in detail. The spectral variation of each OAS and its implications on ambient light field was discussed. The interaction of downwelling irradiance with OAS in open ocean (O), coastal (C) and estuarine (E) waters are also discussed. The different sources and sinks of OAS and its implication on light field are discussed. Chapter 5 deals with the approaches adopted for the development of algorithms to retrieve OAS through Ocean Colour Monitor data. The computation of hyperspectral water leaving radiance, using calibrated radiative transfer model and the radiative transfer theory is described in detail. The effects of OAS on hyperspectral water leaving radiance were then analyzed. An analysis of OAS through remotely sensed data requires a proper incorporation of the effects of atmosphere. Hence this has been discussed in chapter 6. The methodology adopted in computation of atmospheric path radiances is described in detail. The spectral variability of AOT, Angstrom wavelength exponent (α) and turbidity factor (β) in the atmosphere over O, C and E - waters are discussed in detail. Retrieval of OAS through OCM data are included in chapter 7. The spatial and temporal variability of chlorophyll_a, TISM and CDOM in estuarine and coastal waters along with the accuracy of retrieval are given in this chapter. The chapter also explains the application of ocean colour data to analyze coastal and estuarine hydrodynamics. The summary of the research and the significant conclusions, drawn, are given in chapter 8.

Chapter 2

Study area, in situ observations and OCM characteristics

2.1	Study area-----	(10)
2.2	In situ observation and satellite data-----	(14)
2.3	Ocean Colour Monitor characteristics-----	(17)

2.1 Study area

The study area was chosen in such a way that it falls in three different optical environments / domains. These domains were selected on the basis of the variability of properties of OAS (Prieur and Sathyendranath, 1981). The area consists of case I (open ocean waters from Arabian Sea and waters surrounding Kavaratti Island at Lakshadweep) and case II waters (coastal waters and Mandovi – Zuari estuarine system of Goa, west coast of India) (Fig. 2.1.1).

The Arabian Sea, a tropical basin in the western Indian Ocean, is land locked in the northern side by Asiatic continent. The area is under diverse monsoonal forcing with seasonal reversal of wind during summer and winter. During summer monsoon (June – September) winds are mainly from southwest whereas it reverses to northeast during winter monsoon (November to February) (Bauer et al., 1991). These seasonally reversing monsoon winds force Arabian Sea upper ocean circulation to reverse seasonally. During southwest monsoon, upwelling occurs along the boundaries of the Arabian Sea whereas during northeast monsoon cooling and sinking of surface water, as a result of intense evaporation (winter cooling), was witnessed in the north eastern Arabian Sea (Schott et al., 2002). The winter cooling forces convective mixing resulting in the upward pumping of nutrients in the surface waters (Prasanna Kumar et al., 2001) and subsequent formation of algal bloom (Dwivedi et al., 2006). Hence it is very clear that the area is undergoing inter-seasonal and intra-seasonal variability. These diverse conditions produce notable effect on the distribution of OAS and hence optical properties. The water in the Lakshadweep area forms a unique environment in the Arabian Sea having a coral reef ecosystem. The optical signatures characterize this water as pure case I type. Hence

stations covered in this area along with offshore waters of Arabian Sea were grouped into case I category.

The waters along west coast of India from Karwar to Gujarat were selected as a part of study area. The southern part of this area was under the strong influence of the discharge from rivers such as Kali at Karwar and Mandovi – Zuari at Goa (Qasim, 2003). The topography of the northern part was also highly variable with a large continental shelf off Gujarat Coast (Nayak and Sahay, 1985).

Mandovi and Zuari estuaries, an integral part of the study area, symbolize the most complex ecosystem, optically as well as hydrographically. The estuaries are connected through a narrow canal, the Cumbarjua. The width at the mouth of the Mandovi estuary is ≈ 3.5 km which narrows down to ≈ 0.25 km at the upstream and extends up to 75 km. Zuari estuary extends up to 70 km upstream having width ≈ 5.5 km at the mouth which narrows down to less than 0.5 km to upstream. These estuaries have seasonal cycle of variation in their hydrographic properties during pre-monsoon (February – May), monsoon (June – September) and post-monsoon (October – January) period. The average annual rainfall over Goa is 3000 mm, most of which occurs during southwest monsoon (Qasim and Sen Gupta, 1981). With the onset of the monsoon, the estuaries become stratified below 2 – 3 m of the surface resulting in salt wedge type of estuary. As monsoon recedes, the input of freshwater reduces and tidal force starts dominating resulting in breaking of stratification. This led the estuaries to turn into partially mixed during post-monsoon season. During pre-monsoon season the river discharge is almost negligible and the estuaries are completely dominated by the tide. This leads formation of well mixed estuary (Murthy et al., 1976; Shetye et al., 1995).

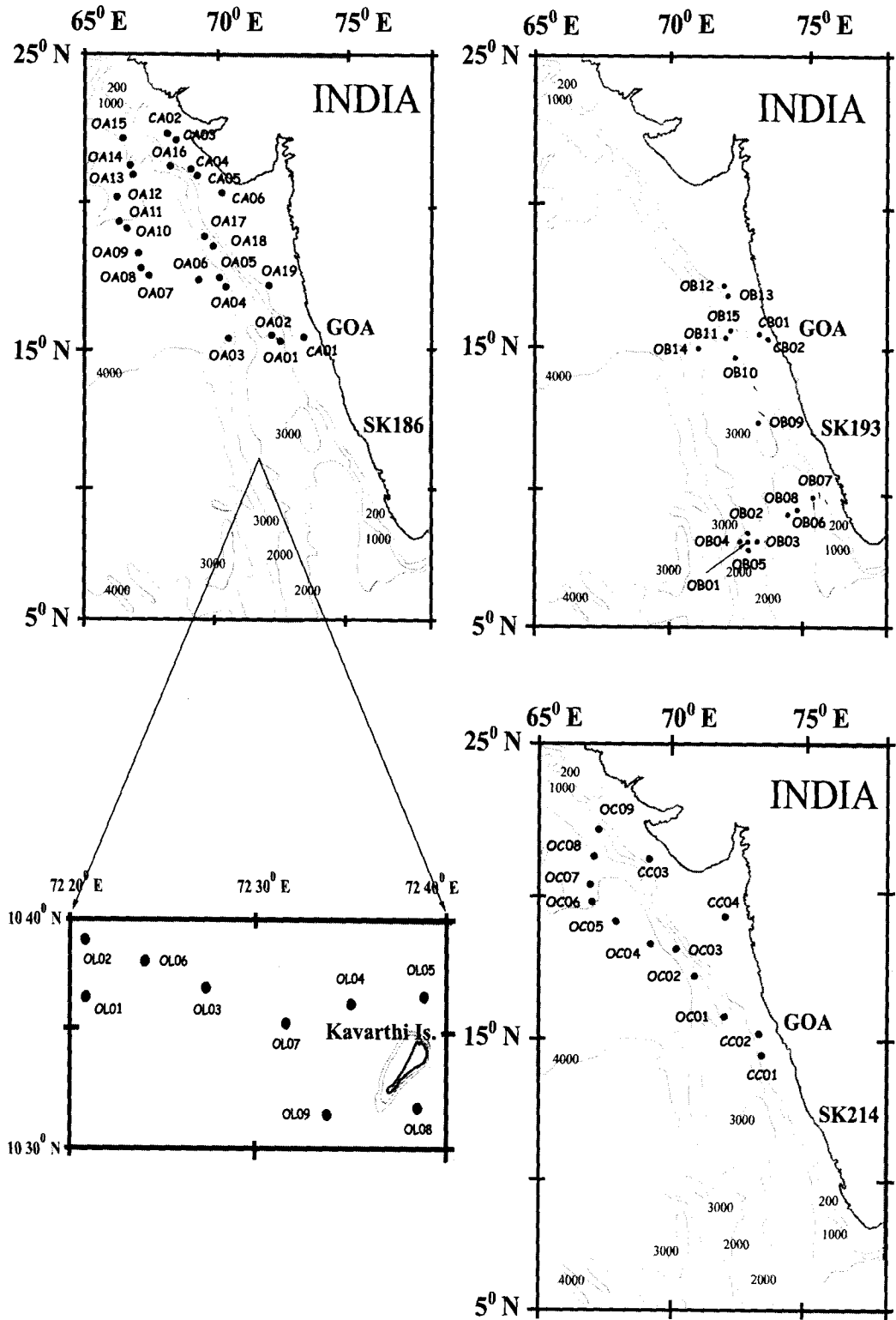


Fig. 2.1.1 (a) Map of study area showing hydrographic stations covered during cruise SK 186, SK 193, SK 214 and in Lakshadweep waters

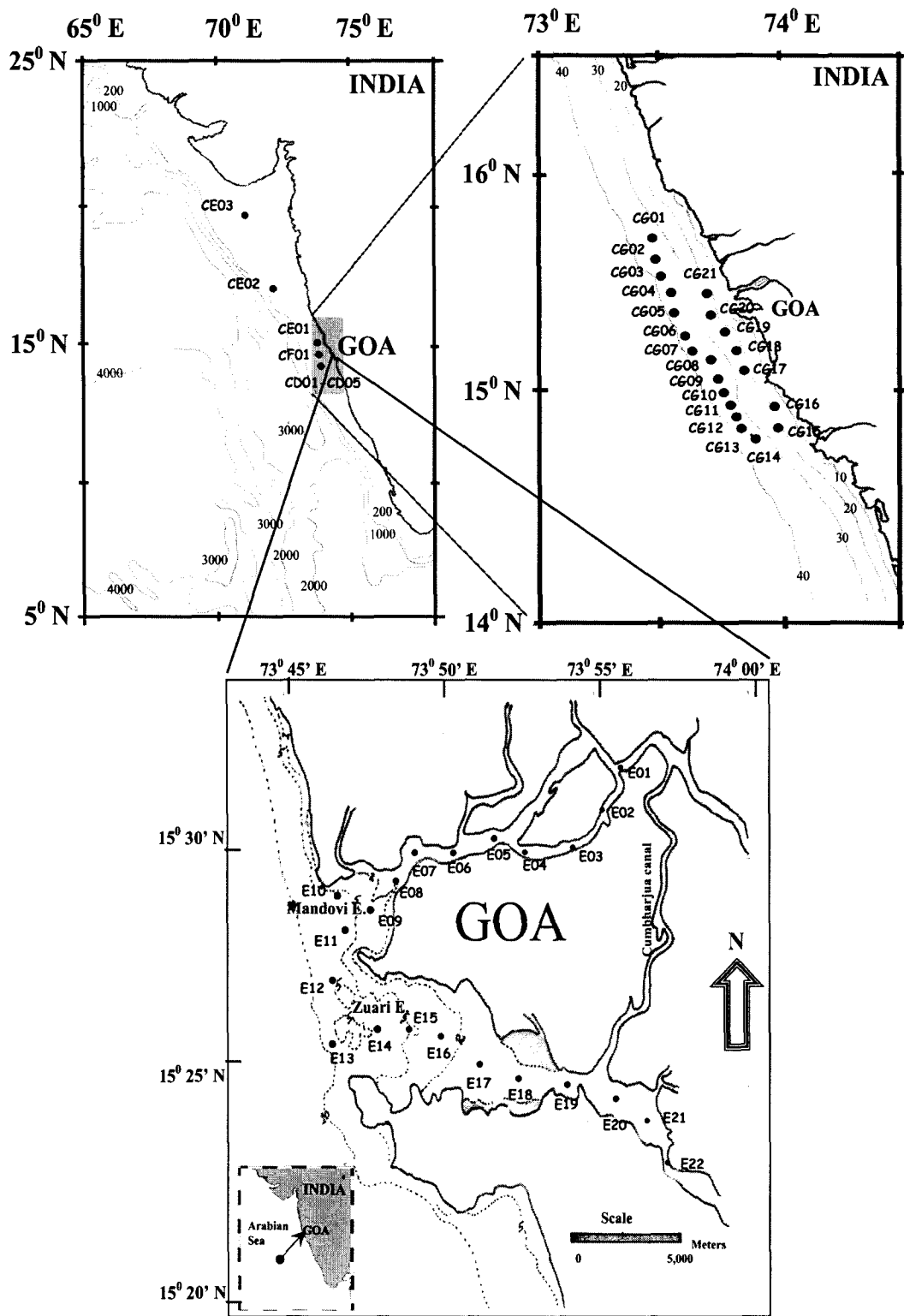


Fig. 2.1.1 (b) Map of study area showing hydrographic stations covered onboard CRV Sagar Purvi (CF01; CG01 – CG21), CRV Sagar Paschimi (CD01 – CD05; CE01 – CE03) and onboard trawler in Mandovi – Zuari estuarine system (E01 – E22) of Goa.

2.2 In situ observation and satellite data

All the field observations were carried out on cloud free days. The sampling gears such as Satlantic Multichannel Radiometer, water sampler, secchi disc, Global Positioning System (GPS), conductivity-temperature-depth (CTD), Photosynthetically Available Radiation (PAR) -natural florescence (PNF) and Microtops II sunphotometer were operated simultaneously from the sunlit portion of the ship / trawler. Details about the instruments are given in subsequent chapters dealing with data from respective instrument. Atmospheric parameters such as air temperature, relative humidity, atmospheric pressure, wind speed and wind direction were obtained from automatic weather station (AWS) installed at the ship. During trawlers surveys, in the estuarine region, these parameters were obtained from AWS installed at Goa University campus. In estuarine waters, being shallow in nature, the station positions were identified on the basis of the transparency of the water column. The transparency was measured using secchi disc. Station positions were chosen in such a way that the depth of the water column was more than three times the secchi disc depth. This has been done to avoid any radiance from bottom of the station (Muller and Austin, 1995).

Three scientific cruises were conducted onboard Ocean Research Vessel (ORV) Sagar Kanya (SK). SK186 (2nd – 20th January 2003) and SK214 (4th – 17th December 2004) was a part of ISRO biological parameters retrieval and validation of OCM derived products programme. Both the cruises were carried out along eastern and northeastern waters of Arabian Sea, covering the area from 15^o N to 23^o N and 66^o E to 74^o E. Total 25 stations were sampled onboard SK186 which includes both open ocean (OA01 – OA19) and coastal (CA01 – CA06) waters. Onboard SK 214, samplings were carried out

at nine stations in open ocean (OC01 – OC09) and four stations in the coastal region (CC01 – CC04).

Cruise ID	Period	No. of Stations	Instruments used	Data generated
SK186	2 nd – 20 th Jan 03	25	W, R, C	IOP, AOP, T, S
SK193	17 th May to 18 th June 03	17	R	AOP
SK214	4 th – 17 th Dec 04	13	W, P, S	IOP, AOP, AOT
Sagar Paschimi	26 th Sept – 30 th Sept 02	05	W, R	IOP, AOP
Sagar Paschimi	3 rd Oct – 5 th Oct 02	03	W, R	IOP, AOP
Sagar Purvi	16 th Oct 03	01	R	AOP
Sagar Purvi	27 th – 30 th Sep 03	09	R	AOP
Sagar Purvi	23 rd – 28 th Nov 04	21	W, S	IOP, AOT
Trawler	14 th Feb 02	08	W, R	IOP, AOP
Trawler	04 th May 02	10	R	AOP
Trawler	12 th Feb 05	14	W, S, C	IOP, AOT, T, SL
Trawler	18 th Mar 05	18	W, S, C	IOP, AOT, T, SL
Trawler	13 th Apr 05	13	W, S	IOP, AOT
Trawler	15 th Apr 05	12	W, S	IOP, AOT
Trawler	11 th May 05	18	W, S, C	IOP, AOT, T, SL
Trawler	15 th Aug 05	17	W, S, C	IOP, AOT, T, SL
Trawler	17 th Sept 05	16	W, S, C	IOP, AOT, T, SL
Trawler	11 th Nov 05	20	W, S	IOP, AOT
Trawler	09 th Dec 05	22	W, S	IOP, AOT

Table 2.2.1

Table showing number of stations sampled, instruments used and data generated during different cruises. The notations are as follows: (W) – water samples, (R) – Radiometer, (C) – Conductivity-Temperature-Depth (CTD), (P) – PAR-Natural Fluorescence profiler, (S) – sunphotometer, (IOP) – Inherent optical properties, (AOP) – Apparent optical properties, (AOT) – Aerosol optical thickness, (T) – Temperature, (SL) – Salinity

SK193 (15th May – 20th June 2003) was carried out in southeastern Arabian Sea, covering the area from 7^o N to 18^o N and 71^o E to 74^o E, as a part of Arabian Sea Monsoon Experiment (ARMEX) programme. Although sampling was conducted at fifteen stations in open ocean (OB01 – OB15) and two in coastal (CB01 – CB02) waters,

only those stations corresponding to clear sky conditions were used for the analysis. These stations were OB01, OB04, OB05, OB08, OB09, OB12 and OB13. The field observations in Lakshadweep waters (OL01 – OL09) were carried out onboard Coastal Research Vessel (CRV) Sagar Purvi in the area surrounding Kavrathi Island from 27th to 30th September 2003 (Fig. 2.1.1a). Satlantic Multichannel Radiometer was operated at all the stations onboard SK186 along with water sample collection for the analysis of OAS whereas at stations sampled onboard SK193 and those covered in Lakshadweep waters only radiometer was operated. Further, stations covered onboard SK 214, PNF profiler was operated along with water sample collection and sunphotometer observation. Apart from this, CTD measurements were carried out at all stations.

The coastal observations were carried out onboard Coastal Research Vessel (CRV) Sagar Paschimi between 26th September and 30th September 2002 (CD01 – CD05), 3rd October and 5th October 2002 (CE01 – CE03). The observations onboard CRV Sagar Purvi were carried out on 16th October 2003 (CF01) and CRV Sagar Purvi from 23rd to 28th November 2004 (CG01 – CG21). All the observations were carried out in coastal waters from Karwar to Gujarat along 20 m to 40 m bathymetry line (Fig. 2.1.1b). At stations CD01 – CD05 radiometric measurements and water sample collections were done whereas at stations CE01 – CE03 and CF01 only radiometer was operated. Further, at stations CG01 – CG21 water samples were collected and sunphotometer was operated. CTD measurements were carried out at all the stations of different cruises.

In Mandovi – Zuari estuarine system, field surveys were conducted, on board trawler, during pre-monsoon (12th February, 18th March, 13th April and 11th May),

monsoon (15th August and 17th September) and post-monsoon (11th November and 9th December) season of the year 2005 (Fig. 2.1.1b). The details about the period of sampling, number of stations and data generated at each cruise is given in table 2.1.1.

2.3 Ocean Colour Monitor characteristics

Moreover, IRS – P4 – OCM data of 08th January 2003 (corresponding to SK186), 10th December 2004 (corresponding to Sk214), 12th January, 12th February, 18th March, 13th April, 11th May, 17th September, 09th October, 11th November and 09th December 2005 (corresponding to field survey in estuarine region) was procured from National Remote Sensing Agency (NRSA).

OCM onboard IRS - P4 was launched in 26th May 1999 in a polar sun synchronous 720 km altitude orbit. The equatorial crossing is at 12 noon \pm 20 min. The main features of the OCM instrument are given in table 2.2.1.

Parameters		Specification
Spatial resolution (m)		360 x 250
Swath (km)		1420
No. of spectral bands		8
Spectral range (nm)		402-885
Revisit time		2 days
Spectral band	Central wavelength (bandwidth) in nm	Saturation radiance (mw-cm ⁻² -sr ⁻¹ - μ m ⁻¹)
C1	412 (20)	35.5
C2	443 (20)	28.5
C3	490 (20)	22.8
C4	510 (20)	25.7
C5	555 (20)	22.4
C6	670 (20)	18.1
C7	765 (40)	9.0
C8	865 (40)	17.2

Table 2.2.1

Table showing the characteristics of Ocean Colour Monitor onboard IRS – P4

The OCM is the first instrument to take advantage of push broom technology for achieving higher radiometric performance and higher spatial resolution while maintaining a large swath to provide high revisit time of 2 days for ocean observations. The sensor spatial resolution is 360 meters across track and 250 meters along the track.

The spectral bands for IRS – P4 – OCM have been selected mindful of the optical properties of phytoplankton pigments (principally chlorophyll_a), TISM, CDOM and the requirements of spectral bands for atmospheric correction (Navalgund and Kiran Kumar, 2001). The first spectral band centered at 412 nm is selected primarily for discriminating CDOM from viable phytoplankton pigment. The band at 443 nm is close to the absorption maximum of chlorophyll_a, which is centered at approximately 435 nm, but it has been selected because its location minimizes interference from a Fraunhofer absorption line at 435 nm. This band is used along with the 555 nm band for determining colour boundaries, low chlorophyll_a concentrations and diffuse attenuation coefficient. The third band, at 490 nm, along with a fourth channel at 510 nm would allow the use of multi-band spectral curvature algorithms and other second derivative algorithms to be applied to derive chlorophyll concentrations in coastal or Case-II waters. The 510 nm band along with a 555 nm channel would also be useful in deriving higher chlorophyll concentrations in Case-I waters. The spectral band at 555 nm is used as a hinge point for determining chlorophyll_a concentration and water optical properties such as diffuse attenuation coefficient. The band at 670 nm is sensitive to backscattering from suspended matter in coastal waters, and is useful in quantifying suspended matter along with the channel at 557 nm. The spectral bands at 768 nm and 867 nm are used in atmospheric correction procedures (Chauhan et al., 2002).

Chapter 3

Light field in the water column

- 3.1 Radiometric measurement----- (20)
- 3.2 Hydrographic and optical zonation of water column----- (22)
- 3.3 Inherent optical properties, apparent optical properties and water colour -- (25)

The transmission of light in to the water column is of fundamental importance to aquatic ecosystems. The process of absorption by dissolved and suspended matter in the ocean affects the distribution of light within the water column as well as that emerging from the ocean. The scattering and absorption by different OAS is described by IOP (Preisendorfer, 1965; Belzile et al., 2004). IOP are solely properties of the media and independent of the ambient light field. IOP being additive, could be directly compared with the presence of OAS irrespective of the ambient light field. The fundamental IOP are absorption (a) and volume scattering function (VSF).

The in situ measurement of absorption ($a(\lambda)$) and attenuation coefficients ($c(\lambda)$) could be easily achieved using available instruments such as ac-9 and ac-s meters. The difficulty lies in the measurement of backscattering coefficient ($b_b(\lambda)$), which is VSF integrated backward and very crucial as far as remote sensing of ocean colour is concerned. The backscattering (b_b) could be estimated by inversion of AOP (Roesler and Perry, 1995). As AOP depend upon IOP as well as ambient radiance distribution, the normalization of AOP with respect to radiance distribution can serve the purpose of computation of backscattering (b_b) (McKee et al., 2003). In the present study, IOP, such as absorption (a) and backscattering coefficient (b_b), have been estimated using AOP. The AOP used for the inversion are remote sensing reflectance ($R_{rs}(\lambda)$) and diffuse attenuation coefficient of downwelling irradiance ($k_d(\lambda)$).

$R_{rs}(\lambda, 0^+)$, the ratio of radiance leaving the water column (upwelling) to irradiance incident on the water (downwelling), indicates the effective reflectance of a water body when viewed by a remote sensor. The $k_d(\lambda)$ is an AOP which defines the variability of light with depth. Being an AOP, it varies with solar zenith angle and with depth even in well mixed water column (Gordon, 1989; Liu et al., 2002). This behavior of k_d has been used by Jerlov (1976) to develop a frequently used

classification scheme for oceanic waters based on its spectral shape. k_d is also an indicator of water quality and is of prime importance in ocean colour remote sensing. $k_d(\lambda)$ also plays a critical role in many studies including photosynthesis and other biological processes in the water column (Sathyendranath et al., 1989) which also determines the turbidity of coastal waters (Kirk, 1994). Hence the chapter deals with the variability of light field within the water column, and its attenuation on the basis of IOP and AOP of OAS at different wavelengths as an implication to ocean colour in different optical domains.

3.1 Radiometric measurement

A Satlantic Profiling Multichannel Radiometer (SPMR) along with Satlantic Multichannel Surface Reference (SMSR) was used to measure the profiles of upwelling radiance ($L_u(\lambda, z)$), downwelling irradiance ($E_d(\lambda, z)$) and downwelling irradiance reaching the sea surface ($E_s(\lambda)$). The instrument operates in seven bands with wavelength centered at 412, 443, 490, 510, 555, 670 and 780 nm with a bandwidth of ± 10 nm in visible bands and ± 20 nm in near infrared (NIR) bands. The measurement was restricted up to euphotic depth (depth at which 1 % surface PAR reaches). The radiometer data was processed using software SATCON and PROSOFT 3c supplied by the manufacturer. As a quality control of the data, those observations, wherein the tilt of the SPMR exceeds 5° and that of SMSR with tilt 10° were discarded.

The PAR was computed using the equation given by Kirk (1994)

$$\text{PAR} = [h c]^{-1} \int_{400}^{700} \lambda E_d(\lambda, z) d\lambda \quad [\text{quanta-m}^{-2}\text{-sec}^{-1}] \quad \text{---- (3.1.1)}$$

Where h is the Planck's constant and c is velocity of light in vacuum. $k_d(\lambda)$ and diffuse attenuation coefficient of PAR ($k_d(\text{PAR})$) over the euphotic depth was then calculated as

$$k_d(\lambda) = - [E_d(\lambda)]^{-1} d [E_d(\lambda)] / dz \quad [\text{m}^{-1}] \quad \text{---- (3.1.2)}$$

$$k_d(\text{PAR}) = - [\text{PAR}]^{-1} d [\text{PAR}] / dz \quad [\text{m}^{-1}] \quad \text{---- (3.1.3)}$$

The water leaving radiance was then extrapolated to the surface following Derecki et al. (2003) as follows

$$L_u(\lambda, \theta^+) = L_u(\lambda, \theta^-) [(1 - \rho(\lambda, \theta)) / \eta_w^2(\lambda)] [\mu\text{w-cm}^{-2}\text{-nm}^{-1}\text{-s}^{-1}] \quad \text{---- (3.1.4)}$$

Where $\rho(\lambda, \theta)$ is Fresnel reflectance index of seawater and η_w is the refractive index of seawater. The remote sensing reflectance ($R_{rs}(\lambda, \theta^+)$) were calculated using downwelling irradiance at the surface ($E_d(\lambda, \theta^+)$) and $L_u(\lambda, \theta^+)$, for wavelengths corresponding to bands of radiometer, as

$$R_{rs}(\lambda, \theta^+) = L_u(\lambda, \theta^+) / E_d(\lambda, \theta^+) \quad [\text{sr}^{-1}] \quad \text{---- (3.1.5)}$$

The total $a(\lambda)$ and $b_b(\lambda)$ of OAS were derived from AOP ($k_d(\lambda)$ and $R_{rs}(\lambda)$) (McKee et al., 2003) as per the following equations

$$a(\lambda) \approx [k_d(\lambda) \cos \theta_s] / 1.0395 [(R_{rs}(\lambda) / 0.083) + 1] \quad [\text{m}^{-1}] \quad \text{---- (3.1.6)}$$

$$b_b(\lambda) \approx [k_d(\lambda) \cos \theta_s] / 1.0395 [(0.083 / R_{rs}(\lambda)) + 1] \quad [\text{m}^{-1}] \quad \text{---- (3.1.7)}$$

3.2 Hydrographic and optical zonation of water column

The data pertaining to ocean colour, collected through various cruise programmes over the eastern and northeastern Arabian Sea (see Chapter 2), show large variability in their hydrographic and optical pattern. Following to Gordon and Morel (1983) and IOCCG (2000), the properties of samples can be classified into three distinct groups namely O, C and E – waters. The first group includes the stations (OA01 – OA19; OB01 – OB15; OC01 – OC09) in deep waters away from the coast. The second group includes the stations (CA01 – CA06; CB01 – CB02; CC01 – CC04; CD01 – CD05; CE01 – CE03; CF01; CG01 – CG21) from shallow waters close to the coast. The third group includes stations (E01 – E22) from estuarine waters. The vertical profiles of temperature, fluorescence and PAR clearly depicts these features (Fig. 3.2.1).

The figure 3.2.1 showed the mean temperature, fluorescence and PAR profiles at different stations in O, C and E – waters. The mean profile of temperature in O and C – waters showed thermal stratification with the average depth of mixed layer as 47 m (± 18 m) and 8 m (± 5 m) respectively. A prominent deep chlorophyll maxima (DCM) settling at an average depth of 48 m (± 10 m) and 10 m (± 3 m) was also seen in the average profile of fluorescence in O and C – waters respectively. Studies carried out by Barlow et al. (2002) showed a similar distribution where DCM was observed in the upper 20 m in the European Shelf and Falkland regions while in the southern oligotrophic waters it was located at depths from 70 to 100 m. In E – waters a clear mixed layer depth (MLD) and DCM was not seen. It was also observed that DCM coincides with the bottom of the mixed layer in O – waters. DCM plays a significant role in altering the spectral signatures emerging out of the water column only if the surface chlorophyll_a concentration is below $0.4 \mu\text{g}\cdot\text{l}^{-1}$. On the contrary its

effect nullifies if located at depths > 65 m (Sathyendranath and Platt 1989; Stramaska and Stramaski, 2005).

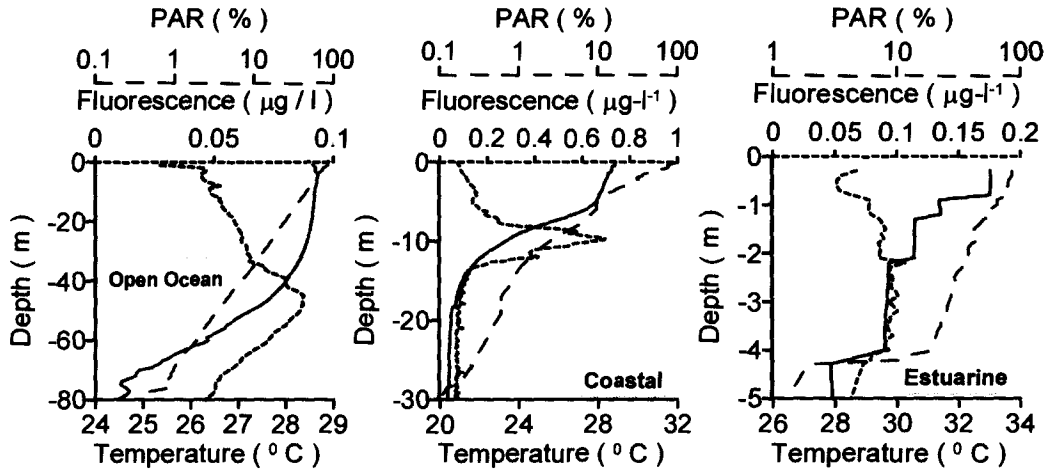


Fig. 3.2.1

Vertical profiles of mean temperature ($^{\circ}\text{C}$), fluorescence ($\mu\text{-g}^{-1}$) and PAR (%) in open ocean (O), coastal (C) and estuarine (E) waters. The vertical distribution of PAR is presented on a logarithmic scale.

The PAR decreases exponentially with depth (linearly decreasing on a logarithmic scale) having a uniform slope in O – waters whereas in C – waters a larger slope could be seen at first few meters. This confirms that in C – waters the attenuation of light was maximum in first few meters. This was also evident from the variability of E_d at 490 nm (Fig. 3.2.2) observed in O, C and E – waters. It was clear that at all the stations, a uniform attenuation with depth were observed in O – waters where as the attenuation of light was maximum in first few meters. Moreover, in O – waters the blue-green light was seen up to 50 m whereas it was 15 m in C – waters and less than 3 m in E – waters. Smith (1981) showed that the penetration of light in deeper waters primarily depends on water clarity and on the wavelength of light considered. In clear oligotrophic waters, where the absorption of light was mainly due to water itself, the red light diffuses maximum with depth indicating presence of blue-green light in deeper waters (McKee et al., 2003; Mishra et al., 2005).

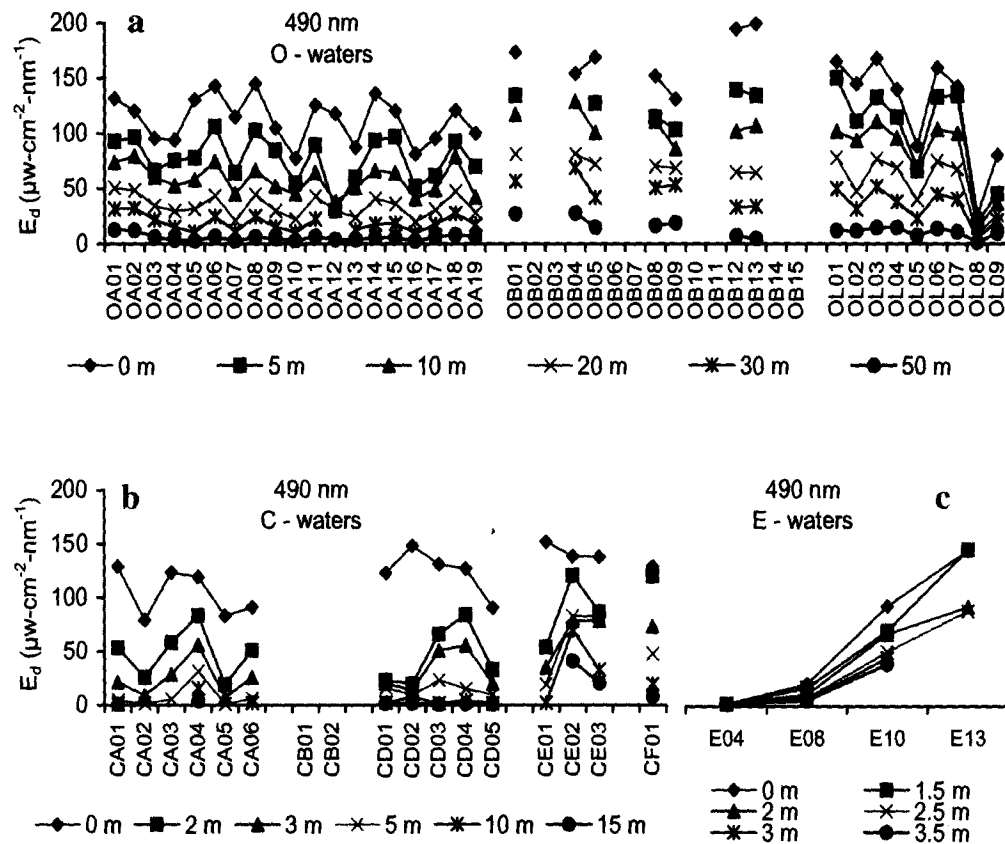


Fig. 3.2.2

Variability of downwelling irradiance (E_d) at 490 nm at different depths at stations corresponding to a) open ocean (O), b) coastal (C) and c) estuarine (E) waters

The average PAR at the surface, during the period of observations, was 8.94×10^{16} ($\pm 2.33 \times 10^{16}$), 8.96×10^{16} ($\pm 2.47 \times 10^{16}$) and 8.89×10^{16} ($\pm 2.11 \times 10^{16}$) quanta-cm⁻²-sec⁻¹ in O, C and E – waters respectively. The mean euphotic depth was found to be extending up to 64 m (± 9 m) and 16 m (± 6 m) in O and C – waters respectively. In E – waters, no prominent euphotic depth was observed. Further, the average PAR at DCM was found to be 2.56×10^{15} (1.25×10^{15}) and 2.40×10^{15} (1.64×10^{15}) in O and C – waters respectively. Although the PAR reaching at DCM almost equals in O and C – waters, the settlement of DCM in O – waters was much deeper as compared to C – waters (Fig. 3.2.1). This may be due to fact that the attenuation of light by OAS was much higher in C – waters as compared to O –

waters. Hence in order to understand the reason for migration of DCM and euphotic depth to deeper layer in O – waters it is mandatory to analyze the constituents prevailing in the water column responsible for attenuation of light within the water column. This could be achieved by understanding IOP and AOP of OAS prevailing in the respective water column.

3.3 Inherent optical properties, apparent optical properties and water colour

The vertical variability of light at different wavelengths in visible part of EMR was quantified by computing k_d , over the euphotic depth, corresponding to wavelengths 412, 443 (blue), 490 (blue-green), 510, 555 (green) and 670 nm (red) (Table 3.3.1). The average values of k_d along with standard deviation for all the stations corresponding to O, C and E waters were presented here. The k_d (PAR) over euphotic depth in O, C and E – waters were also given in the table along with standard deviation.

	k_d (m^{-1})						k_d (PAR) (m^{-1})
	412 nm	443 nm	490 nm	510 nm	555 nm	670 nm	
O – waters	0.092	0.074	0.058	0.065	0.086	0.169	0.079
	± 0.016	± 0.011	± 0.008	± 0.008	± 0.007	± 0.028	± 0.009
C – waters	0.376	0.312	0.230	0.216	0.193	0.489	0.244
	± 0.097	± 0.094	± 0.073	± 0.063	± 0.042	± 0.103	± 0.055
E – waters	2.029	1.720	1.342	1.268	1.066	1.269	2.905
	± 0.684	± 0.537	± 0.417	± 0.391	± 0.328	± 0.266	± 0.410

Table 3.3.1

Mean and standard deviation of downwelling diffuse attenuation coefficient at wavelengths 412, 443 (blue), 490 (blue-green), 510, 555 (green) and 670 (red) nm and diffuse attenuation coefficient of PAR (k_d (PAR)) in open ocean (O), coastal (C) and estuarine (E) waters.

In the view of remote sensing of ocean colour, k_d plays a significant role in determining the satellite penetration depth. Around 90 % of the diffuse reflected light from water body comes from a surface layer of water depth k_d^{-1} (Mishra et al., 2005). The k_d values exhibit a large difference between O, C and E – waters. The magnitude shows that in O – waters, k_d was ten times smaller than C – waters which was further ten times smaller than E – waters. The spectral variability depicts that k_d was least (0.058 ± 0.0084) in blue and maximum (0.1690 ± 0.0283) in red in O – waters. The result was similar to the findings of Belzile et al. (2004) for the studies carried out at 19 stations across the 620 km² oligotrophic lake Taupo in New Zealand. In C – waters, k_d was found to be minimum (0.2164 ± 0.0631) in green and maximum in blue and red with the respective values of 0.3762 ± 0.097 and 0.4886 ± 0.1029 . In their studies Mishra et al. (2005) obtained increased light attenuation from blue to red with a part of green showing lower k_d value which was due to high chlorophyll_a concentration. Further, they also documented a sharp increase in k_d from 560 to 700 nm, with values at blue green and red part of EMR as 0.138, 0.158 and 0.503 m⁻¹ respectively, for study carried out in coastal stations. In E – waters, minimum (1.2694 ± 0.2665) k_d was encountered in red and maximum (2.0292 ± 0.6842) in blue part of EMR. This concludes that in O – waters, blue-green (490 nm) light penetrates to a deeper depth compared to that in C – waters which explains the shift in DCM from shallow to deeper depths between C and O – waters. The k_d (PAR) also showed a large variability between different optical domains. The values depicted ten fold increase from O to C waters and further 10 fold increase from C to E waters. Through numerical modeling, Ross et al. (1994) identified the level of PAR as a factor most likely to determine the time of bloom and primary production.

The availability of light at different levels and settlement of DCM has been explained on the basis of relationship developed between downwelling diffuse attenuation coefficient at 490 nm ($k_d(490)$) and DCM using 52 data points from O, C and E – waters (Fig. 3.3.1a). The coefficient of regression was found to be 0.94. The figure shows an exponential relationship between DCM and $k_d(490)$. Therefore, from the equation [$DCM = 3.2741 k_d(490)^{-0.8874}$], it was evident that for $k_d(490)$ less than 0.1, DCM settles to a depth greater than 25 m. Further, a relationship was developed between $k_d(PAR)$ and $k_d(490)$ using 65 data points having a regression coefficient of 0.98 (Fig. 3.3.1b). Hence using this relationship [$k_d(PAR) = 0.8891 k_d(490) + 0.0338$] $k_d(PAR)$ could easily be computed from $k_d(490)$.

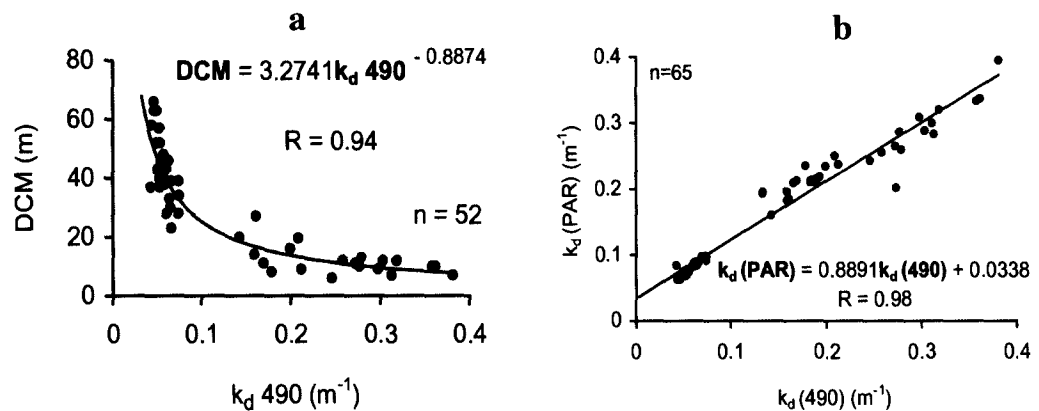


Fig. 3.3.1

Regression between a) DCM and downwelling diffuse attenuation coefficient (k_d) at 490 nm and b) downwelling attenuation coefficient of PAR ($k_d(PAR)$) and downwelling diffuse attenuation coefficient (k_d) at 490 nm

The variability of k_d clearly illustrates the differential pattern of attenuation with respect to wavelength and optical environment. But k_d gives the vertical variation of attenuation, which is the combined contribution of both absorption and scattering (Kirk, 1994). Therefore, in order to trace the spectral signatures of the light emerging out of the water column, it is necessary to analyze the spectral patterns of

remote sensing reflectance which results due to IOP such as absorption and backscattering (Babin et al., 2003).

The R_{rs} is a function of 'a' and 'b_b'. Zaneveld (1982) used an analytical approach based on a radiative transfer equation to relate the IOP and AOP such as 'a', 'b_b' to R_{rs} . Hence the components defining R_{rs} includes 'a' and 'b_b'. Therefore, at first instance, the spectral variation of 'a' and 'b_b' derived through AOP have been analyzed.

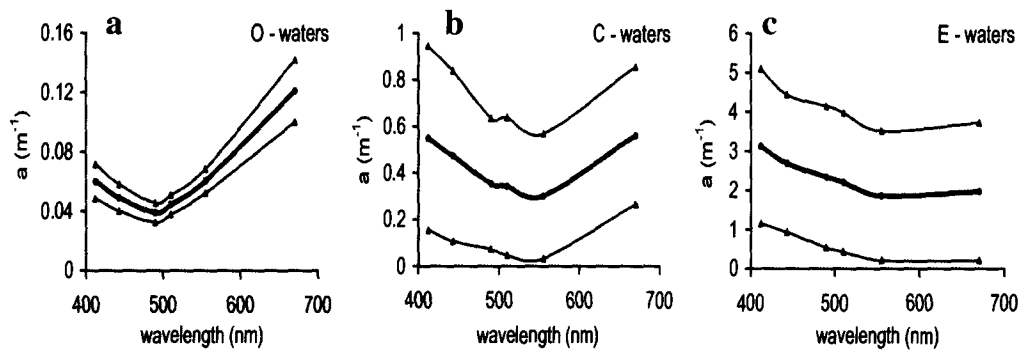


Fig. 3.3.2

Spectral variation of total absorption coefficient (a) corresponding to stations in open ocean (O), coastal (C) and estuarine (E) waters. The thick line indicates the mean and the thin line above and below the thick lines indicates the standard deviation.

The spectral variation of total 'a' is given in fig 3.3.2 and 3.3.3 gives the spectral total 'b_b'. The spectra presents clear inter and intra regional differences. In O – waters, absorption coefficient showed a fairly uniform pattern from 412 nm to a 490 nm after which it increased drastically up to 670 nm. Hence it was observed that absorption was minimum in blue and maximum in red part of EMR. The scenario was different in C – waters where the absorption coefficient decreased from 412 nm to attained minimum absorption at 555 nm after which it showed an increase towards longer wavelength to a maximum at 670 nm. The absorption coefficient in E – waters

showed a completely different pattern. Here the absorption coefficient was found to be decreasing from 412 nm to around 555 nm after which the absorption was almost uniform in longer wavelength (670 nm).

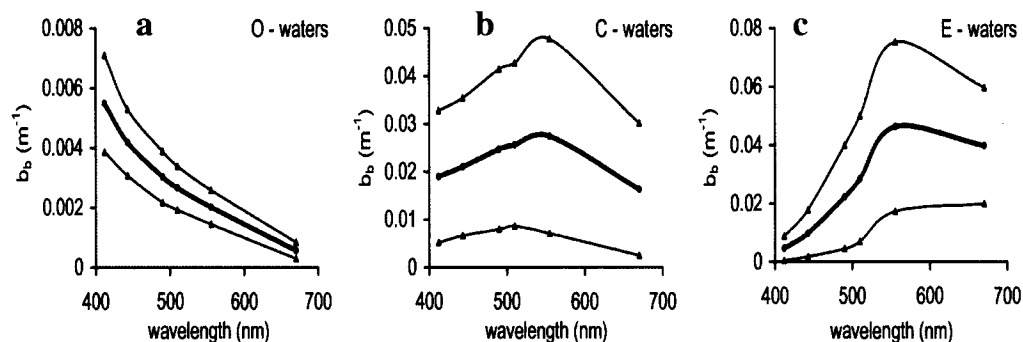


Fig. 3.3.3

Spectral variation of total backscattering coefficient (b_b) corresponding to stations in open ocean (O), coastal (C) and estuarine (E) waters. The thick line indicates the mean and the thin line above and below the thick lines indicates the standard deviation.

In O – waters the range of concentration of chlorophyll_a, TISM and CDOM were 0.16 – 0.67 $\mu\text{g}\cdot\text{l}^{-1}$, 3.08 – 6.20 $\text{mg}\cdot\text{l}^{-1}$ and 0.8 – 1.2 m^{-1} respectively. In C – waters chlorophyll_a varied between 0.1 – 4.2 $\mu\text{g}\cdot\text{l}^{-1}$, TISM 1.23 – 16 $\text{mg}\cdot\text{l}^{-1}$ and CDOM 1.2 – 21.9 m^{-1} . In E – waters chlorophyll_a varied between 1.0 – 22.1 $\mu\text{g}\cdot\text{l}^{-1}$, TISM 5 – 33 $\text{mg}\cdot\text{l}^{-1}$ and CDOM 2.12 – 6.2 m^{-1} . The resultant absorption spectra in O – waters were chiefly due to water molecule. A gentle effect of CDOM could also be observed at the shorter wavelength from 400 to 500 nm. In C – waters, absorption spectrum was due to the combine effect of chlorophyll_a and CDOM. The absorption at blue band was due to chlorophyll_a and CDOM, whereas in red band it was only due to chlorophyll_a. Green and Sosik (2004) reported that in shelf waters, dominated by chlorophyll_a and CDOM, the absorption spectrum showed minimum in green. Further, in E – waters the absorption spectrum was found to be a function of CDOM

and TISM with TISM having more weightage (Doxaran et al., 2006). Similar results were obtained by Belzile et al. (2000) in turbid water dominated by suspended sediment.

The total backscattering coefficient (b_b) showed an inverse relationship to that of absorption coefficient (Fig. 3.3.3). In O – waters, the spectral variation of b_b was such that it decreases exponentially from shorter to longer wavelength inferring maximum backscattering in blue and minimum in red band of EMR. This confirms the dominance of water molecules in O – waters. The C – waters depicted a gradual increase in b_b from 412 to 55 nm, which further decreases towards longer wavelength at 670 nm. This indicated that b_b was minimum in blue and red and maximum in green part of EMR. As CDOM doesn't scatter (Kowalczyk et al., 2005), b_b was totally dominated by chlorophyll_a. The b_b in E – waters showed an increase from 412 to 555 nm after which it attained a uniform pattern up to 670 nm. This showed that in E – waters red light backscatters maximum whereas blue light minimum. The suspended sediment concentration was much higher in this water which absorbs strongly at shorter wavelength and dominates b_b at longer wavelength (Gallie and Murtha, 1992).

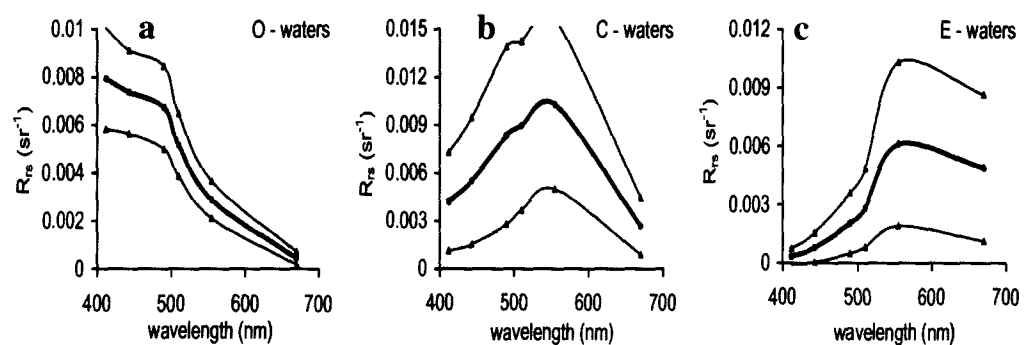


Fig. 3.3.4

Spectral variation of remote sensing reflectance (R_{rs}) corresponding to stations in open ocean (O), coastal (C) and estuarine (E) waters. The thick line indicates the mean and the thin line above and below the thick lines indicates the standard deviation.

The spectral R_{rs} is of prime importance as far as ocean colour remote sensing is concerned. R_{rs} showed one-to-one correspondence with b_b (Fig. 3.3.4). In O – waters spectral signatures of R_{rs} showed a fairly uniform pattern from 412 to 490 nm with a slight decrease followed by a drastic decrease from 490 to 670 nm. R_{rs} was found to be negligible at longer wavelengths. The maximum reflectance in blue region points towards the fact that this water appeared blue in colour. In C - waters, R_{rs} attained maxima at 555 nm (green) with minimum in blue and red region. This indicates that the maximum energy reaching at optical sensor was in green band of EMR and hence the ocean colour. In an area dominated by chlorophyll_a and CDOM, R_{rs} peaks in green band giving greenish to yellow appearance to the water column (Darecki et al., 2003; Green and Sosik, 2004). In E – waters, the spectral variation of R_{rs} was such that it has minimum reflectance at 412 nm which increases gradually to 555 nm after which the variation was almost uniform up to 670 nm. This demonstrated that the peak energy emerging out of the water column was from yellow to red band of EMR making the water highly optically complex and giving yellow to red colour to the water column. The peak in the longer wavelength was an indication of dominance of suspended sediment in an area. Despite the absorption by chlorophyll_a and CDOM, Suspended sediment absorbs strongly at shorter wavelength and its backscattering dominated at longer wavelength resulting in spectral signatures in longer wavelength (Doxaran et al., 2002, 2003). Froidefond et al. (2002) identified four different types of R_{rs} spectra for the studies carried out at French Guiana coast. The first characterizing clear blue waters where R_{rs} are typically high in blue. The second pattern was seen at the continental shelf where R_{rs} was low especially in blue domain resulting due to intrusion of CDOM from Amazonia waters. The third in green waters close to coast where maximum R_{rs} was seen at about 570

nm and fourth in the mouth of the Mahury River where sediment concentration was very high. Here the spectral R_{rs} was low in blue and green and increased towards red end of the spectra.

The analysis of R_{rs} clearly illustrated the variability of ocean colour in different optical domains. Hence, in order to understand the contribution of a and b_b to total attenuation of light within the water column and its effect on the energy coming out of the water column, scatter plots of a and $a + b_b$ against k_d were generated in O, C and E – waters. The slope of the curves μ_a (a v/s k_d) and μ_b ($a + b_b$ v/s k_d) depends mainly on the ambient light field and gives the rate at which light diffuses with depth (Gordon, 1989; Darecki et al., 2003).

Wavelength (nm)	O – water		C – waters		E – waters	
	a v/s k_d	a + b_b v/s k_d	a v/s k_d	a + b_b v/s k_d	a v/s k_d	a + b_b v/s k_d
412	0.62	0.67	0.69	0.73	0.81	0.88
443	0.62	0.67	0.68	0.73	0.80	0.87
490	0.62	0.67	0.69	0.75	0.81	0.88
510	0.63	0.67	0.68	0.74	0.83	0.93
555	0.65	0.67	0.67	0.73	0.83	0.97
670	0.67	0.68	0.70	0.71	0.81	0.96
Mean (r)	0.81	0.8	0.78	0.80	0.96	0.91

Table 3.3.2

Slope of the scatter plot of a v/s k_d and $a + b_b$ v/s k_d at 412, 443, 490, 510, 555 and 670 nm in open ocean (O), coastal (C) and estuarine (E) waters. The mean coefficient of regression (r) is given in the bottom row.

The slope of the scatter plot μ_a and μ_b at 412, 443, 490, 510, 555 and 670 nm in O, C and E – waters is given in table 3.3.2. The average coefficient of regression was also given. On the analysis of numeric values of slopes from the table it was clear that μ_a ranges from 0.62 to 0.67 in O – waters, 0.68 to 0.7 in C – waters and 0.80 to 0.83 in E – waters. In their studies, Derecki et al. (2003) reported μ_a values between

0.68 and 0.70 for the studies carried out in Irish Shelf and Baltic Sea. They documented typical values of 0.8 under diffuse light condition. They also reported that μ_a has a little spectral dependence also largely depends on absorption coefficient. Further, the difference between μ_a and μ_b in O – waters and increases to C and E – waters. The difference between the two slopes is the indication whether the media was absorbing or scattering. As b_b approaches zero, the difference between the two slopes also approaches to a minimum value (Derecki et al., 2003).

In general it was observed that, in all three optical domains, absorption dominates the backscattering in determining attenuation. In an area dominated by chlorophyll_a and CDOM, k_d is mainly determined by absorption (Derecki et al., 2003; Green and Sosik, 2004). The backscattering was found to be increasing from O to E – waters with intermediate in C – waters. Looking at the spectral dependence, in O – waters, μ_a depicted lesser values at the shorter wavelengths. This confirms O – waters as a typical case I water with the dominance of water molecule on reflection spectra. Also the difference in slopes clearly indicates negligible b_b and most of which contributing at the shorter wavelength.

The C – waters were also found to be an absorbing media with absorption contributing to attenuation. The larger μ_a were found to be in blue and red part of EMR. Also the difference between the slopes showed that b_b contributing less than 'a' to total attenuation and most of it at green band (510 and 555 nm). This further confirms the presence of CDOM in high concentration along with chlorophyll_a in C – waters wherein the absorption at shorter wavelengths was maximum. And the increase in backscattering at green band was due to presence of chlorophyll_a (D'sa and Miller, 2003).

The difference in the slope of both the plots in E – waters illustrated the increase in b_b as compared to that of O and C – waters. Although there was a significant contribution of b_b to k_d , this waters still serve as an absorbing media. The increase in b_b at longer wavelength clearly indicates the dominance of suspended sediment in E – waters. As suspended sediment also absorbs significantly at shorter wavelength, the major contributor to the k_d was a, but b_b also contributed significantly to total k_d .

To understand the contribution of each OAS to the total absorption spectra it is necessary to analyze the absorption spectra of each OAS separately. This could be achieved by generation of spectra through water sample analysis.

Chapter 4

Bio – optical properties through water sample analysis

4.1	Generation of optical properties-----	(36)
4.2	Optically active substances in different optical domains-----	(39)
4.3	Interaction of downwelling irradiance with optically active substances-----	(41)
4.4	Inherent optical properties in different optical domains-----	(43)
	4.4.1 Spectral variability of specific absorption coefficient of chlorophyll_a--	(44)
	4.4.2 Spectral variability of specific absorption coefficient of total inorganic suspended matter -----	(48)
	4.4.3 Spectral variability of specific absorption coefficient of coloured dissolved organic matter-----	(52)
4.5	Spatial variability of optically active substances in different optical domains-	(54)
4.6	Sources and sinks of optically active substances in different optical domains-	(58)

The OAS in the natural environment can be classified into dissolved and particulate. The matter that passes through a filter paper of 0.2 μm is termed as dissolved (Blough and Del Vecchio, 2002) whereas that retained on 0.45 μm filter paper is called as particulate. The optically active constituent of the dissolved fraction mainly consists of fulvic and humic acid and is referred to as CDOM (Coble, 1996). The composition of suspended matter is very complex and can be divided into organic and inorganic. The organic fraction includes phytoplankton containing chlorophyll_a, its major fraction, and its accessory pigments. The inorganic component includes sediment and all non-living particles. Apart from these, water molecules also produce a considerable amount of absorption and scattering. Remote sensing accounts for reflection, refraction and diffraction of the energy received from the sun. The reflection mainly occurs at the air-sea boundaries and within the water column. The subsurface reflectance ($R(\lambda)$) is the information carrier as far as ocean colour remote sensing is concerned. The accurate assessment of ocean colour analysis can be achieved only by understanding the effect of each OAS on signals emerging out of the water column. The procedure of retrieving OAS from an optical sensor is very simple in case I waters. The difficulties lay in case II waters. In case II waters the signals from different OAS overlap each other. Hence the radiometer, with six discrete channels and a large bandwidth, does not suffice the need for understanding the effect of OAS on optical properties. For a better understanding of the optical complexity of the case II waters, it is necessary to generate high resolution optical properties of each OAS. This can be achieved by using a hyperspectral radiometer or by generating hyperspectral reflectance ($R(\lambda, 0)$) through water sample analysis. In the present study, inherent optical properties of phytoplankton pigment, chlorophyll_a,

TISM and CDOM were generated for every 1 nm (between 400-700 nm). Subsequently using hyperspectral IOP, the reflectance has been computed. The present chapter deals with the spectral and spatial variability of OAS in different optical domains viz. open ocean, coastal and estuarine waters.

4.1 Generation of optical properties

In order to analyze the OAS such as chlorophyll_a, TISM and CDOM, water samples were collected using Niskin sampler from a depth just below the surface.

For the estimation of chlorophyll_a, water samples were filtered onboard through Whatman GF/C filter paper. 1 ml of saturated MgCO₃ was spread on the filter paper at the end of filtration to avoid any bacterial degradation. The filter paper was then crushed, soaked in 90% acetone and kept in dark at low temperature for 20 - 24 hrs for the pigment to get extracted. The extract was then centrifuged at 3000 r.p.m. for 10 to 15 min. The sample optical density (OD) was then measured through Perkin Elmer Lambda 35 UV/VIS spectrophotometer using 1 cm cell, in the spectral range 400 to 700 nm with an interval of 1 nm against the cell containing 90% acetone as blank (Strickland and Parson, 1972). The OD at 750 nm was subtracted from the entire spectrum and converted to absorbance unit as,

$$a_c(\lambda) = 2.303 OD_c(\lambda) 100 \quad [m^{-1}] \quad \text{----- (4.1.1)}$$

Chlorophyll_a specific absorption coefficient (a^*_c) was estimated for the spectral range 400 to 700 nm using the measured chlorophyll_a concentration (C_c) in $\mu g-l^{-1}$ (Strickland and Parson, 1972) and the spectral absorption coefficient as per Mobley (1994).

$$a^*_c(\lambda) = 0.06 * C_c^{0.62} * a_c(\lambda) \quad [m^2 \cdot mg^{-1}] \quad \text{----- (4.1.2)}$$

The scattering coefficients of chlorophyll_a were then calculated over the spectral range 400 – 700 nm as per Gordon and Morel (1983).

$$b_c(\lambda) = 0.3 C_c^{0.62} (550/\lambda) \quad [m^{-1}] \quad \text{----- (4.1.3)}$$

Absorption coefficient due to CDOM was estimated spectrophotometrically by the methodology suggested by Kowalczyk and Kaczmark (1996). Water samples were filtered onboard through 0.2 μ m Sartorius cellulose membrane filters. 0.4 ml of 0.5 M HgCl₂ was added to 200 ml of sample to avoid any bacterial degradation. The sample was then preserved at low temperature until analysis in the laboratory. The sample transparency was measured using Perkin Elmer Lambda 35 UV/VIS spectrophotometer over the same spectral range 400 to 700 nm with an interval of 1 nm against distilled water as blank.

The spectral absorption coefficient of CDOM was calculated by normalizing with respect to 440 nm (Kowalczyk and Kaczmark, 1996). These have been done as chlorophyll_a has a primary absorption at 440 nm. (Carder et al., 1989; Bowers et al., 2000).

$$a_{CDOM}(\lambda) = a_{CDOM}(440) \exp [-s(\lambda - 440)] \quad [m^{-1}] \quad \text{-----(4.1.4)}$$

Where, $a_{CDOM}(440)$ is the absorption measured at 440 nm and s is the slope coefficient which was calculated as the slope of the curve resulted by plotting logarithm of a_{CDOM} against wavelength (λ). The magnitude of $a_{CDOM}(440)$ gives the concentration while the

spectral slope (s) indicates its composition (Stedmon and Markager, 2003). The absorption coefficients were then corrected for backscattering of small particles and colloids, which pass through filters (Green and Blough, 1994).

$$a_{\text{CDOM_corr}}(\lambda) = a_{\text{CDOM}}(\lambda) - a_{\text{CDOM}}(700) * (\lambda/700) \quad [\text{m}^{-1}] \quad \text{----- (4.1.5)}$$

To determine the absorption coefficient due to TISM, water samples were filtered through pre-weighted 0.45 μm membrane filter paper. The filter paper was dried in a hot air oven at 70°C for 20 min and weighed again. The residue on the filter paper was then added to 10 ml distilled water and OD was measured over wavelength range 400 – 700 nm with an interval of 1 nm. Specific absorption coefficients due to TISM were calculated through the following equation (Menon et al., 2005)

$$a^*_s(\lambda) = a_s(\lambda) / C_s \quad [\text{m}^2\text{-g}^{-1}] \quad \text{----- (4.1.6)}$$

Where $a_s(\lambda)$ is the absorption coefficient due to TISM and C_s is concentration in mg-l^{-1} .

The scattering coefficient of TISM (b_s) can be expressed as (Morel, 1988)

$$b_s(\lambda) = b_s(550) C_s (550/\lambda) \quad [\text{m}^{-1}] \quad \text{----- (4.1.7)}$$

Subsequently the hyperspectral subsurface reflectance ($R(\lambda)$) was computed using a two-flow bio-optical model (Doerffer, 1992).

$$R(\lambda) = [k_u(\lambda) - a(\lambda)] / [k_u(\lambda) + a(\lambda)] \quad \text{----- (4.1.8)}$$

The total upwelling diffuse attenuation coefficient ($k_u(\lambda)$) was computed as per Menon (2004)

$$k_u(\lambda) = [a(\lambda) + b(\lambda)] / \cos \theta_v \quad [m^{-1}] \quad \text{----- (4.1.9)}$$

Where, $a(\lambda)$ is total absorption and $b(\lambda)$ is total scattering coefficient and θ_v is satellite zenith angle. $a(\lambda)$, $b(\lambda)$ and $k_u(\lambda)$ were then fractionized with respect to OAS as per Doerffer (1992).

$$k_u(\lambda) = k_{uw}(\lambda) + k_u^*c(\lambda) C_c + k_u^*s(\lambda) C_s(\lambda) + k_u^*CDOM(\lambda) C_{CDOM} \quad [m^{-1}] \quad \text{----- (4.1.10)}$$

$$a(\lambda) = a_w(\lambda) + a^*c(\lambda) C_c + a^*s(\lambda) C_s(\lambda) + a^*CDOM(\lambda) C_{CDOM} \quad [m^{-1}] \quad \text{----- (4.1.11)}$$

$$b(\lambda) = b_w(\lambda) + b^*c(\lambda) C_c + b^*s(\lambda) C_s(\lambda) \quad [m^{-1}] \quad \text{----- (4.1.12)}$$

The subscript w, c, s and CDOM refer to water molecule, chlorophyll_a, TISM and CDOM substance respectively. The absorption coefficients for pure water molecules were taken from Pope and Fry (1997) and scattering coefficient were taken from Morel (1974).

4.2 Optically active substances in different optical domains

Adopting the methodology, as mentioned above, the absorption coefficients of each OAS were derived for the samples collected from O, C and E – waters. Spectral absorption coefficient of each OAS at a selected station from O, C and E – waters were given in fig 4.2.1.

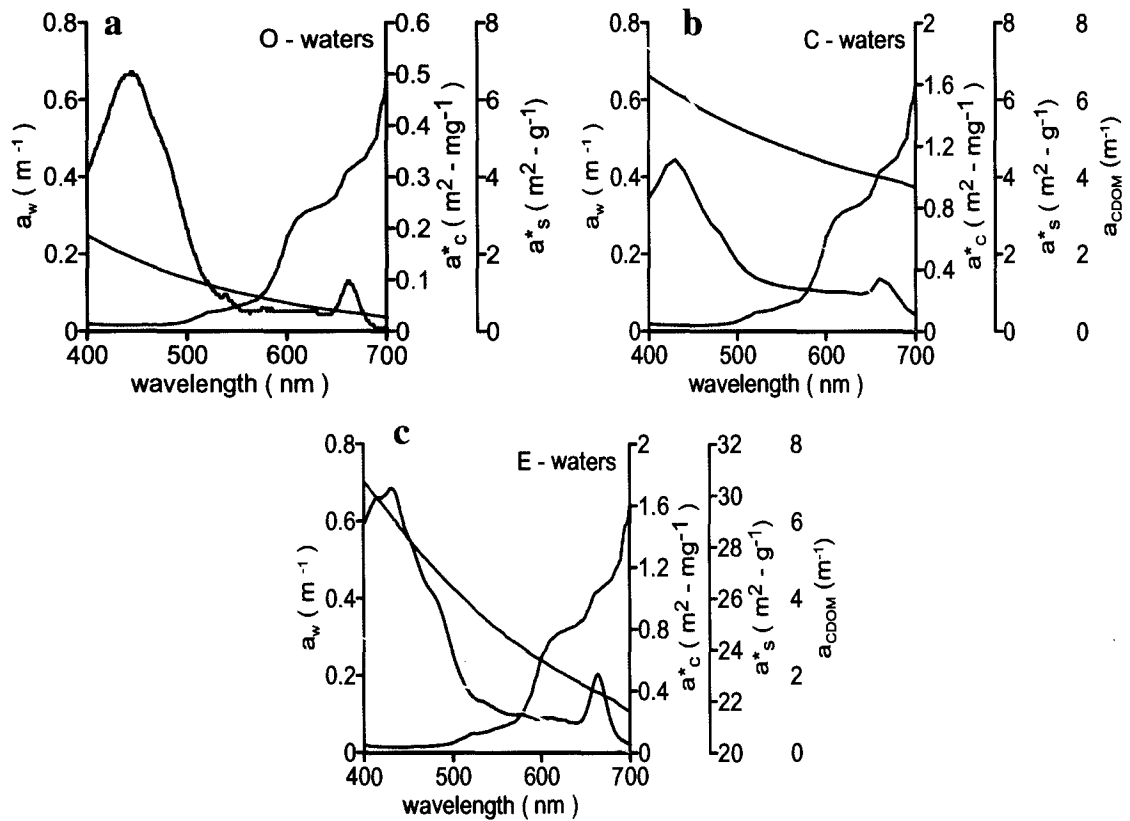


Fig. 4.2.1

Spectral variability of absorption coefficient due to pure water (a_w), specific absorption coefficient due to chlorophyll_a (a^*_c), TISM (a^*_s) and absorption coefficient due to a_{CDOM} at a selected stations from open ocean (O), coastal (C) and estuarine (E) waters.

The spectral variation of absorption coefficient due to water molecule (a_w) was very small and almost uniform at the shorter wavelength and exhibits an increasing trend from 500 nm onwards. The specific absorption due to chlorophyll_a (a^*_c) showed a bimodal distribution. The primary peak was seen at blue whereas the secondary peak was observed at red part of EMR. A very small and almost uniform values of a^*_c exhibited along the green part of the spectrum. The specific absorption coefficient due to TISM and CDOM showed an exponentially decreasing trend with higher value in blue and lower value in red part of EMR.

The competition for light in different optical domains by OAS was clearly indicated in fig 4.2.1. In O – waters chlorophyll_a along with water molecule dominates total absorption spectra. TISM also contributes to the total absorption spectra but its contribution was not significant. C and E – waters were typical case II waters. Here the contribution of TISM and CDOM were significant along with chlorophyll_a. Hence it was observed that, in case II waters, energy at shorter wavelength was utilized by all the three OAS. The relative contribution of OAS in absorbing the light reaching the water column has been discussed in subsequent section.

4.3 Interaction of downwelling irradiance with optically active substances

The amount of light absorbed by prevailing OAS was quantified by forcing the normalized absorption coefficient to downwelling irradiance reaching the sampling depth. The downwelling irradiance just above the sea surface ($E_d(\lambda, 0^+)$) was measured by SMSR and just below the sea surface ($E_d(\lambda, 0^-)$) was calculated as per Magnuson et al. (2004).

$$E_d(\lambda, 0^-) = 0.98 E_d(\lambda, 0^+) \quad \text{----- (4.3.1)}$$

The irradiance at the sampling depth was computed as per Beer - Lambert law which states that intensity of light decreases exponentially as a function of depth in the water column and is described mathematically as

$$E_d(\lambda, z) = E_d(\lambda, 0^-) * e^{-k_d(\lambda) * z} \quad \text{----- (4.3.2)}$$

Where $k_d(\lambda)$ is the downwelling diffuse attenuation coefficient for waters of different optical domains and the respective values were discussed in the previous chapter. To get

the amount of light absorbed by each OAS, $E_d(\lambda, z)$ at different stations were multiplied by normalized absorption due to each OAS. For example the normalized absorption coefficient of chlorophyll_a is as follows.

$$a_c(\text{nor}) = a_c / (a_w + a_c + a_s + a_{\text{CDOM}}) \quad \text{----- (4.3.3)}$$

Where a_w , a_c , a_s and a_{CDOM} were absorption due to water molecules, chlorophyll_a, TISM and CDOM respectively. The values of a_w were taken from Pope and Fry (1997).

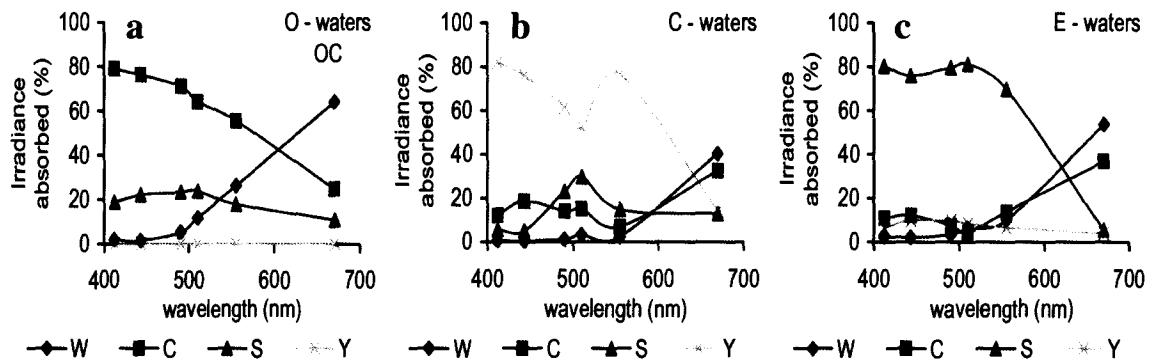


Fig. 4.3.1

Spectral variability of percent irradiance, entering the water column, absorbed by pure water (W), chlorophyll_a (C), TISM (S) and CDOM (Y) in a) open ocean (O), b) coastal (C) and c) estuarine (E) waters.

The OAS in the water column absorbs a considerable amount of light reaching at that depth. Fig. 4.3.1 demonstrates the average percentage of irradiance absorbed by each OAS out of the total irradiance absorbed in O, C and E – waters. From the figure it is clear that different OAS dominated different optical domains. In O – waters, most of the irradiance were absorbed by chlorophyll_a in blue and green region. The chlorophyll_a absorbs 70 – 80 % in blue, 58 – 70 % in green and 20 – 30 % in red region of EMR. The contribution from TISM was in the range of 15 – 22 % over the entire spectrum. CDOM

has no significant contribution in the absorption of irradiance in O – waters. At longer wavelength, in red part of EMR, water molecules override chlorophyll_a. About 60 – 70 % of the irradiance was absorbed by water molecules at longer wavelength.

In C – waters CDOM dominates the absorption at the shorter wavelengths. The total absorption by CDOM was 82 % at 412 nm which decreases to 57 % at 510 nm. At this point, TISM absorption was increased to 30 %. The absorption by CDOM was increased again to 72 % at 555 nm. The contribution from CDOM was only 18 % at 670 nm in the red region of EMR. In the red region chlorophyll_a has a significant contribution of 37 % along with water molecules. The water molecules absorb 42 % of the irradiance at 670 nm.

The E – waters were completely dominated by TISM. TISM absorbs 70 – 80 % of the irradiance in blue and green part of EMR. As seen in the previous case, the chlorophyll_a and water molecules dominate the absorption in the longer wavelength. This indicated that CDOM has no contribution towards absorption in the red part of EMR. In all the three cases chlorophyll_a absorbs around 40 % of the irradiance in red part of EMR.

4.4 Inherent optical properties in different optical domains

The composition of OAS, responsible for complex optical environment, can be inferred from the spectral variability of IOP (Chang and Dickey, 2001; Gallegos and Neale, 2002). In the view of development of algorithm, for the retrieval of OAS, the knowledge of spectral variation of IOP and spatial distribution of OAS were all the more important. Hence in the present study, complexity in O, C and E – waters have been

studied using the spectral variability of IOP and spatial variability of OAS present in the environment. The variability of the absorption coefficient in case I waters has been thoroughly documented over the last decades. In such waters, all components often covary with chlorophyll_a concentration (Morel and Prieur, 1977; Prieur and Sathyendranath, 1981). But in coastal and inland (case II) waters OAS do not covary with chlorophyll_a concentration. In such waters, variations in the shape and magnitude of the spectrum are poorly documented.

The estuaries are optically complex systems due to mixing of land derived freshwater and tidally forced sea water (Qasim, 2003). Therefore to have a better understanding of this optical complexity, the estuarine environment was divided into three zones, namely upper (head), middle and lower (mouth). The zonation was based on the variations in its optical properties, hydrographic features and geomorphology. The surface area of upper estuary was too small to resolve by OCM. Further, due to the cloud cover, no satellite information was available during monsoon. Therefore the spectral variability of OAS in the upper zone and that during monsoon was not presented in the thesis.

4.4.1. Spectral variability of specific absorption coefficient of chlorophyll_a

4.4.1.1. Open ocean waters

The spectral variability of mean specific absorption coefficient of chlorophyll_a (a^*_c) in O – waters was given in fig. 4.4.1.1. The mean spectra showed two distinct peaks. The primary peak was in blue (434 nm) where as the secondary peak was in the red part (665 nm) of EMR. Also a steep increase was observed from 400 to 430 nm. The

variations in the magnitude of the spectra were analyzed through the standard deviation. The maximum deviation was observed in the blue region (400 – 500 nm) whereas the deviation was uniform in green and red part of EMR.

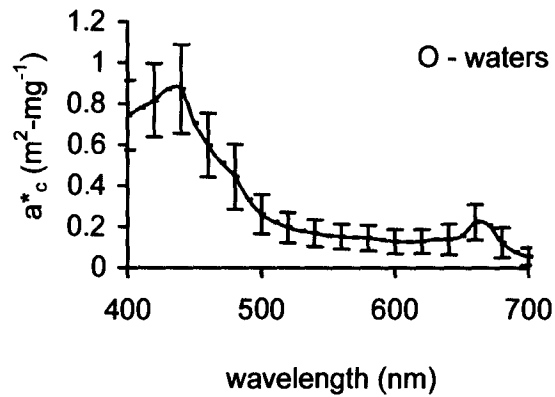


Fig. 4.4.1.1

Spectral variability of mean specific absorption coefficient due to chlorophyll (a^*_c) in open ocean (O) waters. The vertical bars indicate the standard deviation.

4.4.1.2. Coastal waters

The spectral variation of a^*_c in the C – waters (Fig. 4.4.1.2) was similar to that in the O – waters. Unlike O – waters, the primary peak was at 430 nm and the secondary at 662 nm. Increase from 400 nm to first absorption peak was gradual. The maximum variation in the magnitude was in the blue (400 to 500 nm) region. The red region from 640 to 680 nm was also found to have a significant deviation. The variations in the magnitude in green band were seen to be fairly uniform. The variability in a^*_c was more in the C – waters as compared to that in O – waters.

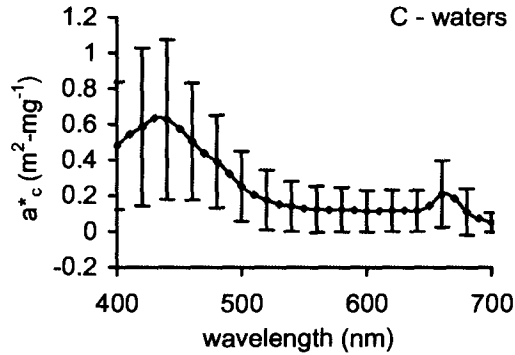


Fig. 4.4.1.2

Spectral variability of mean specific absorption coefficient due to chlorophyll (a^*_c) in coastal (C) waters. The vertical bars indicate the standard deviation.

4.4.1.3. Estuarine waters

The spectra of a^*_c in E – waters have a similar shape in all the zones and in all seasons (Fig. 4.4.1.3). There was no spatial and temporal variability in the mean shape of the spectra in E – waters. In this water, the primary peak was observed at 438 nm whereas the secondary peak was at 670 nm. The shape of the spectra was more distinct as that in O and C – waters. The a^*_c increased gradually from 400 to 420 nm and thereafter, a steep increase was seen till the primary peak. Subsequently a steep decrease was observed from primary peak till 460 nm. Beyond 460 nm, a^*_c , decreased gradually till 480 nm and further a steep decrease was observed till 510 nm. The magnitude of a^*_c from 510 to 640 nm was very close to zero. A large variability was encountered in the magnitude of a^*_c both spatially as well as temporally. The maximum variations were seen in the blue (400 to 500 nm) part of EMR in all the cases.

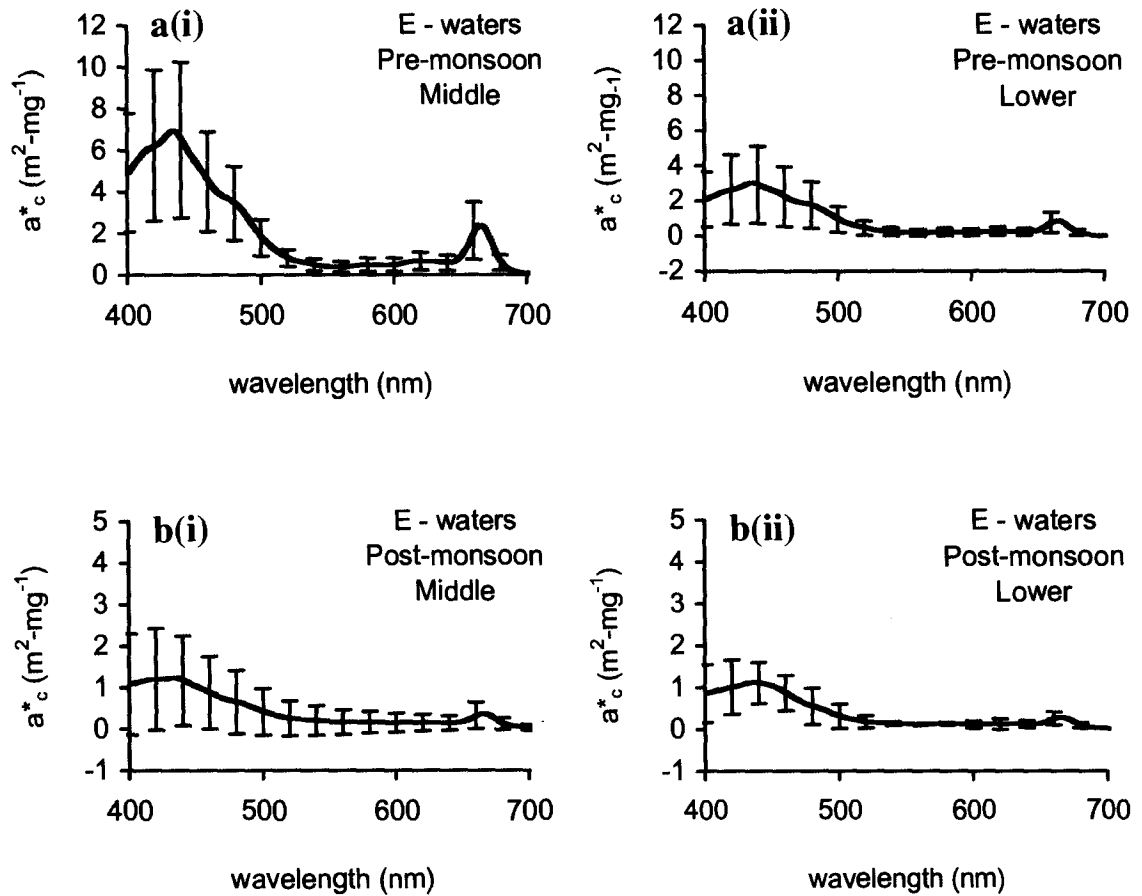


Fig. 4.4.1.3

Spectral variability of mean specific absorption coefficient due to chlorophyll_a (a^*_c) in estuarine (E) waters during (a) pre-monsoon in (i) middle and (ii) lower estuary and (b) post-monsoon in (i) middle and lower estuary. The vertical bars indicate the standard deviation.

The variability in the spectral shape of absorption coefficients were probably related to the phytoplankton species prevailing in the ambient waters. The variability in the absorption coefficient in blue region is primarily due to the influence of accessory pigments, or plant pigments other than chlorophyll_a that capture photons of light for photosynthesis. Hence the variations in blue may result from the combined influences of package effect from the total cellular pigment content as well as the pigment composition of the cell (Bricaud et al., 1995; Fujiki and Taguchi, 2002; Ciotti et al., 2002). In their

studies Suzuki et al. (1998) examined the variety in shape and magnitude of the in vivo chlorophyll_a specific absorption spectra of phytoplankton in relation to differences in pigment composition in the northwestern Pacific (off Sanriku). They concluded that the absorption and pigments of phytoplankton are characteristic of each water mass of the study area. This result strongly supports that oceanic waters should be partitioned based on the regional absorption characteristics and such features could be used to improve remote-sensing algorithms for the area. Sathyendranath et al. (2005) studied general trend between phytoplankton community composition with chlorophyll_a concentration using data on optical properties and phytoplankton communities from 1,600 samples of marine phytoplankton collected from different areas and its implications for remote sensing of ocean colour. The specific absorption coefficient due to chlorophyll_a was found to vary inversely with cell size. The seasonal distribution of phytoplankton in the Mandovi - Zuari estuarine system from November 1979 to October 1980 was described by Devassy and Goes (1988). Of the 82 species of phytoplankton recorded, diatoms (63 species) showed an overwhelming predominance over dinoflagellates (14 species), blue-green algae (three species) and green algae (two species).

4.4.2. Spectral variability of specific absorption coefficient of total inorganic suspended matter

The TISM in the water column are excellent at reflecting light and depicts well in visible band of satellite sensors. In order to make quantitative estimates of the particle concentration and its effect on the penetration of sunlight into the sea, it is necessary to know how the absorption, scattering and backscattering coefficients of these inorganic

particles change with concentration, the nature of the particles, and with wavelength (Bowers and Binding, 2006). The colour ratios (the ratio of two reflection coefficients) are less sensitive to variations in scattering (Bowers and Binding, 2006) which controls the brightness and more sensitive to the absorption which controls the contrast of the water column.

4.4.2.1. Open ocean waters

The spectral variability in mean specific absorption coefficient of TISM (a^*_s) in O – waters were shown in Fig. 4.4.2.1. The general trends reflects exponential decrease of a^*_s with increasing wavelength. The concentration of TISM was considerably low in O – waters and the spectra of a^*_s also showed very less variability. The deviation was maximum in blue (400 – 500 nm) region of EMR. In red (600 to 700 nm) region of EMR the variability in a^*_s was negligible.

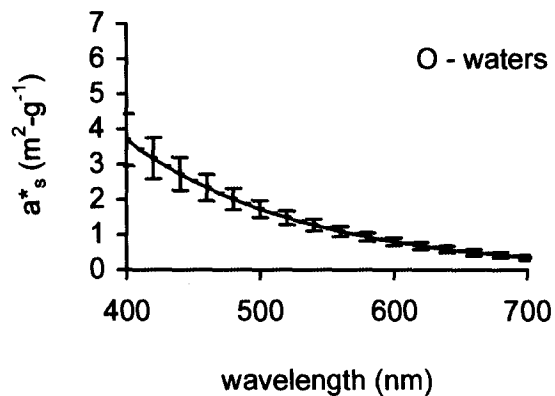


Fig. 4.4.2.1

Spectral variability of mean specific absorption coefficient due to TISM (a^*_s) in open ocean (O) waters. The vertical bars indicate the standard deviation.

4.4.2.2. Coastal waters

The spectral variation of mean a^*_s along with standard deviation is given in Fig. 4.4.2.2. The spectra of a^*_s , in C – waters, was very much distinct as compared to that in O – waters. In C – waters, spectral variation of a^*_s was almost independent of wavelength. The mean a^*_s varied between 0.8 (400 nm) to 0.7 $\text{m}^2\text{-g}^{-1}$ (700 nm). A large deviation, of the order 1.0 $\text{m}^2\text{-g}^{-1}$ was encountered throughout the spectra.

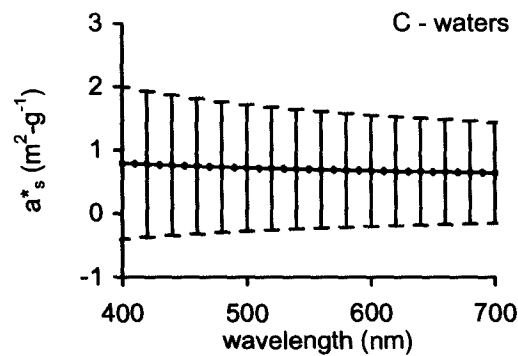


Fig. 4.4.2.2

**Spectral variability of mean specific absorption coefficient due to TISM (a^*_s) in coastal (C) waters.
The vertical bars indicate the standard deviation.**

4.4.2.3. Estuarine waters

In E – waters, during pre-monsoon, mean spectral variation of a^*_s was from 18 to 15 $\text{m}^2\text{-g}^{-1}$ in middle and 20 to 16 $\text{m}^2\text{-g}^{-1}$ in lower zone. Whereas during post-monsoon the variation was from 26 to 21 $\text{m}^2\text{-g}^{-1}$ in middle and from 23 to 17 $\text{m}^2\text{-g}^{-1}$ in the lower zone. A fairly uniform deviation (10 $\text{m}^2\text{-g}^{-1}$) was observed during pre-monsoon in middle zone. In lower zone, during pre-monsoon, very high standard deviation was observed. The deviation was of the order 22 $\text{m}^2\text{-g}^{-1}$ in blue and 15 $\text{m}^2\text{-g}^{-1}$ in red part of EMR. Further, it was also observed that, the spectral slope was almost uniform in particular season and zone.

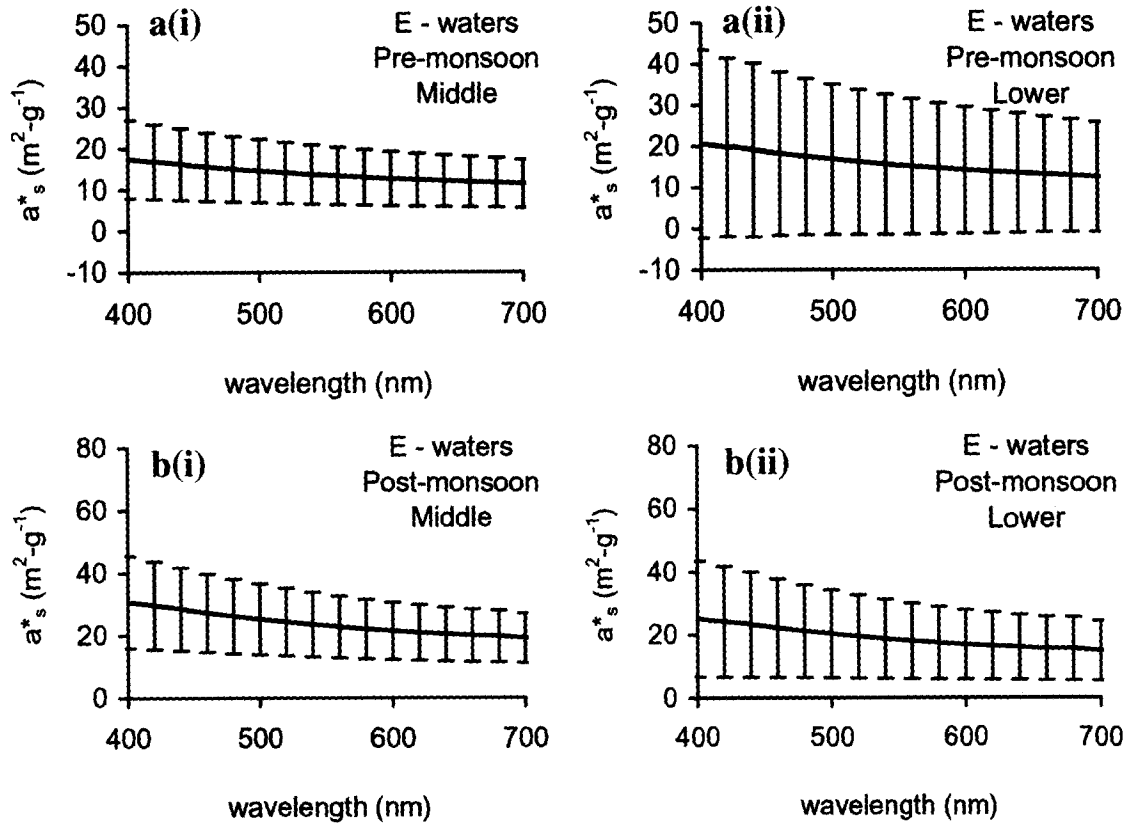


Fig. 4.4.2.3

Spectral variability of mean specific absorption coefficient due to TISM (a^*_s) in estuarine (E) waters during (a) pre-monsoon in (i) middle and (ii) lower estuary and (b) post-monsoon in (i) middle and lower estuary. The vertical bars indicate the standard deviation.

The variability in the spectral distribution of a^*_s is often an indicator of the size and shape of the particles (Binding et al., 2005). The attenuation of light by these particles is generally the first-order determinant of reflectance variability in C and E – waters (case II). Consequently, the load of suspended particles would be the quantity estimated with most confidence from reflectance in such waters when measured in the field or from space (Sathyendranath et al., 1989).

4.4.3. Spectral variability of absorption coefficient of coloured dissolved organic matter

The DOM is a complex and poorly understood mixture of organic polymers that plays an influential role in regulating light in aquatic ecosystems. The CDOM can be used as a tracer for the dynamics and characteristics of the total DOM pool (Colin et al., 2003). The dynamics in the CDOM distribution has been studied through its spectral variability. $a_{\text{CDOM}440}$ is the index of its concentration while the spectral slope (s) provides the estimation of its composition (Twardowski et al., 2004). As the concentration of CDOM in O – waters was negligible, the section is not presented here.

4.4.3.1. Coastal waters

The general trend in the spectral variation of a_{CDOM} was such that absorption decreases exponentially towards longer wavelength. The maximum deviation in a_{CDOM} was at the shorter wavelength (400 nm) which decreases to 700 nm. The spectral variation of mean a_{CDOM} in C – waters is given in Fig. 4.4.2.1. The maximum deviation was 6.9 m^{-1} . A large variability was observed in the spectral slope of a_{CDOM} . The spectral slope in C – waters ranges from 0.0015 to 0.0137 nm^{-1} . The maximum slope was encountered at station CA01.

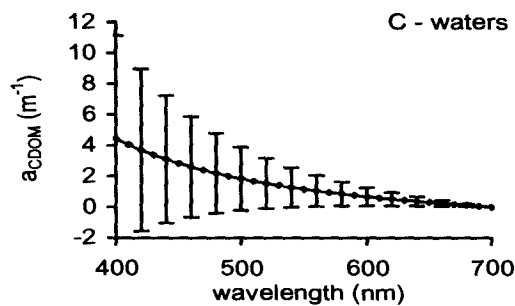


Fig. 4.4.3.1

Spectral variability of mean absorption coefficient due to CDOM (a_{CDOM}) in coastal (C) waters. The vertical bars indicate the standard deviation.

4.4.3.2. Estuarine waters

The spectral variation of mean a_{CDOM} in E – waters during pre and post-monsoon in the middle and lower estuary is given in fig. 4.4.2.2. It was very clear from the standard deviation that the variability in slope was very high within the zones as well as within different seasons. The mean slope during pre-monsoon in middle zone was 0.0042 ± 0.0024 and in lower zone was 0.0051 ± 0.0055 . During post-monsoon the mean slope in middle zone was 0.0025 ± 0.0018 and in lower zone was 0.0053 ± 0.0036 . The slope in lower zone of E – waters was larger as compared to that in the middle zone.

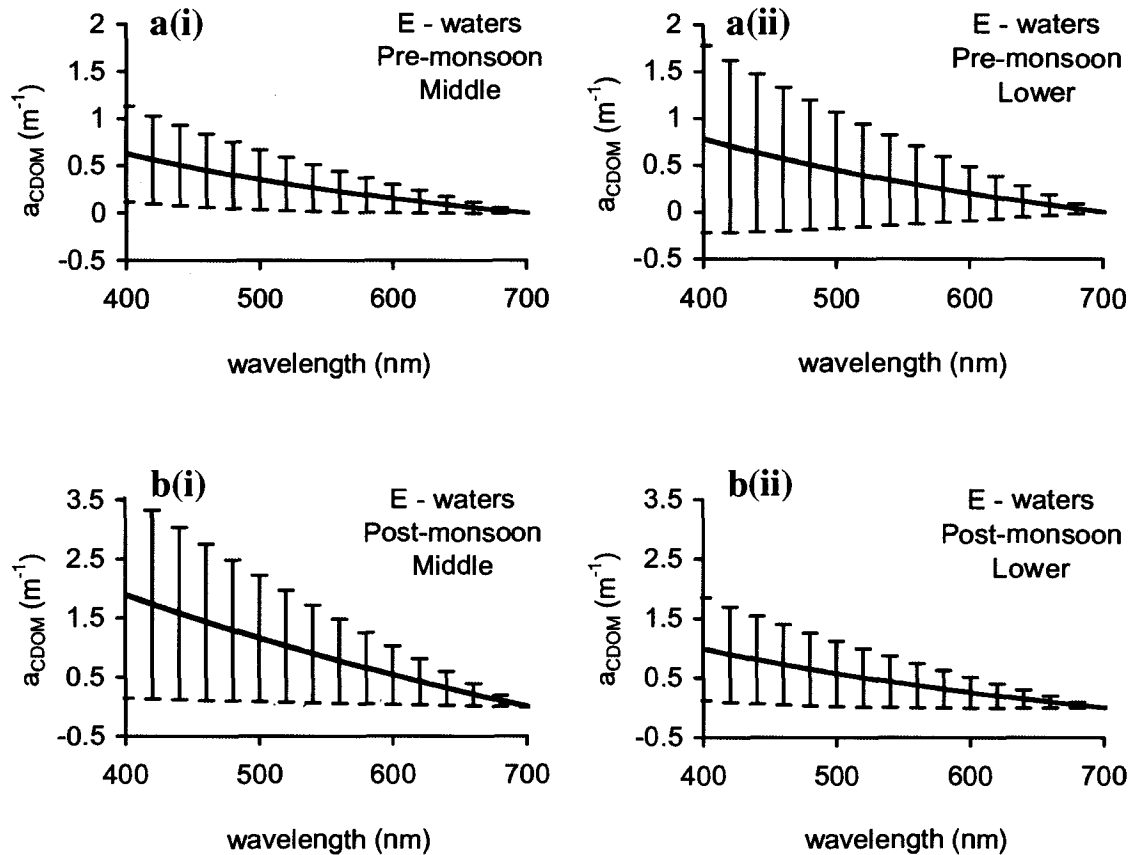


Fig. 4.4.3.2

Spectral variability of mean absorption coefficient due CDOM (a_{CDOM}) in estuarine (E) waters during (a) pre-monsoon in (i) middle and (ii) lower estuary and (b) post-monsoon in (i) middle and lower estuary. The vertical bars indicate the standard deviation.

The result of the slope analysis in different optical domains showed an increasing trend from E to C – waters. Variability in the spectral slope coefficients reflects CDOM changes resulting from production, removal and mixing of different water masses characterized by contrasting optical properties of CDOM. In their studies Vodacek et al. (1997) pointed out that the increase in slope was due to the in-situ production of CDOM. Also the variability in slope can be a result of the change in the stratification. Stabenau and Zika (2004) analyzed spectral slope of a_{CDOM} in Florida river plume. The study showed that the steepest slope and highest correlation between optical and mass spectral properties are observed in rivers with strongly absorbing waters originating in the Florida Everglades and lowest in rivers draining clearer waters from widely variable and anthropogenic influenced regions. A similar result was obtained by Kowalczyk et al. (2003) from the study carried out in an organic-rich river and surrounding coastal ocean in the South Atlantic Bight. In their study, Blough and Green (1995) showed that spectral slope of a_{CDOM} was highly variable in coastal and oceanic waters. This was mainly due to changes in the origin of dissolved material (terrestrial v/s oceanic) and CDOM photo-oxidation (into optically inactive forms of dissolved organic carbon) under high surface irradiances in stratified systems.

4.5 Spatial variability of optically active substances in different optical domains

The distribution of OAS was analyzed in O, C and E – waters. As the present research involves in the study of the variability of OAS in different optical domains, the mean value of OAS is presented here. The variability within the particular optical domain was explained using the standard deviation.

4.5.1. Open ocean waters

Fig. 4.5.1 gives the variability of mean chlorophyll_a and TISM in O – waters. The concentration of OAS in O – waters were very low. The chlorophyll_a was in the range of 0.2 to 0.7 $\mu\text{g}\cdot\text{l}^{-1}$ and TISM was in the range of 3.0 to 8.0 $\text{mg}\cdot\text{l}^{-1}$.

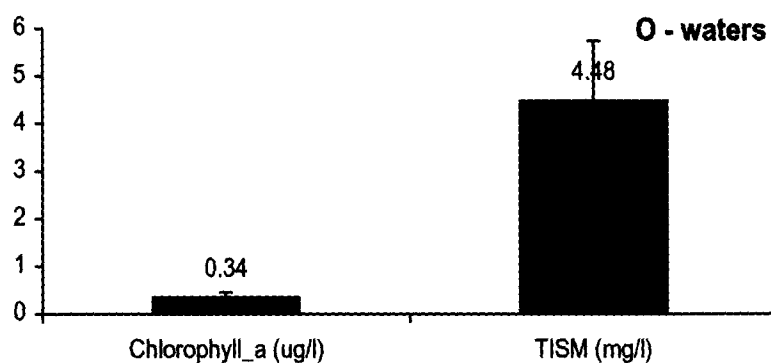


Fig. 4.5.1

Variability of mean chlorophyll_a and TISM in open ocean (O) waters. The vertical bars indicate the standard deviation.

4.5.2. Coastal waters

In C – waters, concentration of chlorophyll_a was fairly low and was in the range of 0.10 to 4.20 $\mu\text{g}\cdot\text{l}^{-1}$. TISM concentration was double than that in O – waters and was in the range of 3.70 to 16.30 $\text{mg}\cdot\text{l}^{-1}$ (Fig. 4.5.2). The most dynamic OAS in the C – waters was CDOM. The variability of $a_{\text{CDOM}440}$ was in the range of 1.00 to 22.00 m^{-1} . Therefore analysis of distribution of OAS, in C – waters clearly indicates that these waters fall in case II category. Further the variation of $a_{\text{CDOM}440}$ clearly indicates the dominance of CDOM.

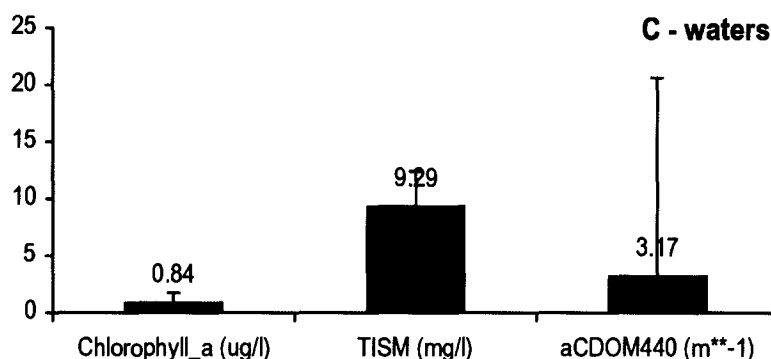


Fig. 4.5.2

Variability of mean chlorophyll_a, TISM and a_{CDOM440} in coastal (C) waters. The vertical bars indicate the standard deviation.

4.5.3. Estuarine waters

The spatial variability of OAS in E – waters with respect to different seasons were presented in Fig. 5.5.3. The general trend shows that the concentration of OAS during post-monsoon was less than that during pre-monsoon in both the zones except for a_{CDOM440} in the middle zone.

The chlorophyll_a was in the range of 1.32 to 9.62 $\mu\text{g-l}^{-1}$ and 1.00 to 5.95 $\mu\text{g-l}^{-1}$ in the middle and lower zones during pre-monsoon respectively. During post-monsoon, chlorophyll_a was in the range of 0.23 to 3.85 $\mu\text{g-l}^{-1}$ and 0.13 to 2.80 $\mu\text{g-l}^{-1}$ in middle and lower zone respectively. The TISM, during pre-monsoon, was in the range of 12.1 to 32.3 mg-l^{-1} in middle zone and 4.4 to 25.8 mg-l^{-1} in lower zone. During post-monsoon, TISM was in the range of 6.5 to 26.7 mg-l^{-1} in middle zone and 2.0 to 12.1 mg-l^{-1} in lower zone. a_{CDOM} was in the range of 0.13 to 1.52 m^{-1} in the middle and 0.2 to 3.47 m^{-1} lower zone during pre-monsoon and 0.19 to 6.16 m^{-1} in middle and 0.1 to 2.50 m^{-1} lower zone during post-monsoon.

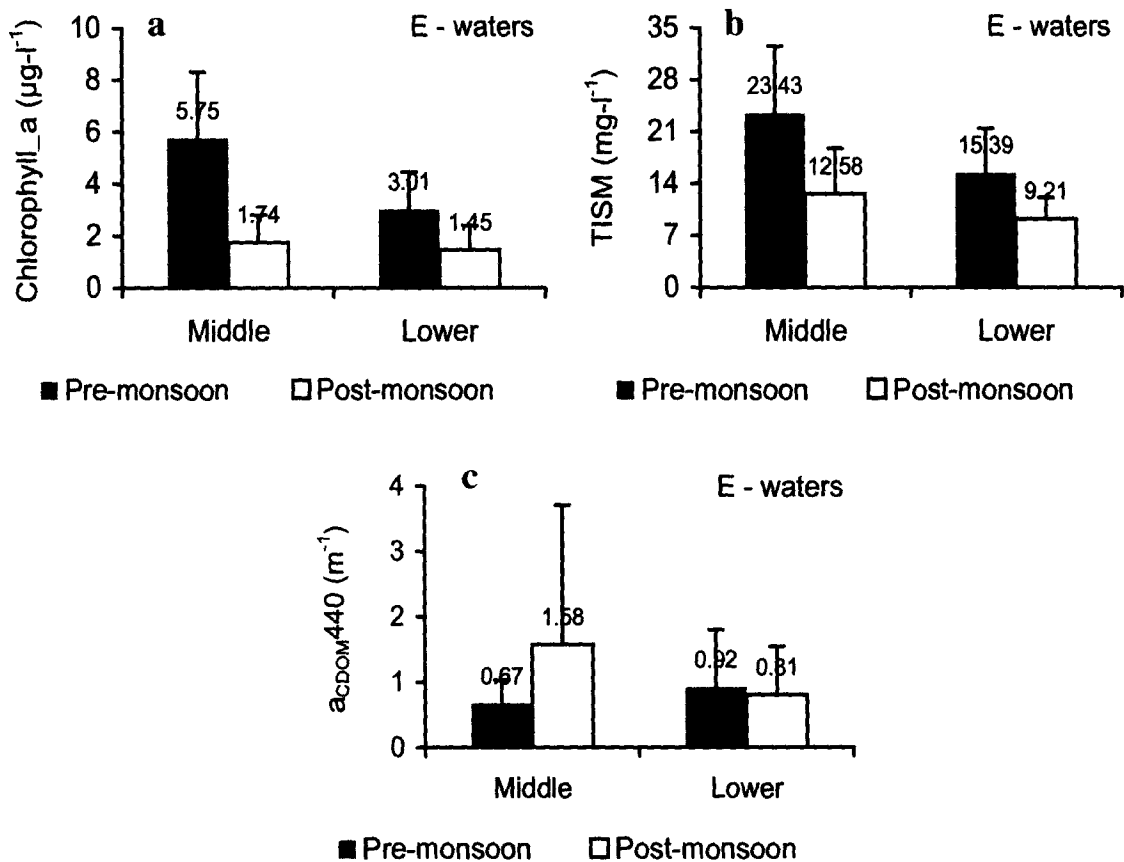


Fig. 4.5.3

Variability of mean (a) chlorophyll_a in middle and lower zone during pre-monsoon and post-monsoon season, (b) TISM in middle and lower zone during pre-monsoon and post-monsoon season and (c) a_{CDOM440} in middle and lower zone during pre-monsoon and post-monsoon season in estuarine (E) waters. The vertical bars indicate the standard deviation.

In E – waters the concentration of chlorophyll_a and TISM was very high as compared to that in O and C – waters. Krishna Kumari et al. (2002) observed that mean chlorophyll_a content in estuarine and coastal waters of Goa are 5.8 µg-l⁻¹ and 1.94 µg-l⁻¹. The biological production (primary and secondary) becomes intense at low salinities (5-8) because of their preference to a variety of planktonic organisms (marine, brackish and fresh water) at low salinity (Kibirige and Perissinotto, 2003). The availability of nutrients has been recognized as one of the major factors controlling primary production (Krishna Kumari et al., 2002). Estuaries, the dynamic water bodies in the coastal area are

the cradle grounds for phytoplankton growth because they receive constant nutrients supply from rivers and other land based discharges. Among nutrients, nitrogen (N) and phosphorous (P) are commonly referred as limiting nutrients (Neill, 2005) support the growth of phytoplankton to establish a suitable pelagic food web. Besides the availability of nutrients, the physical variables such as flushing rate, salinity and turbidity also largely influence the distribution and abundance of plankton communities in estuaries (Gerhardt et al., 2003).

The CDOM concentration from the coastal waters was higher than the estuarine waters. In their studies, Devassy et al. (1978) reported *Trichodesmium* bloom in the coastal waters of Goa during the spring season. Similarly, Madhupratap et al. (2000) reported a thick bloom of *Phaeocystis globosa* in the central Arabian Sea. In the present study, although CDOM in the C waters was high there was no concomitant rise in chlorophyll_a, probably because the sample was taken during a senescent phase. All the sampling from E – waters coincided with low tide. Hence, the stations having more proximity to the land show a comparatively high incidence of CDOM.

4.6 Sources and sinks of optically active substances in different optical domains

The developments of any site specific algorithms require a proper understanding of the distribution of OAS in the ambient waters. The distribution of OAS in any environment largely depends upon their sources and sinks. Hence in the present study an attempt has been made to understand the sources and sinks of OAS in O, C and E – waters using a statistical approach. This exercise was not applied in the O – waters as a well defined algorithm is prevalent in the open ocean.

The distribution of chlorophyll_a in water column depends upon nutrient concentration in the ambient water, insolation and carbon (Raymont, 1980). In tropics, insolation is not a limiting factor. In surface waters, carbon dioxide is in saturation with atmosphere. Therefore, the chlorophyll_a concentration largely depends upon the supply of nutrients. The TISM load generally derived from the land drainage. The remains of the zooplankton also form the TISM (Eisma and Kalf, 1987; Bowers and Binding, 2006). There were three distinct sources of CDOM identified in the world ocean (Coble, 1996; Stedmon and Markanger, 2001; Kowalczul et al., 2005). The major source of CDOM is from land drainage. Apart from this, in situ degradation of phytoplankton and generation from microbes in bottom sediment also forms a significant source of CDOM. Table 4.6.1 shows the regression matrix of chlorophyll_a, TISM and $a_{CDOM440}$ in C - waters. A significant relationship was observed between chlorophyll_a and $a_{CDOM440}$. This clearly indicates that the major source of CDOM in C – waters was from in situ degradation.

C – waters	Chlorophyll_a	TISM	$a_{CDOM440}$
Chlorophyll_a	1		
TISM	0.43	1	
$a_{CDOM440}$		0.17	1

Table 4.6.1

Table showing the correlation coefficient (R^2) between chlorophyll_a, TISM and $a_{CDOM440}$ in coastal (C) waters

Table 4.6.2 shows the regression matrix of chlorophyll_a, TISM and $a_{CDOM440}$ in middle and lower zone during pre-monsoon and post-monsoon season in E – waters. In middle zone TISM relates significantly with chlorophyll_a and $a_{CDOM440}$. Therefore it can be inferred that the major source of CDOM in this zone was from bottom

resuspension of microbially generated CDOM in bottom sediments. However the significant relationship between chlorophyll_a and $a_{CDOM440}$ in the middle zone during post-monsoon indicate that in-situ production also responsible for CDOM in this zone.

E - waters			Chlorophyll_a	TISM	$a_{CDOM440}$
Chlorophyll_a	Pre-monsoon	Middle	1		
		Lower	1		
	Post-monsoon	Middle	1		
		Lower	1		
TISM	Pre-monsoon	Middle	0.01	1	
		Lower	-0.23	1	
	Post-monsoon	Middle	0.75	1	
		Lower	0.25	1	
$a_{CDOM440}$	Pre-monsoon	Middle	-0.09	0.55	1
		Lower	-0.02	0.45	1
	Post-monsoon	Middle	0.22	0.22	1
		Lower	0.32	0.32	1

Table 4.6.2

Table showing the correlation coefficient (R^2) between chlorophyll_a, TISM and $a_{CDOM440}$ in estuarine (E) waters during pre-monsoon and post-monsoon season in middle and lower zones

Twardowski et al. (2004) stated that changes in values of the spectral slope coefficient may be regarded as an indicator of compositional changes in CDOM, if this source of error is reduced and effects associated with conservative mixing filter-out. Variability in the spectral slope coefficients reflects CDOM changes resulting from production, removal and mixing of different water masses characterized by contrasting optical properties of CDOM. In the present study, in order to differentiate between terrestrially derived and in-situ produces CDOM, the slope parameters were plotted

against $a_{\text{CDOM}440}$. The relation was linear in the C – waters and exponential in E – waters. The shape of curve in E – waters was similar to that presented by Stedmon and Markager (2001). Following the interpretation of Kowalczyk et al. (2005), E – waters exhibits two sources of CDOM whereas in C – waters a single source of CDOM exists.

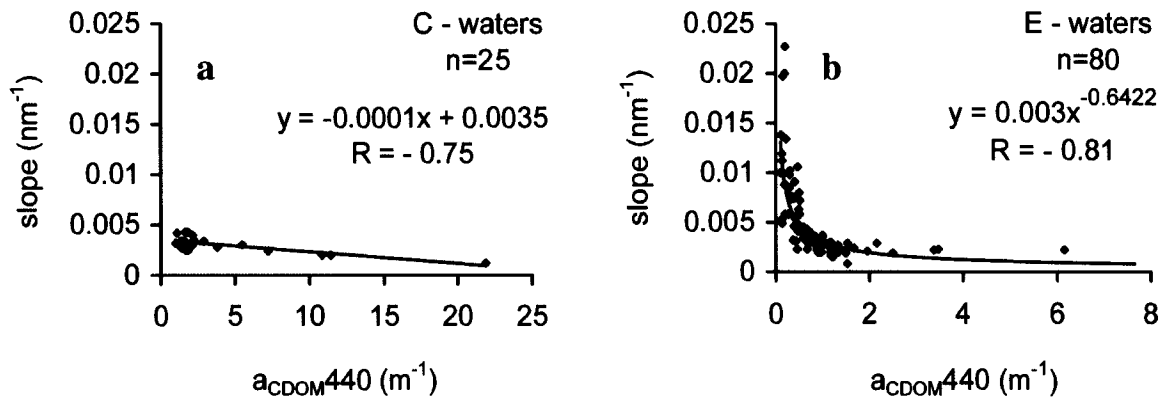


Fig. 4.6.1

Variability of slope coefficient with $a_{\text{CDOM}440}$ in (a) coastal (C) and (b) estuarine (E) waters.

The analysis of OAS in waters of different optical domains and their interaction with visible part of EMR (400 – 700 nm) was properly documented. The next step is to simulate hyperspectral water leaving radiance and develop an algorithm to retrieve these OAS through a visible satellite sensor. This has been presented in next chapter.

Chapter 5

Development of Algorithms

5.1	Hyperspectral water leaving radiance-----	(63)
5.1.1	Theory-----	(63)
5.1.2	Effect of optically active substances on hyperspectral water leaving radiance-----	(66)
5.1.3	Sensitivity analysis of measured and computed absorption coefficient and water leaving radiance-----	(68)
5.2	Identification of wavelengths to derive optically active substances -----	(70)
5.2.1	Qualitative approach-----	(71)
5.2.2	Quantitative approach-----	(74)

The satellite based retrieval of ocean colour parameters involves a major task of development of an accurate bio-optical algorithm for water parameter retrieval (Gordon et al., 1980). There are many approaches to develop algorithm for the retrieval of OAS of case II waters through a visible satellite sensor. These are band-ratio approach (O'Reilly et al., 1998), inverse modeling approach (Doerffer and Fisher, 1994), principal component analysis (Lorenz and Cai, 2006) and artificial neural network approach (Gross et al., 1999). In the present study first approach is adopted.

The development of a reliable remote sensing algorithm for any water body depends upon an understanding of the contribution of different OAS to variation of spectral absorption and scattering properties of the water body. The procedure is straight forward in case I waters where the algorithm is based on the fact that phytoplankton pigment, chlorophyll_a, absorbs primarily in blue and reflects in green segment of EMR. This indicates that with increase in chlorophyll_a concentration the water appears green in colour. Hence a ratio of energy received by the blue and green bands of visible sensor serves as a good indicator of chlorophyll_a concentration (O'Reilly et al., 1998). The task of development of algorithm to retrieve OAS in case II waters is highly complex due to the presence of TISM and CDOM along with chlorophyll_a. An examination of the spectral variation of IOP of OAS indicates that all OAS utilizes energy in the wavelength range 400 – 500 nm. The underwater radiometer with six spectral bands in visible part of EMR and a bandwidth of ± 10 nm was not sufficient to analyze the spectral response of IOP. Also these bands were not evenly spaced and were concentrated in blue and green wavelengths. A large gap exists between the green (555 nm) and red (670) nm. Hence in order to analyze the spectral signatures of each OAS on signal leaving the water column,

hyperspectral water leaving radiance is crucial (Chang et al., 2004). There were two ways to achieve the same. Either to use a hyperspectral underwater radiometer or to generate hyperspectral water leaving radiance through water sample analysis. The present study uses the second approach. The detail about the same is given in subsequent section.

5.1 Hyperspectral water leaving radiance

The hyperspectral water leaving radiance was computed using a calibrated radiative transfer model (Menon, 2004) following the approach of Doerffer (1992). A brief detail about the radiative transfer model is as follows.

5.1.1 Theory

The transfer of radiation through the atmosphere to the sea, into it, back to surface, through atmosphere and finally to the sensor of the satellite is termed as radiative transfer (RT). Hence RT is the study of the propagation of radiation through an absorbing and scattering medium. When solar radiation passes through the atmosphere, it undergoes attenuation (scattering and absorption). Scattering is by means of air molecules (Rayleigh scattering) aerosols (mie scattering), while absorption is by gaseous molecules. Radiation reaching the sea surface is partly reflected/refracted at the intermediate layer of the atmosphere and at the sea surface (sun glint), while certain amount of radiation is transmitted through the water column. The transmitted radiation is either absorbed and/or scattered by the OAS present in it. The amount of energy emerging from the sea depends on the optical properties of OAS. Hence by assuming a single scattering albedo,

Radiative transfer between sun, atmosphere and water medium have been formulated by Gordon (1978).

$$L_T(\lambda) = L_w(\lambda) T_d(\lambda) + L_g(\lambda) T(\lambda) + L_p(\lambda) \quad \text{----- (5.1.1.1)}$$

Where, L_T is total radiance received by the sensor, L_w is radiance leaving the water column (water leaving radiance), L_g is radiance reflected at the sea surface (sunglint radiance), L_p is total atmospheric path radiance, which is the sum of aerosol and rayleigh radiance ($L_a + L_r$), T is direct transmission coefficient, T_d is diffuse transmission coefficient at wavelength (λ).

The subsurface reflectance (R) at wavelength (λ) was formulated as per Doerffer (1992) as

$$R(\lambda) = E_u(\lambda) / E_d(\lambda) \quad \text{----- (5.1.1.2)}$$

Where, $E_u(\lambda) = Q(\lambda) L_w(\lambda)$ is upwelling irradiance and L_w is water leaving radiance.

The radiance field within the water column is not isotropic and depends upon the AOP and dynamics of the water body. This non-isotropic nature is described by bi-directional reflectance coefficient expressed by a factor 'Q' which is the ratio of upwelling irradiance to upwelling radiance (Morel et al., 1995). Hence using the above equations

$$Q(\lambda, \theta_s) = R(\lambda) / R_{rs}(\lambda) \quad \text{[sr]} \quad \text{----- (5.1.1.3)}$$

Adopting the above equation, $Q(\lambda, \theta_s)$ has been derived for all six wavelengths (412, 443, 490, 510, 555 and 670 nm) of the radiometer. The average value of Q – factor along with standard deviation is given in table 5.1.1.1.

	Q – factor (sr)					
	412 nm	443 nm	490 nm	510 nm	555 nm	670 nm
O – waters	3.939	3.899	3.800	3.755	3.610	3.778
	± 0.088	± 0.066	± 0.080	± 0.061	± 0.033	± 0.006
C – waters	3.788	3.759	3.697	3.693	3.683	3.901
	± 0.098	± 0.117	± 0.148	± 0.143	± 0.157	± 0.073
E – waters	3.565	3.599	3.624	3.718	3.825	3.958
	± 0.031	± 0.054	± 0.108	± 0.121	± 0.169	± 0.119

Table 5.5.1.1.1

Mean and standard deviation of coefficient of bi-directional reflectance, Q-factor, at wavelengths 412, 443, 490, 510, 555 and 670 nm in open ocean (O), coastal (C) and estuarine (E) waters.

The downwelling irradiance ($E_d(\lambda)$) was computed as (Wang, 1999; Yang and Gordon, 1997)

$$E_d(\lambda) = F_s(\lambda) \cos(\theta_s) T(\lambda) \quad \text{----- (5.1.1.4)}$$

Where, $F_s(\lambda)$ is solar irradiance at the top of the atmosphere and taken from Nickel and Labs (1984), θ_s is solar zenith angle and $T(\lambda)$ is atmospheric transmittance which was calculated as per Wang (1999)

$$T(\lambda) = \text{Exp} [-(\tau_a(\lambda) + \tau_r(\lambda)) / 2 + \tau_o(\lambda)] / \cos \theta_s \quad \text{----- (5.1.1.5)}$$

Where, τ_a , τ_r , and τ_o are optical thickness for aerosol, air molecule and ozone scattering respectively. The aerosol optical thickness was measured using Sunphotometer where as optical thickness due to air molecules and ozone were computed as per Doerffer (1992).

Therefore, from above equations, water leaving radiance was computed as

$$L_w(\lambda) = [R(\lambda) F_s(\lambda) \cos(\theta_s) T(\lambda)] / Q(\lambda) \quad [\text{W}\cdot\text{m}^{-2}\cdot\text{nm}^{-1}\cdot\text{sr}^{-1}] \text{ -- (5.1.1.6)}$$

The subsurface reflectance ($R(\lambda)$) was computed using IOP of OAS. The details of which is explained in section 4.1.

5.1.2 Effect of optically active substances on hyperspectral water leaving radiance

The water leaving radiance was computed for every 1 nm (hyperspectral) at all the stations from O, C and E waters. In order to show the effect of OAS on hyperspectral water leaving radiance, three stations were presented here. Two stations from C and one from E – water. Out of two stations in C – waters, CA04 showed normal distribution of OAS and CA01 showed dominance of CDOM. The station from E – water (E07) showed dominance of TISM. At station CA04 the distribution of hyperspectral water leaving radiance was normal with a minimum concentration of OAS ($C_c = 0.2 \mu\text{g-l}^{-1}$, $C_s = 5.44 \text{ mg-l}^{-1}$ and $a_{\text{CDOM}440} = 2.76 \text{ m}^{-1}$). At station CA01 $a_{\text{CDOM}440}$ was 21.67 m^{-1} , C_c was $0.37 \mu\text{g-l}^{-1}$ and TISM was 7.45 mg-l^{-1} . At station E07, sampled on 14th February 2002, the concentration of TISM was 22 mg-l^{-1} . The concentration of chlorophyll_a and $a_{\text{CDOM}440}$ at this station were $0.96 \mu\text{g-l}^{-1}$ and 1.15 m^{-1} respectively. The results were presented in fig. 5.1.2.2. Having a resolution of 1 nm, the simulated values clearly show the effect of each OAS on spectral distribution and thus sensitivity of the model.

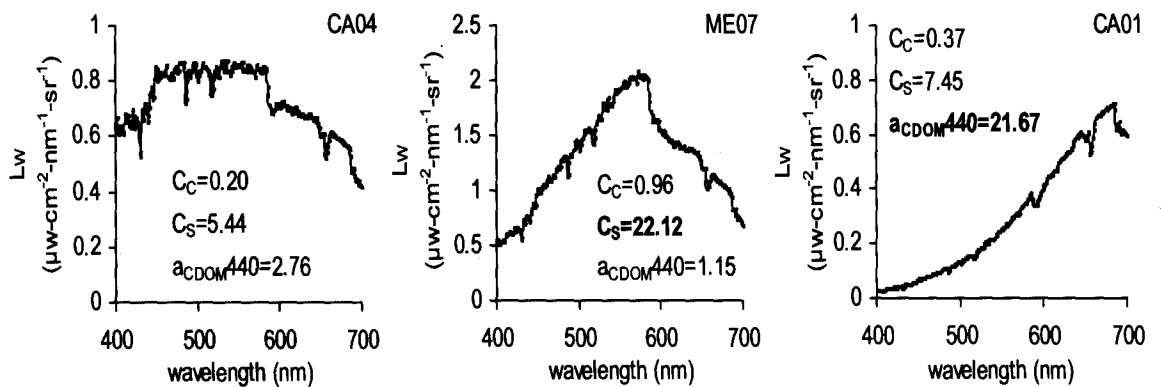


Fig. 5.1.2.1

Spectral variation of computed hyperspectral water leaving radiance (L_w) at stations CA04, E07 and CA01

The spectral shape of water leaving radiance at station CA04 showed an increase from blue to green region and a decreasing trend from green to red region. The increase was found to be gradual from 400 to 437 nm followed by a drastic increase from 437 to 450 nm, after which again a gradual increase was observed till 535 nm. The minimum value was seen at 431 nm ($0.52 \mu\text{w}\cdot\text{cm}^{-2}\cdot\text{nm}^{-1}\cdot\text{sr}^{-1}$) where as the maximum at 535 nm ($0.87 \mu\text{w}\cdot\text{cm}^{-2}\cdot\text{nm}^{-1}\cdot\text{sr}^{-1}$). Beyond 535 nm, the spectra had a decreasing trend. Although a high was seen at 605 nm and 664 nm, the spectra decreases gradually till 700 nm. Unlike this station, E07 showed primary minima in blue, secondary in red and maxima in yellow region. The minimum value was observed at 400 nm ($0.52 \mu\text{w}\cdot\text{cm}^{-2}\cdot\text{nm}^{-1}\cdot\text{sr}^{-1}$), beyond which radiance increased gradually with a maximum value of $2.1 \mu\text{w}\cdot\text{cm}^{-2}\cdot\text{nm}^{-1}\cdot\text{sr}^{-1}$ at 573 nm. Further a gradual decrease was seen up to 658 nm after which an increase was observed till 664 nm. Beyond this wavelength, spectra decrease gradually till 700 nm. This concludes that with increase in TISM concentration the peak energy shifts to longer wavelength. Similar results were obtained by Doxaran et al. (2002) for the data generated in the turbid waters of Gironde estuary. It was observed that, R_{rs} was near zero at 850 nm for low TISM concentration ($< 13 \text{ mg}\cdot\text{l}^{-1}$) which increased to 110 % for highest concentration ($985 \text{ mg}\cdot\text{l}^{-1}$) of TISM. The recent study carried out by Karabulut and Ceylan (2005) shows that though increasing TISM concentration produces a significant wavelength shift in the reflectance pattern, the spectral signatures of algal pigment remained unchanged. At CA01, the spectral shape of water leaving radiance indicated a gradual increase from blue to red region. The minimum value was encountered at 400 nm ($0.02 \mu\text{w}\cdot\text{cm}^{-2}\cdot\text{nm}^{-1}\cdot\text{sr}^{-1}$) after which a gradual increase was seen in radiance till 685 nm ($0.71 \mu\text{w}\cdot\text{cm}^{-2}\cdot\text{nm}^{-1}\cdot\text{sr}^{-1}$) beyond which a slight decrease till 700 nm. The secondary

minimum was not seen like other two stations. The values at longer wavelengths at all three stations were almost similar which points towards the fact that decrease in radiance at shorter wavelength at CA01 was due to strong absorption of CDOM. The effect of CDOM absorption was seen up to 650 nm. In the region of high incidence of CDOM, light absorption can extend largely into the visible channel dominating the phytoplankton absorption in the blue part of EMR (Vodacek et al., 1997; Stedmon et al., 2000).

5.1.3 Sensitivity analysis of measured and computed absorption coefficient and water leaving radiance

The computation of water leaving radiance is very much sensitive to accuracy of IOP (Gordon et al., 1997). Therefore at first instant the absorption coefficient generated through water sample analysis was compared with that derived using radiometric measurements. The methodology for generating absorption coefficient through water sample analysis was given in section 4.1. The derivation of absorption coefficient through radiometric measurement was given in section 3.1. The results showed that the measured and computed absorption coefficients were in good agreement. The correlation coefficient (R^2) of 0.78, 0.78, 0.87, 0.87, 0.86 and 0.88 were obtained at 412, 443, 490, 510, 555 and 670 nm bands respectively (Fig. 5.1.2.1).

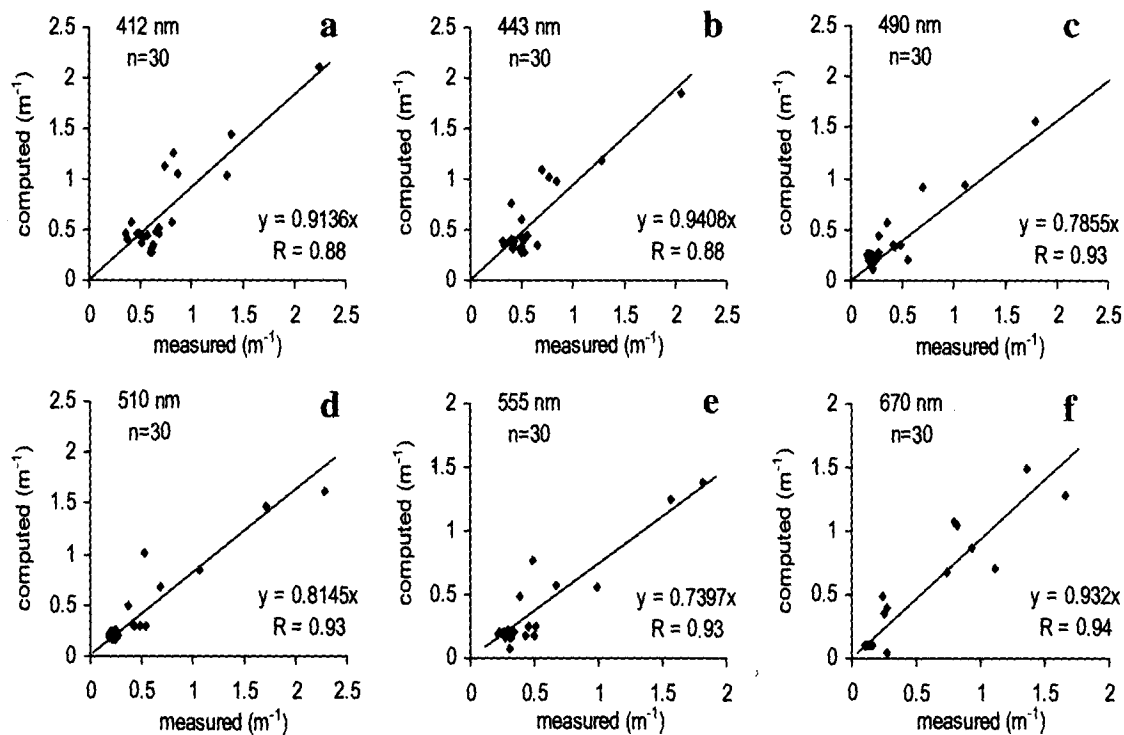


Fig. 5.1.3.1

Correlation between absorption coefficient (a) generated through water sample analysis (computed) and that derived through radiometric measurements (measured) for wavelengths a) 412 nm, b) 443 nm, c) 490 nm, d) 510 nm, e) 555 nm and f) 670 nm

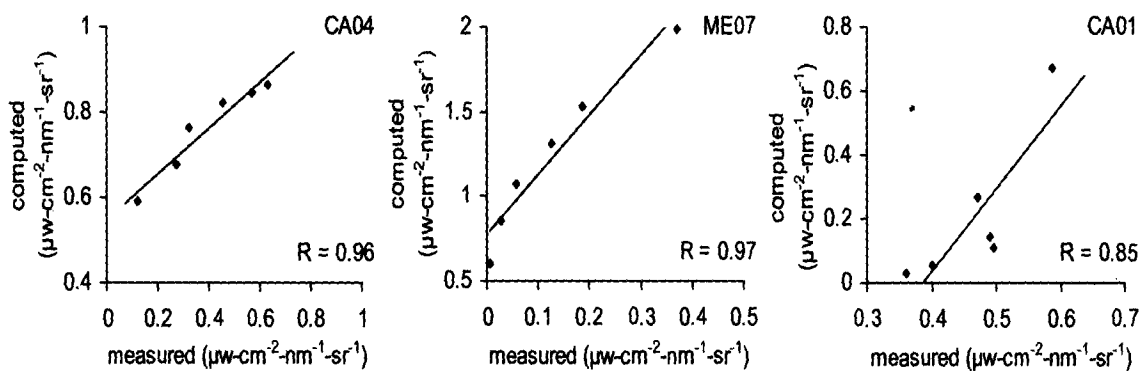


Fig. 5.1.3.2

Correlation between measured and computed water leaving radiance (L_w) at stations CA04, E07 and CA01

The accuracy of computed water leaving radiance was determined by comparing it with measured one, at six bands of radiometer in visible part of EMR. The correlation coefficient (R) at CA04, E07 and CA01 was found to be 0.96, 0.97 and 0.85 respectively (Fig. 5.1.3). The results showed that model computed water leaving radiance was in good agreement with measured. Though there was a good correlation, the computed values at CA04 and E07 were found to be higher than the measured values. Also an offset was seen on the computed axis at CA04 and E07 where as it was on computed axis CA01. This discrepancy might be due to the factors such as manual error while operating the instrument or instrument calibration error or time lag between instrument operation and water sample collection.

5.2 Identification of wavelengths to derive optically active substances

Adopting the band-ratio approach, algorithms were developed to map chlorophyll_a concentration, TISM concentration and absorption due to CDOM at 440 nm ($a_{CDOM440}$). The procedure for identification of wavelengths was based on the differential response of each OAS to absorption and scattering of visible part of EMR at each wavelength. At first instant a qualitative scheme was adopted to find out which OAS has minimum and maximum effect on IOP and at what wavelength.

5.2.1 *Qualitative approach*

The motivation of qualitative approach has been adopted from Babin et al., 2003. In their studies Babin et al., 2003 analyzed the dominance of OAS, at wavelengths 412, 443, 490, 510, 555 and 670 nm, in coastal waters around Europe using ternary plots. A similar approach has been adopted in the present study. Fig. 5.2.1 shows the ternary plots illustrating the relative contribution of absorption due to chlorophyll_a (a_c), TISM (a_s) and CDOM (a_{CDOM}) in waters of different optical domains i.e. open ocean including Lakshadweep waters (O – waters), coastal (C – waters) and estuarine (E – waters).

The plots shows that at 412 and 443 nm (Blue) chlorophyll_a absorption dominates the spectra for the samples collected in O – waters whereas it was CDOM in C – waters and TISM in E – waters. Chlorophyll_a has a primary absorption peak in blue and due to absence of any other OAS the total absorption was dominated by chlorophyll_a (Bricaud et al., 1998). This depicts O – waters as a pure case I and hence blue band could be chosen to retrieve chlorophyll_a from this water. As discussed earlier in section 4.4, the spectral shape of absorption due to TISM and CDOM has a similar pattern which was exponentially decreasing with increasing wavelength. Hence all three OAS contributes in absorption of light at shorter wavelength.

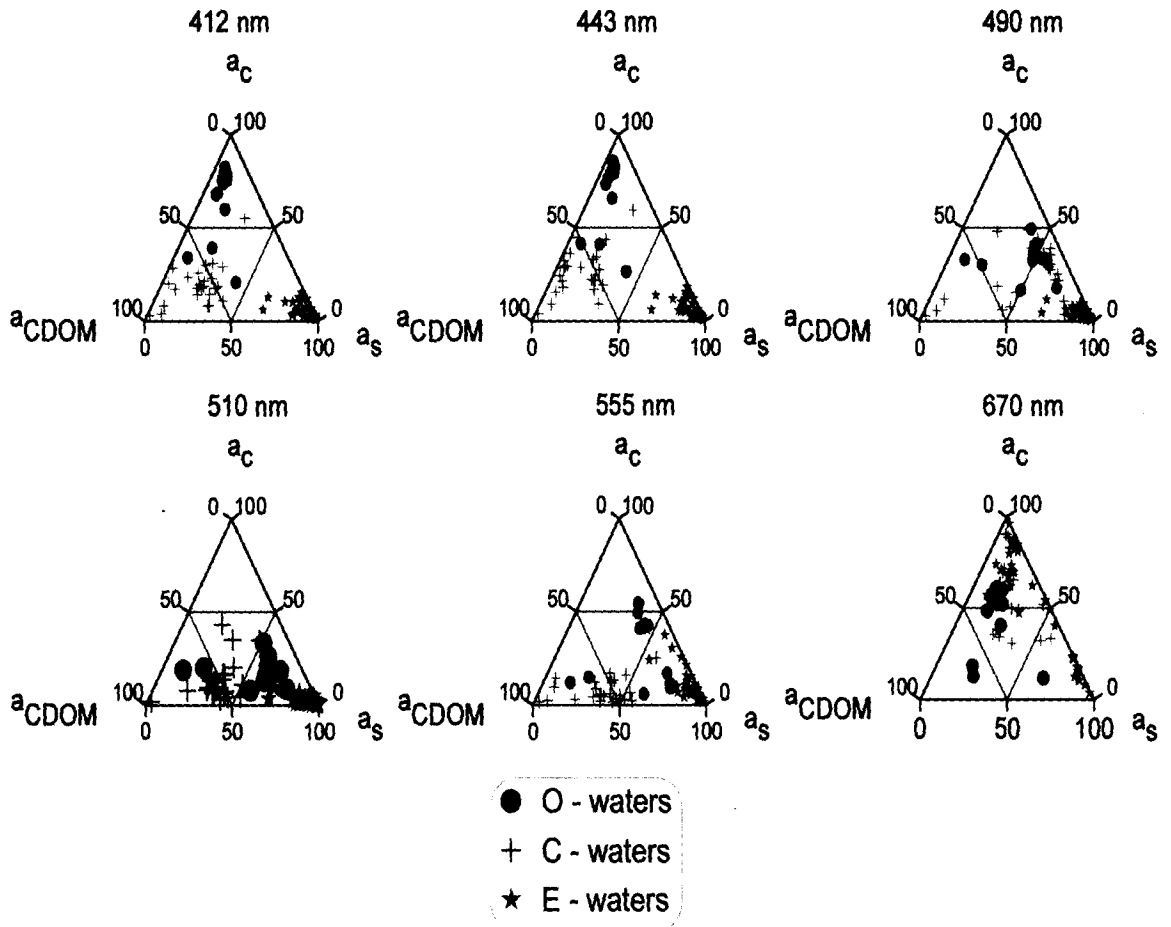


Fig. 5.2.1.1

Ternary plots illustrating the relative contribution of chlorophyll_a (a_c), TISM (a_s) and a_{CDOM} to absorption for stations in open ocean (O – waters), coastal (C – waters) and estuarine (E – waters) waters at wavelengths 412, 443, 490, 510, 555 and 670 nm. The labels correspond to maximum fraction.

From the fig. 5.2.1.1 it was clear that CDOM dominated in C – waters and TISM in E – waters at 412 nm. This was because of their relative concentration in respective waters. As TISM have a large refractive index which can produce spectra that is several times greater than that of CDOM or chlorophyll_a present in high concentration. As originally noted by Morel and Prieur (1977), the waters dominated by CDOM and TISM produces high absorption in shorter wavelength compared to one with high

phytoplankton concentration. Therefore this wavelength region is not ideal for the retrieval of chlorophyll_a concentration in such waters (Szekielda, 2005). The scenario was different at 490 nm (Blue-Green). Here the effect of TISM was found to be relatively higher than chlorophyll_a and CDOM in all three waters except for stations CA01, CA02 and CD12 in C – waters where $a_{\text{CDOM}440}$ was 21.67 m^{-1} , 9.19 m^{-1} and 13.82 m^{-1} respectively. The effect of chlorophyll_a was totally withdrawn at this wavelength. The similar situation was observed at 510 and 555 (Green) wherein it was seen that both TISM and CDOM contribute to the total absorption. At 670 nm (Red), it was observed that, chlorophyll_a absorption again dominates the total absorption except for stations OC01, OC02 and OC03 in O – waters and those stations in E – waters which were sampled during pre-monsoon and monsoon from mid estuary. Chlorophyll_a has a secondary peak in red part of EMR. The recent studies carried out by Szekielda (2005) showed that although chlorophyll_a absorption intensity at concentration $> 20 \mu\text{g-l}^{-1}$ was partly offset by scattering by phytoplankton cells, resulting in shift of the peak position towards longer wavelengths, it still has a significant absorption at wavelengths 670 – 710 nm. Also due to exponentially decreasing pattern of absorption due to CDOM and TISM their contribution to total absorption coefficient reduces at this wavelength. In their study, Han et al. (1994) verified that TISM has little or no effect on the position of the red part of the chlorophyll_a absorption band.

5.2.2 Quantitative approach

From the qualitative approach, the relative contributions of IOP to its constituents were very well understood. But in order to derive an algorithm it was necessary to quantify the result. Hence the quantitative approach was employed to get the equations which could be directly applied to the satellite data to map all three OAS. The method was first applied to retrieve OAS from E – waters. The details are given below.

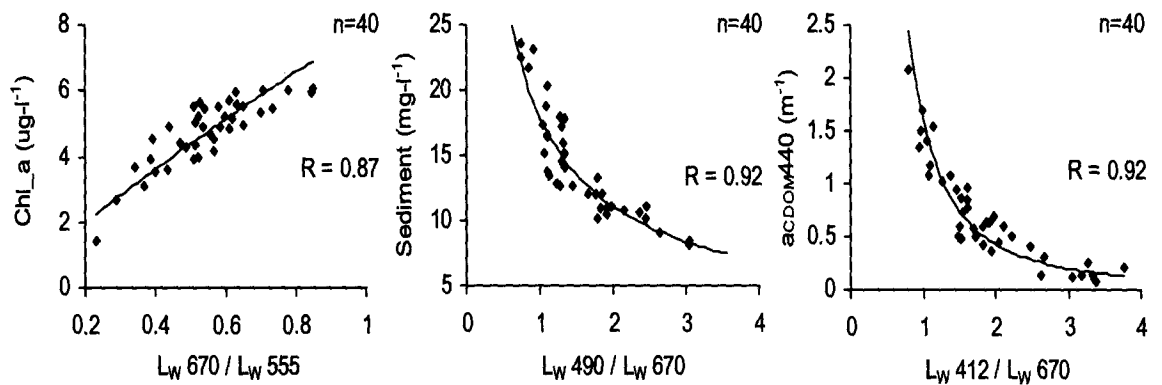


Fig. 5.2.2.1

Regression between a) chlorophyll_a concentration and the ratio of water leaving radiance at 670 and 555 nm, b) TISM (sediment) concentration and the ratio of water leaving radiance (L_w) between 490 and 670 nm and c) $a_{CDOM440}$ and the ratio of water leaving radiance (L_w) between 412 and 670 nm.

One station was selected with a minimum concentration of OAS. The hyperspectral water leaving radiance computed at this station was considered as base line spectra. Then by varying only chlorophyll_a concentration and keeping all other parameters constant, water leaving radiance was computed. The range of chlorophyll_a was selected on the basis of its ambient concentration in the respective environment. Then each hyperspectral radiance was divided by the baseline spectra. Subsequently wavelengths having minimum and maximum effects of chlorophyll_a concentration were identified. The same method was adopted for TISM and $a_{CDOM440}$. The suitable

wavelengths for the retrieval of chlorophyll_a, TISM and $a_{CDOM440}$ were found to be 670 and 555 nm, 490 and 670 nm, 412 and 670 nm. The study carried out by Szekiolda (2005) showed that the ratio of MODIS channels 13 (678 nm) and 14 (667 nm) gives a good relation with surface chlorophyll_a concentration. The ratio of water leaving radiance having maximum and minimum effect of the respective OAS was then regressed with the concentration of that OAS to get the algorithm. Fig. 5.2.2.1 shows the regression between OAS and the respective ratio of the water leaving radiance at wavelengths having maximum and minimum effect of that OAS. The regression coefficient (R) was 0.87 for chlorophyll_a and 0.92 for TISM and $a_{CDOM440}$. The plots showed a power relation between the ratios and its respective concentration which comes to a saturation point at a particular concentration. Hence it can be concluded that for the concentration of OAS outside the limit of analysis different algorithms have to be used indicating that the algorithms are site specific. The respective algorithms are

$$\text{chlorophyll_a} = 5.5931 (L_w 670 / L_w 555)^{0.615} \quad [\mu\text{g-l}^{-1}] \text{----- (5.2.2.1)}$$

$$\text{TISM} = 17.11 (L_w 490 / L_w 670)^{-0.3596} \quad [\text{mg-l}^{-1}] \text{----- (5.2.2.2)}$$

$$a_{CDOM440} = 2.9393 (L_w 412 / L_w 670)^{-2.2486} \quad [\text{m}^{-1}] \text{----- (5.2.2.3)}$$

A similar approach was adopted in development of algorithms for the northesatern Arabian Sea. In this case the ratio of R_{rs} was used instead of water leaving radiance (L_w). As the geometric area of Arabian Sea is much larger than Mandovi-Zuari estuarine system, the latitudinal variability of incoming solar irradiance could be

expected to much larger extend. Hence, in order to develop an algorithm to get a synoptic picture, it is necessary to normalize the energy leaving the water column to that received by the water column so as to get the relative energy received by the satellite sensor. Further, as the concentration of chlorophyll_a in these waters was lower, as compared to that in estuarine, the wavelengths identified were 670 and 510 nm instead of 555 nm. The wavelengths used for TISM were 490 and 670 nm where as for CDOM they were 412 and 670 nm. Moreover, a high variability in CDOM was observed between offshore waters and northern inshore waters (above 20⁰ N). Hence to retrieve chlorophyll_a and TISM from both inshore and offshore waters, the algorithm was polynomial while it was multi-spatial in the case of CDOM, linear in the offshore and polynomial in the inshore waters (Fig. 5.2.2.2). The respective algorithms are

$$\text{chlorophyll_a} = -2.6889 A^3 + 4.365 A^2 - 2.2424 A + 0.7222 [\mu\text{g}\cdot\text{l}^{-1}] \quad \text{-- (5.2.2.4)}$$

$$\text{TISM} = 3.0416 B^3 - 17.803 B^2 + 33.03 B - 15.145 \quad [\text{mg}\cdot\text{l}^{-1}] \quad \text{-- (5.2.2.5)}$$

$$a_{\text{CDOM}440} = 1.0066 C^2 - 12.238 C + 37.503 \quad \text{inshore } [\text{m}^{-1}] \quad \text{-- (5.2.2.6)}$$

$$a_{\text{CDOM}440} = 0.0561 C + 0.8047 \quad \text{offshore } [\text{m}^{-1}] \quad \text{-- (5.2.2.7)}$$

Where, $A = R_{rs}(670) / R_{rs}(510)$, $B = R_{rs}(490) / R_{rs}(670)$ and $C = R_{rs}(412) / R_{rs}(670)$

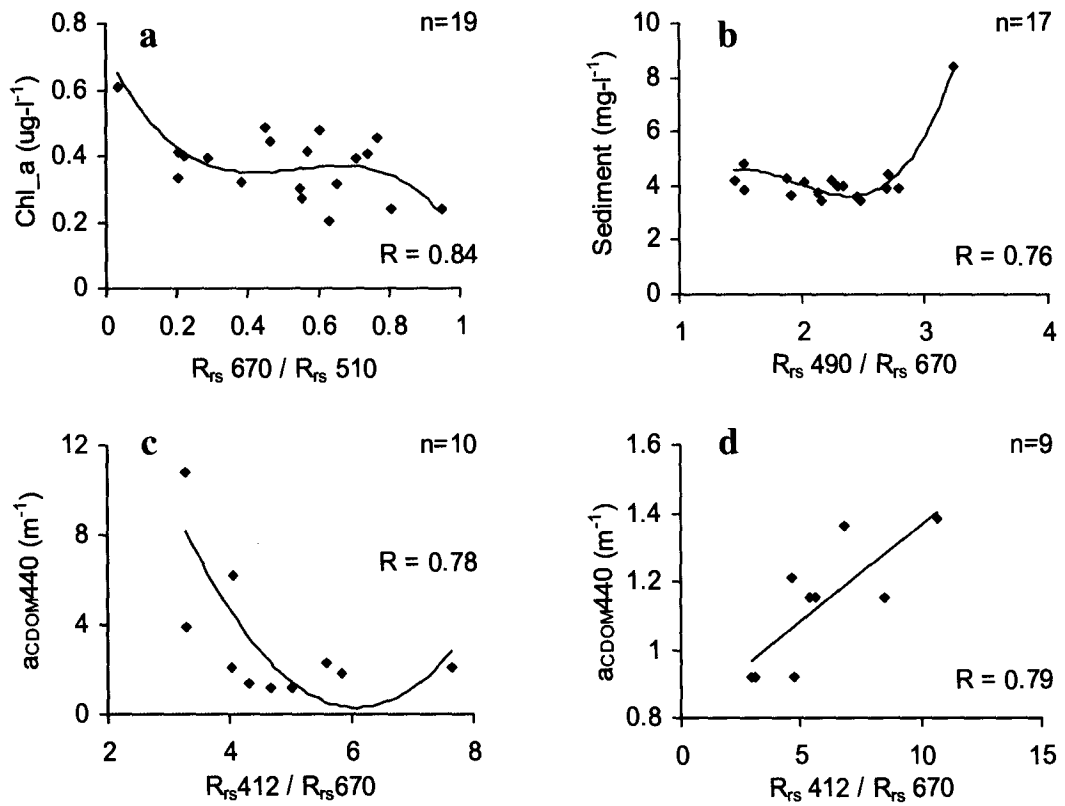


Fig. 5.2.2.2

Regression between a) chlorophyll_a concentration and remote sensing reflectance (R_{rs}) at 670 and 510 nm, b) TISM (sediment) concentration and the ratio of remote sensing reflectance (R_{rs}) at 490 and 670 nm, c) a_{CDOM440} and the ratio of remote sensing reflectance (R_{rs}) at 412 and 670 nm in inshore waters and d) a_{CDOM440} and the ratio of remote sensing reflectance (R_{rs}) at 412 and 670 nm in offshore waters

An analysis of OAS through remotely sensed data requires a proper incorporation of the effects of atmosphere (Mukai et al., 2000; Moulin et al., 2001). The study carried out by Gordon (1997) revealed that around 85 % of the total radiance received by an optical sensor is from atmosphere. Hence this exemplifies that aerosols along with air molecules play a vital role in applying atmospheric correction to analyze OAS through a visible satellite sensor. The elimination of aerosol and Rayleigh radiances (path radiance) from each pixel of an optical sensor refers to atmospheric correction. The radiance received from air molecule (Rayleigh radiance) can be accurately modeled as a function of atmospheric pressure, zenith and azimuth angle (Doerffer, 1992). The main difficulty in the correction of atmospheric effects is due to the presence of aerosols, for which optical characteristics are variable in both space and time. (Charlson et al., 1992). In order to make local estimates of direct aerosol radiative forcing, several key aerosol properties must be measured or estimated. These include the relative amounts of light scattering by the aerosol, the fraction of the incident solar radiation that is scattered upward to space by the suspended particles and the optical thickness of the aerosols (Sheridan et al., 2001). Most of the studies related to aerosols in the past were based on the in-situ observations thus lacking synoptic coverage. However very few studies were conducted to map AOT synoptically using Mesosat-5 (Leon et al., 2001), NOAA – AVHRR (Rajeev and Ramnathan, 2002), MODIS – TERRA (Vinoj et al., 2004; Kaufman et al., 1997) and IRS – P4 – OCM (Das et al., 2002).

6.1 Atmospheric path radiance

The atmospheric radiances are collectively termed as path radiance ($L_p(\lambda)$). Hence the path radiance can be expressed as sum of contributions from aerosols (aerosol radiance, L_a) and that from air molecules (Rayleigh radiance, L_r) (Eq. 5.1.1.1).

$$L_p(\lambda) = L_a(\lambda) + L_r(\lambda) \quad [\mu\text{W}\cdot\text{cm}^{-2}\cdot\text{nm}^{-1}\cdot\text{sr}^{-1}] \quad \text{----- (6.1.1)}$$

The simulation procedure for the path radiance was adopted from Doerffer (1992) as follows.

$$L_x = F_s \cdot \tau_x \omega_{ox} \cdot P_x / 4\pi \cos(\theta_v) \quad [\mu\text{W}\cdot\text{cm}^{-2}\cdot\text{nm}^{-1}\cdot\text{sr}^{-1}] \quad \text{----- (6.1.2)}$$

[x = a for aerosol and x = r for Rayleigh]

Where, $F_s(\lambda)$, extraterrestrial solar irradiance, taken from Nickel and Labs (1984), τ is the optical thickness, ω_o is single scattering albedo, and θ_v is the satellite view angle. The scattered part of the radiance, P_x , was computed as per Doerffer (1992) as follows

$$P_x(\gamma) = P_x(\gamma^+) + [R(\theta_v) + R(\theta_s)] P_x(\gamma^+) \quad \text{----- (6.1.3)}$$

Where R is the Fresnel reflectance of the water surface, θ_s is the solar zenith angle and γ^\pm is the forward/backward scattering angle. The Rayleigh phase function scattering is given by

$$P_r(\gamma^\pm) = (3/4) [1 + \cos^2(\gamma^\pm)] \quad \text{----- (6.1.4)}$$

Following Doerffer (1992), one can approximate the scattering phase function for marine aerosols by a two term Heyney-Greenstein phase function of the form

$$P_a(\gamma^\pm) = A f(\gamma^\pm, g1) + (1 - A) f(\gamma^\pm, g2) \quad \text{----- (6.1.5)}$$

Where

$$f(\gamma^\pm, g) = (1 - g^2) / [1 + g^2 - 2g \cos \gamma^\pm]^{3/2} \quad \text{----- (6.1.6)}$$

With $A = 0.985$, $g_1 = 0.8$ and $g_2 = 0.5$ for marine aerosols (Sturm, 1980; Doerffer, 1992). The forward/backward scattering angles are related to the sensor viewing and solar illumination directions through

$$\cos \gamma^\pm = \pm \cos \theta_v \cos \theta_s - \sin \theta_v \sin \theta_s \cos \Phi \quad \text{----- (6.1.7)}$$

Where Φ is the azimuth difference between the sensor viewing and solar illumination directions. Further the Fresnel reflectance (for unpolarized radiation) is given by

$$R(\theta_i) = 0.5 [\sin^2(\theta_i - \theta_j) / \sin^2(\theta_i + \theta_j) + \tan^2(\theta_i - \theta_j) / \tan^2(\theta_i + \theta_j)] \quad \text{---- (6.1.8)}$$

Where θ_j is determined through the relation (Snell's law)

$$\sin \theta_i / \sin \theta_j = n \quad \text{----- (6.1.9)}$$

Where n is the refractive index of water

The Rayleigh radiance (L_r) was computed with the knowledge of atmospheric pressure and sun zenith angle. The difficulty lies in the calculation of aerosol radiance (L_a) as its magnitude and wavelength dependence can vary greatly with position, time and due to variations in aerosol concentration and aerosol optical properties. The most important aerosol property required is AOT. The characterization of the spectral dependence of AOT, documented as Angstrom wavelength exponent (α), is important for modeling the radiative effects of aerosol on the atmosphere/surface system, retrieval of aerosol parameters from satellite remote sensing, and in identification of aerosol source regions (O'Neill and Royer, 1993). The Angstrom turbidity factor (β), which accounts for the total atmospheric turbidity due to aerosols, is also one of the important parameters in understanding the radiative processes in the atmosphere. Hence the aerosol characteristics were analyzed in atmospheres of different optical domains. The details are given in subsequent section.

6.2 Aerosol characterization in different atmospheric optical domains

The spectral AOT was measured using Microtops II sunphotometer. The Microtops II is five bands (380, 440, 500, 675 and 870 nm) hand held sunphotometer, which measures AOT with a full field view of 2.5° . The instrument calculates AOT at each wavelength based on the energy received at the target, its calibration constants, atmospheric pressure, time and position of observation. A built-in pressure sensor was provided to measure the atmospheric pressure, which is mainly used to compute Rayleigh optical depth. A hand held GPS interfaced with the sunphotometer gives the accurate measure of time, position and solar zenith angle.

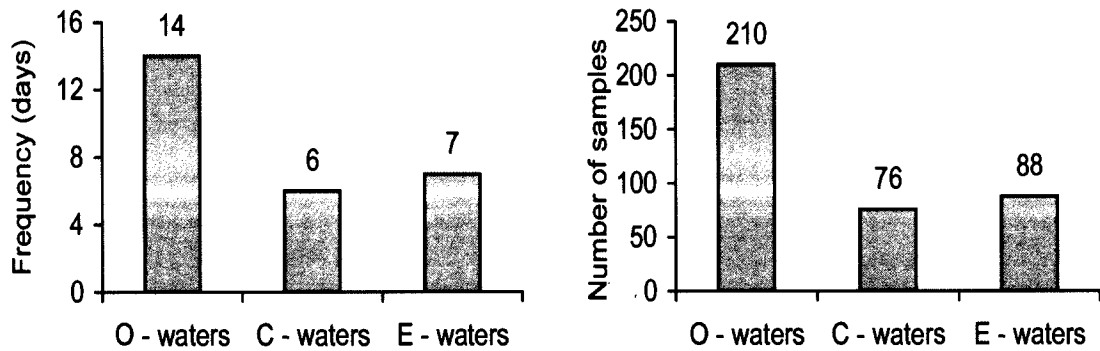


Fig. 6.2.1

Sampling frequency of AOT measurements over open ocean (O), coastal (C) and estuarine (E) waters

Fig. 6.2.1 shows the sampling frequency. The sunphotometer measurements were carried out for 14 days in open ocean (O) – waters (SK 214), 6 days in coastal (C) – waters (Sagar Purvi) and 7 days in estuarine (E) – waters (fishing trawler). The total number of measurements in O, C and E - waters were 210, 76 and 88 respectively (Fig. 6.2.1).

The spectral variations of AOT over the atmospheres of different optical domains (O, C and E – waters) were analyzed. Through spectral analysis of AOT, aerosol size index (Angstrom wavelength exponent, α) and turbidity factor (β) were derived using the following relation by Angstrom (1961, 1964).

$$\tau_a(\lambda) = \beta * \lambda^{-\alpha} \quad \text{----- (6.2.1)}$$

$$\alpha = \text{Ln} [\tau_a(\lambda_1) / \tau_a(\lambda_2)] / \text{Ln} (\lambda_2 / \lambda_1) \quad \text{----- (6.2.2)}$$

Where, λ_1 and λ_2 are two different wavelengths on the exponentially decreasing curve of spectral AOT. In the present study the two wavelengths selected were 675 and 870 nm.

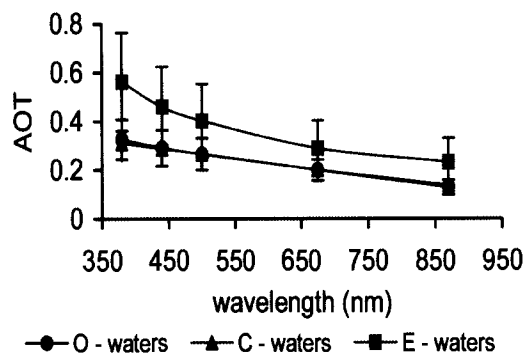


Fig. 6.2.2

Spectral variation of mean AOT over open ocean (O), coastal (C) and estuarine (E) waters. The vertical bars indicate standard deviation.

The spectral variability of mean AOT over atmospheres of different optical domains, i.e. in O, C and E - waters was shown in fig. 6.2.2. The vertical bars indicate standard deviation. The general trend shows an exponential decrease in AOT with increasing wavelength. The lowest values of AOT were encountered over O - waters and the highest over E - waters. The variability of AOT was also maximum over E - waters as seen through standard deviation. The aerosol particles brought from the continents have different origins and hence different chemical compositions. The most common among

the particles are the mineral dust, carbonaceous particles and sulfates. Because of their different chemical compositions, their refractive index differs and hence they have different scattering and absorption efficiencies for different wavelengths. Though it was difficult to estimate the individual contribution from these different aerosol types to the measured AOT, the larger variations seen in the smaller wavelength regions indicate that it is the sub-micron particles. Jayaraman and Ramachandran (2002) studied the AOT in five spectral bands from 400 to 1050 nm using a sun-photometer and aerosol mass concentration in ten size ranges from 0.05 to 25 μm diameter using a sensitive quartz crystal cascade impactor system over the Arabian Sea and the Indian Ocean during the winter months. They found that the general feature was that the AOT spectrum was more or less flat in the perfect air with values below about 0.1 at all wavelengths whereas in the turbid region, close to the coastal areas, a steep increase in AOT was observed at lower wavelengths (resulting in a higher wavelength exponent, α).

The mean spectrum of AOT in O - waters was similar to that over C - waters. The AOT spectrum over E - waters shows a steep slope at lower wavelengths as compared to that of C and O - waters. The scenario was different at the longer wavelengths i.e. beyond 670 nm. The AOT spectrum over E - waters shows lesser slope as compared to that over C and O - waters. In order to have the better understanding of such variability, the Angstrom wavelength exponent (α) and turbidity factor (β) have been analyzed.

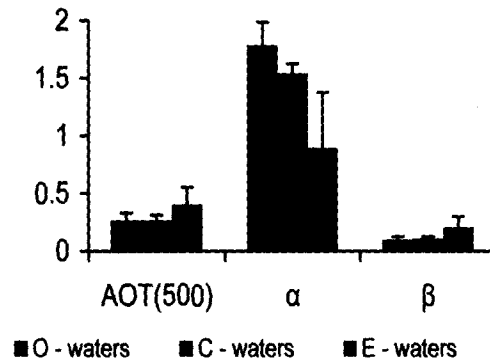


Fig. 6.2.3

Variability of mean AOT at 500 nm, Angstrom wavelength exponent (α) and turbidity factor (β) over open ocean (O), coastal (C) and estuarine (E) waters. The vertical bars indicate standard deviation.

Fig. 6.2.3 shows the variability of AOT at 500 nm (AOT (500)), α and β over O, C and E - waters. The vertical bars indicate the standard deviation. In general AOT (500) increases from O – waters (0.26 ± 0.07) to C – waters (0.40 ± 0.15) with an intermediate value over E – waters (0.27 ± 0.05) atmosphere. The Angstrom wavelength exponent, α , was found to vary with AOT. The higher and lower values of α correspond to the lower and higher values of AOT). The α fluctuations reflect the variations of the aerosol size distributions. The α value increases when the particles size decreases. The maximum value of α equal to 4 corresponds to particles of size of single molecule (Masmoudi et al., 2003; Suresh and Desa, 2005). In their studies, Ramachandran (2004b) encountered α around 1.5 over Coastal India, Arabian Sea, and Tropical Indian Ocean. The 5-year mean β was about 0.14 over Coastal India, 0.10 over Arabian Sea, and about 0.05 over Tropical Indian Ocean indicating the less polluted nature of Tropical Indian Ocean.

The β values were maximum over E - waters (0.21 ± 0.09) and minimum over O - waters (0.10 ± 0.03) with an intermediate values over C - waters (0.11 ± 0.02). This clearly indicates that atmosphere over E – waters was more turbid as compared to that of

O - waters. Also the aerosols exhibit the latitudinal gradient in their variabilities. Similar results were obtained by Ramachandran (2004a) for the study carried out at coastal India, Arabian Sea and tropical Indian Ocean during northeast monsoon. It was observed that over the entire study area, AOT at smaller wavelength 400 nm were more than 3 times higher than those measured at the higher wavelength of 850 nm, indicating the dominance of smaller size aerosols over these oceanic regions.

6.3 Satellite retrieval of atmospheric optical properties

The precise retrieval of ocean colour parameters requires the accurate retrieval of aerosol radiances for which the better understanding of the atmospheric optical properties were required. Aerosol radiance has been derived through IRS – P4 – OCM using Angstrom wavelength exponent approach. The methodology is explained below.

By assuming that the phase function and single scattering albedo were spectrally invariant, the ratio of Eq. 6.1.2 at two different wavelengths yields

$$\alpha = [\text{Log} (L_{a1}/F_{o1}) - \text{Log} (L_{a2}/F_{o2})] / \text{Log} (\lambda_2) - \text{Log} (\lambda_1) \quad \text{----- (6.3.1)}$$

Where L_{a1} and L_{a2} are aerosol radiances corresponding to 765 nm and 865 nm while F_{s1} and F_{s2} are the respective extraterrestrial solar irradiances. As ratio of path radiance between two wavelengths was taken, assumption of spectrally invariant phase function and single scattering albedo won't lead to any discrepancy in the α values. For mapping α , band 7 (765 nm) and band 8 (865 nm) of OCM were chosen. L_a at 765 and 865 nm was

calculated by subtracting L_r from each pixel (Doerffer, 1992; Menon, 2004). Further L_a is mapped for all bands of OCM using the following relationship.

$$L_a (\lambda < 750 \text{ nm}) = L_a (765 \text{ nm}) [F_s (\lambda) / F_s (765 \text{ nm})] [(\lambda / 765)^{-\alpha}] \text{ ----- (6.3.2)}$$

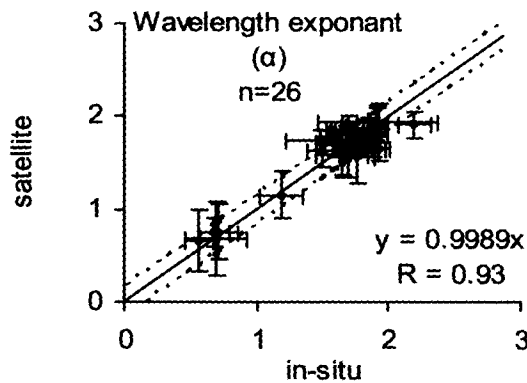


Fig. 6.3.1

Correlation between satellite derived and in-situ Angstrom wavelength exponent (α). The dotted lines were plotted at 95% confidence level. The error bars indicates standard deviation for the data in respective grid.

The validation of α is shown in Fig. 6.3.1. Satellite derived α (Fig. 6.3.1. a) were in good agreement with in-situ measurements. The coefficient of regression (R) was 0.93. The data were tested at 95 % confidence level and found to be significant.

Yan et al. (2002) showed that NIR bands of Sea WiFS 765 nm and 865 nm have water leaving radiance component when the water column / area of study was turbid. Therefore in E – waters, water leaving radiance was expected even in the longer wavelength (NIR bands). Therefore atmospheric correction through identification of dark pixels (by assuming that water leaving radiance is zero in near infrared bands) will not be the right approach to eliminate the effect of atmosphere from each pixel of visible bands. Therefore in the present study, the aerosol radiance was computed over E – waters using

a calibrated radiative transfer model (Menon, 2004). Thus the atmospheric correction to OCM data in E – waters was achieved by eliminating aerosol and rayleigh radiance from each pixel. For the elimination of Rayleigh radiance, methodology given by Doerffer (1992) was adopted.

The accuracy of satellite derived aerosol radiance at 490 nm (L_a490) was given in fig. 6.3.2. The satellite derived L_a490 were significant at 95 % confidence level. The correlation shows a good agreement between satellite derived and in situ values with the coefficient of correlation (R) as 0.97.

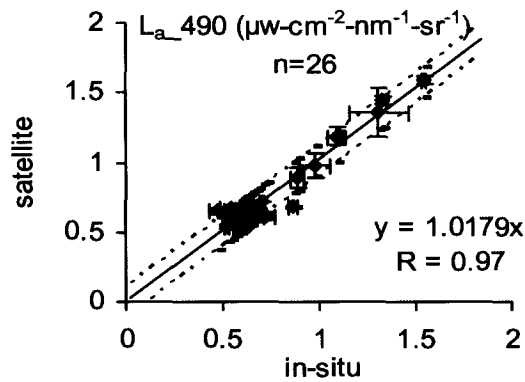


Fig. 6.3.2

Correlation between satellite derived and in situ aerosol radiance (L_a) at 490 nm. The dotted lines indicate 95% confidence level. The error bars indicates standard deviation for the data in respective grid.

Chapter 7

Retrieval of optically active substances from Ocean Colour Monitor

7.1	Satellite data processing -----	(88)
7.2	Synoptic distribution of optically active substances in estuarine waters-----	(89)
7.2.1	Validation of satellite derived optically active substances in estuarine waters-----	(93)
7.3	Synoptic distribution of optically active substances in northeastern Arabian Sea-----	(94)
7.3.1	Validation of satellite derived optically active substances in northeastern Arabian Sea -----	(97)

Optical observations of the marine environment, giving information on ocean colour, have been increasingly used to provide an insight into a number of biogeochemical and physical processes. The subsequent sections deal with the analysis of optically active substances through ocean colour analysis.

7.1 Satellite data processing

IRS – P4 – OCM data was processed using ERDAS IMAGINE 8.4. The data was supplied as unsigned 16-bit binary format. The data was imported into imagery format. Importing was done using IMPORT / EXPORT option in ERDAS IMAGINE icon panel. The information required such as image record length, number of rows, number of columns, line header bytes and file header bytes was obtained from LEADER.OCM. The geometric correction was then performed using Ground Control Points (GCP). The scene input and reference coordinates were taken in the file LEADER.OCM. The coordinates were given in terms of Longitude and Latitude corresponding to pixel and scan. The geometric correction was performed as polynomial. An appropriate polynomial order was set and the images were then projected as 'Geometric Lat / Long'. Subsequently land masking was done to highlight ocean features. For masking the land, binary masking scheme was adopted (Assign, Land=0 and Ocean=1). Then digital numbers (DN) were converted into radiance by dividing the DN values by different constants (Table 7.1.1) corresponding to different bands. The unit of radiance values was $\mu\text{W}\cdot\text{cm}^{-2}\cdot\text{nm}^{-1}\cdot\text{sr}^{-1}$. Subsequent to this, atmospheric correction was applied to different pixel of each visible band as per the method given in chapter 6. Further, the retrieval algorithms were applied to generate chlorophyll_a, TISM and CDOM. Then the images were classified and

composed in a presentable format having colour scale, spatial scale, north arrow, grid lines, tick marks and geographic coordinate labels.

Band No.	Wavelength (nm)	DN conversion factor
1	402 - 422	1334
2	433 - 453	2275
3	480 - 500	2783
4	500 - 520	2972
5	545 - 565	3573
6	660 - 680	4647
7	745 - 785	9974
8	845 - 885	5979

Table 7.1.1

Table showing the constant factor used to convert digital numbers (DN) to the unit of radiance at bands corresponding to that of Ocean Colour Monitor (OCM)

7.2 Synoptic distribution of optically active substances in estuarine waters

The algorithms were applied to OCM data of 12th January, 12th February, 18th March, 13th April, 11th May, 17th September, 09th October, 11th November and 09th December 2005. The synoptic distribution of chlorophyll_a, TISM and CDOM were presented in Fig. 7.2.1, 7.2.2 and 7.2.3 respectively. These scenes were chosen to show the ability of the algorithm in retrieving the OAS during different hydrodynamics of the estuary prevailing in different non-monsoon periods.

The spatial distribution of chlorophyll_a showed that the maximum was in the upper reaches of the estuary throughout the year. The range of concentration prevailing within the estuaries was between 2.0 to 5.0 $\mu\text{g}\cdot\text{l}^{-1}$. Heavy precipitation of the order of 250 – 300 cm yr^{-1} and land runoff (Qasim and Sengupta, 1981) during southwest monsoon period (June – September) brings in huge quantities of nutrients making the estuaries highly productive (Devassy and Goes, 1989). The chlorophyll_a concentration was found to be maximum and almost of the same order of magnitude at the head of the estuaries

during all the months. A large gradient was observed in the distribution of chlorophyll_a, from head to mouth of the estuaries during post-monsoon season (September to December). This gradient diminished gradually as season advances from post-monsoon to pre-monsoon. At the end of the pre-monsoon (during May), the gradient was totally eliminated and the basin was homogenized.

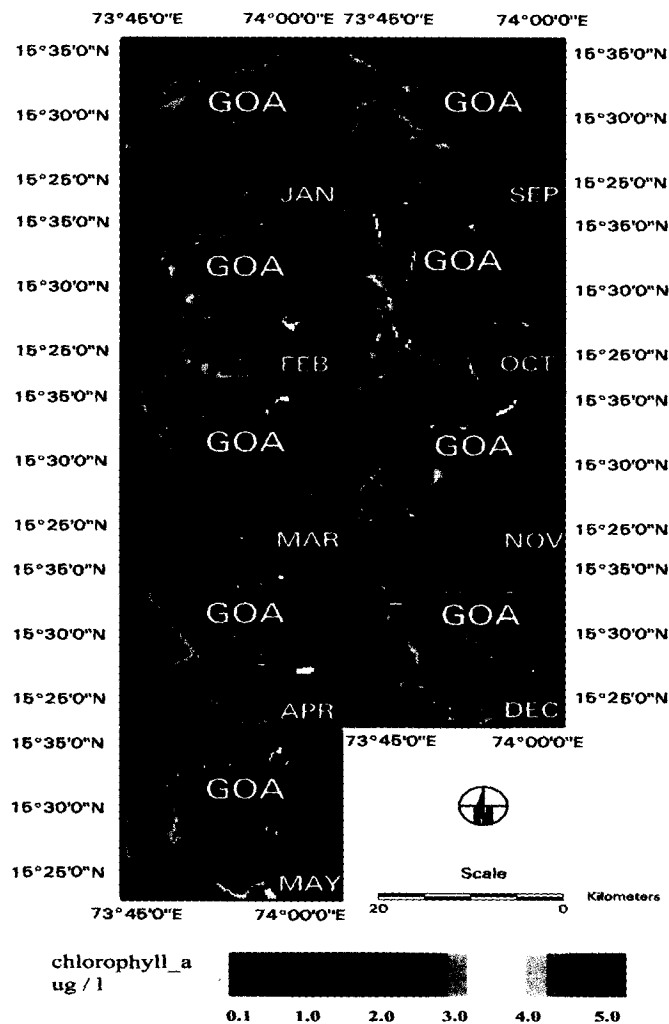


Fig. 7.2.1
 Synoptic distribution of chlorophyll_a in Mandovi and Zuari estuaries of Goa, West coast of India on 12th January, 12th February, 18th March, 13th April, 11th May, 17th September, 09th October, 11th November and 09th December 2005.

The concentration of TISM in the estuarine region was in the range of 14.0 – 22.0 mg-l⁻¹. As seen in the previous case, the sediment maxima were seen in the upper estuary. The distribution pattern in TISM was similar to that of chlorophyll_a. During post-monsoon season, the spatial gradient from head to mouth was high which decreases with progressing month. At the end of the pre-monsoon the gradient was totally diminished and entire estuary was homogenized with the uniform distribution of TISM.

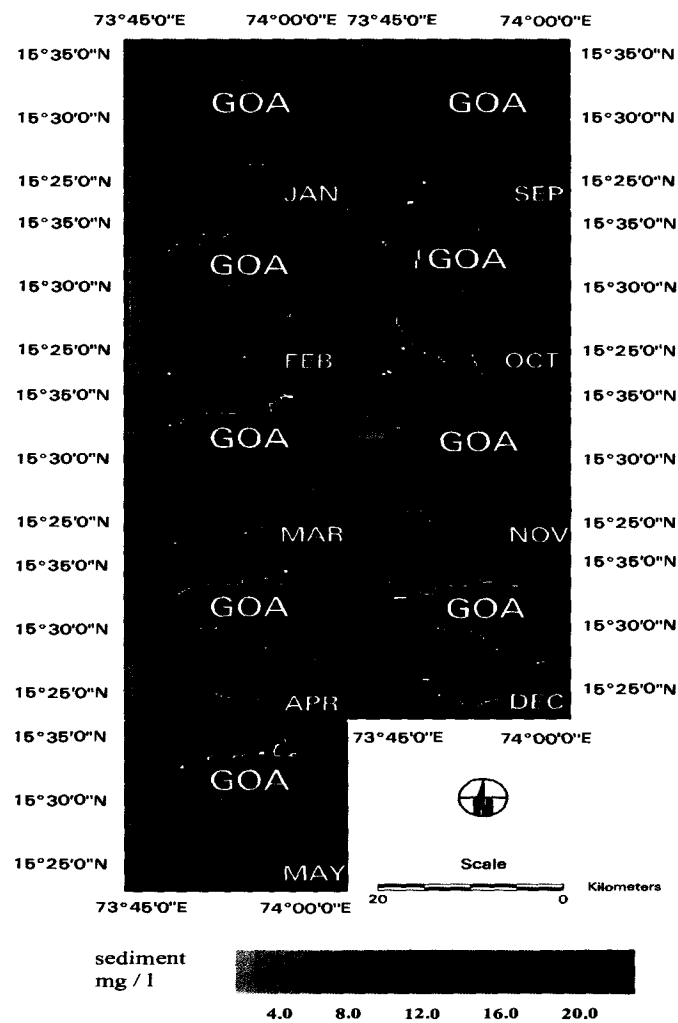


Fig. 7.2.2

Synoptic distribution of TISM in Mandovi and Zuari estuaries of Goa, West coast of India on 12th January, 12th February, 18th March, 13th April, 11th May, 17th September, 09th October, 11th November and 09th December 2005.



Fig. 7.2.3

Synoptic distribution of $a_{CDOM440}$ in Mandovi and Zuari estuaries of Goa, West coast of India on 12th January, 12th February, 18th March, 13th April, 11th May, 17th September, 09th October, 11th November and 09th December 2005.

The $a_{CDOM440}$ was in the range of 0.9 to 2.2 m^{-1} in the estuarine waters. The gradient in the spatial distribution from head to mouth was prominent during post-monsoon. During May, the distribution was uniform throughout the estuarine waters. Further, the distribution of $a_{CDOM440}$ was coinciding with TISM in mid estuary. In their studies Nayak and Bukhari (1992) observed a region of high sediment concentration (22 $mg-l^{-1}$) in the midstream of the estuary. The reason for such a high concentration was

ascribed to the drastic decrease in estuarine depth from mouth to upstream and the effect of tide. This process was enhanced by softer nature of the sediments (Rao and Rao, 1974) and by convergence of currents at the constriction and increasing currents towards the narrow part of the estuary (Pundare, 1989).

The analysis of OAS during different months clearly showed the varying hydrodynamics of the estuaries. The studies on the hydrography and circulation made by Murthy and Das (1972), Verma et al. (1975) and Qasim and Sengupta (1981) showed that estuaries behaved like a homogeneous during pre – monsoon, partially mixed during post-monsoon and salt wedge type during monsoon. Hence they are tidally dominated during pre-monsoon, tide and fresh water influx control them during monsoon and post-monsoon seasons. Therefore through ocean colour analysis, it was possible to study such hydrodynamic features of the estuary.

7.2.1 Validation of satellite derived optically active substances in estuarine waters

The accuracy of the algorithms was tested by validating the results obtained through satellite data with that derived in-situ.

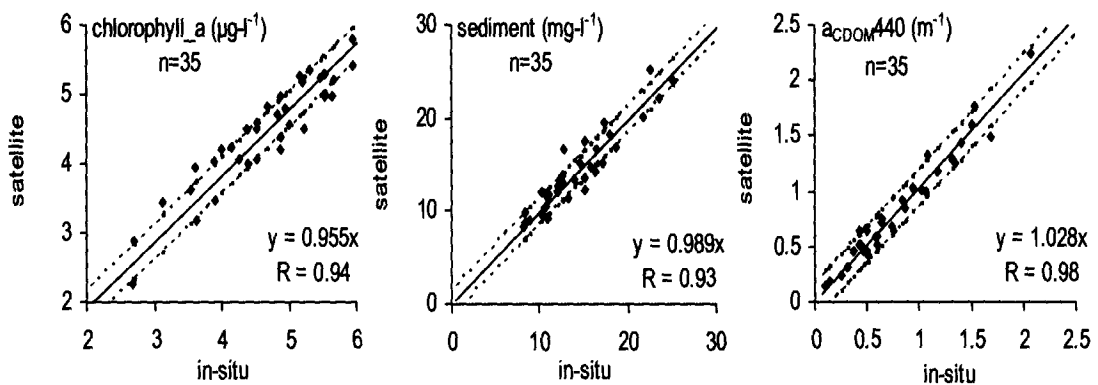


Fig. 7.2.1.1

Correlation between in-situ and satellite derived chlorophyll_a, TISM and $a_{\text{CDOM}440}$ in estuarine waters. The dotted lines represent 95% confidence level.

Fig. 7.2.1.1 shows the regression between satellite derived and in-situ chlorophyll_a, TISM and $a_{CDOM440}$ in Mandovi – Zuari estuarine system of Goa. The results shows that satellite derived and in situ OAS were in good agreement with correlation coefficient (R) 0.94, 0.93 and 0.98 for chlorophyll_a, TISM and $a_{CDOM440}$ respectively. The data were tested at 95% confidence level and was found significant. The RMS error in the retrieval of these OAS in estuarine waters was 15.6 %, 12.9 % and 18.8 % for chlorophyll_a, TISM and $a_{CDOM440}$ respectively.

7.3 Synoptic distribution of optically active substances in northeastern Arabian Sea

The algorithms developed for the northeastern Arabian Sea were applied to two scenes of OCM on 08th January 2003 and 10th December 2004. The scene of 08th January was chosen to account for the robustness of the algorithms in understanding the distribution of OAS during latter phase of the bloom occurred in the Arabian Sea (Dwivedi et al., 2006). The in situ observation carried out during December 2004 onboard SK214 showed that the water was very clear with negligible CDOM during this period. Hence the OCM data of 10th December was processed to validate the algorithms. The algorithms were polynomial in the case of chlorophyll_a, while it was multi-spatial in the case of CDOM, linear in the offshore and polynomial in the inshore waters.

An analysis of OAS during 10th December 2004 showed that chlorophyll_a was in the range of 0.3 to 0.5 $\mu\text{g-l}^{-1}$ and TISM was in the range of 1.0 to 10 mg-l^{-1} . The highest concentration of TISM was found along southern west coast of India.

As seen in the in-situ observations, the satellite derived maps (Fig 7.3.1.) also depicted elevated concentrations of CDOM, chlorophyll_a and sediment in the inshore

waters and uneven patchy nature in the offshore waters. Though chlorophyll_a and CDOM have a similar distribution pattern, sediment distribution differs. In the upper waters it follows that of chlorophyll_a and CDOM while in lower waters unlike chlorophyll_a and CDOM the sediment concentration was more along the inshore than offshore waters. The distribution of chlorophyll_a was fairly uniform with high chlorophyll_a in southeastern Arabian Sea and decreases towards northwest.

The scenario was different during 08th January 2003. An elevated concentration of chlorophyll_a and $a_{\text{CDOM}440}$ were encountered above 20° N and east of 65° E. the chlorophyll_a in this area was between 0.6 to 1.0 $\mu\text{g}\cdot\text{l}^{-1}$ and $a_{\text{CDOM}440}$ was in the range of 6.0 to 12.0 m^{-1} . The possible reasons in such a high $a_{\text{CDOM}440}$ could be fresh water plume or the in situ degradation of phytoplankton. As the inshore waters were not in the vicinity of any fresh water discharge, the first possibility was ruled out. The studies carried out by Prassana Kumar et al. (2001) revealed that the waters above 12° N and east of 64° E display a high degree of physical variability due to the presence of coastal currents and influence of upwelling. This area is also subjected to an intense winter cooling and hence sinking of surface waters (Schott et al., 2002). Therefore high biological activity in the area, through out the year, resulted in higher CO₂ pressure (P_{CO_2}) in surface waters than in the atmosphere (Sarma et al., 1998).

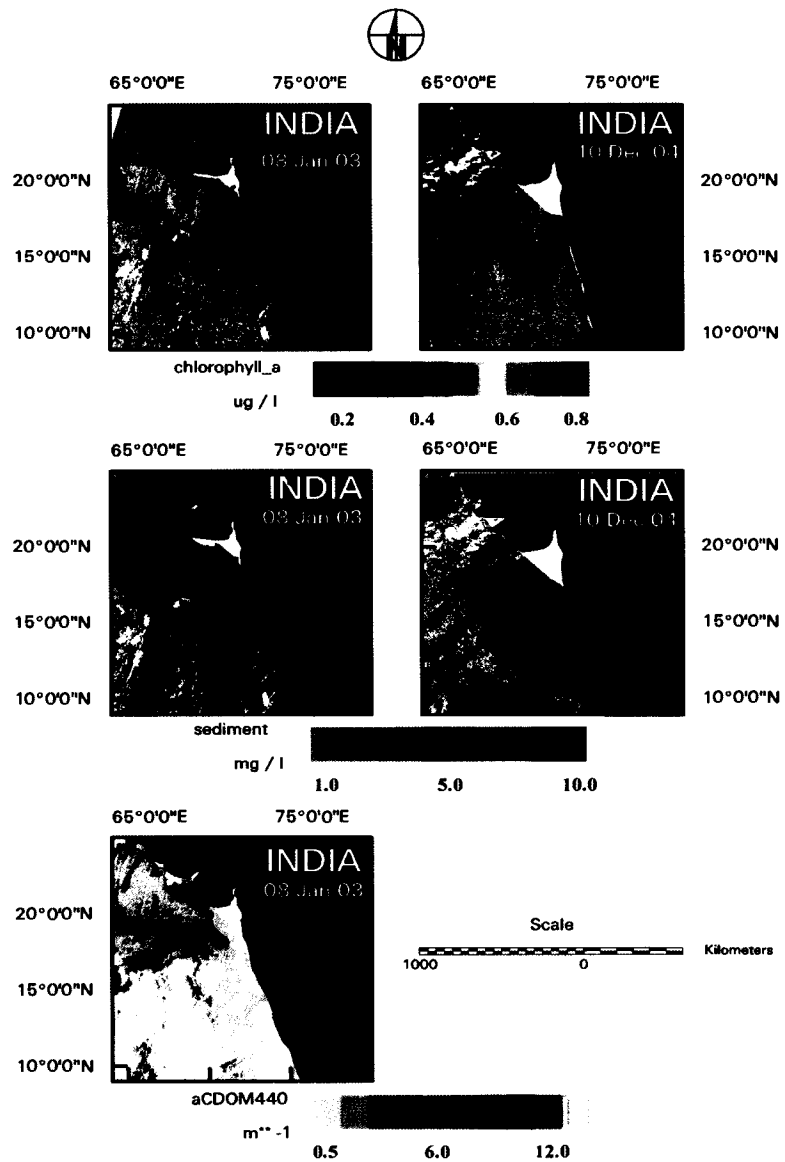


Fig. 7.3.1

Synoptic distribution of a) chlorophyll_a during (i) 08th January 2003 and (ii) 10th December 2004, b) TISM during (i) 08th January 2003 and (ii) 10th December 2004, c) CDOM during 08th January 2003.

7.3.1 Validation of satellite derived optically active substances in northeastern Arabian Sea

The validation of satellite derived OAS in northeastern Arabian Sea were carried out by regressing it with in situ observation. The same data were also processed using standard algorithm for chlorophyll_a (O'Reilly et al., 1998) and sediment (Tassan, 1994) in order to check the accuracy of new algorithm.

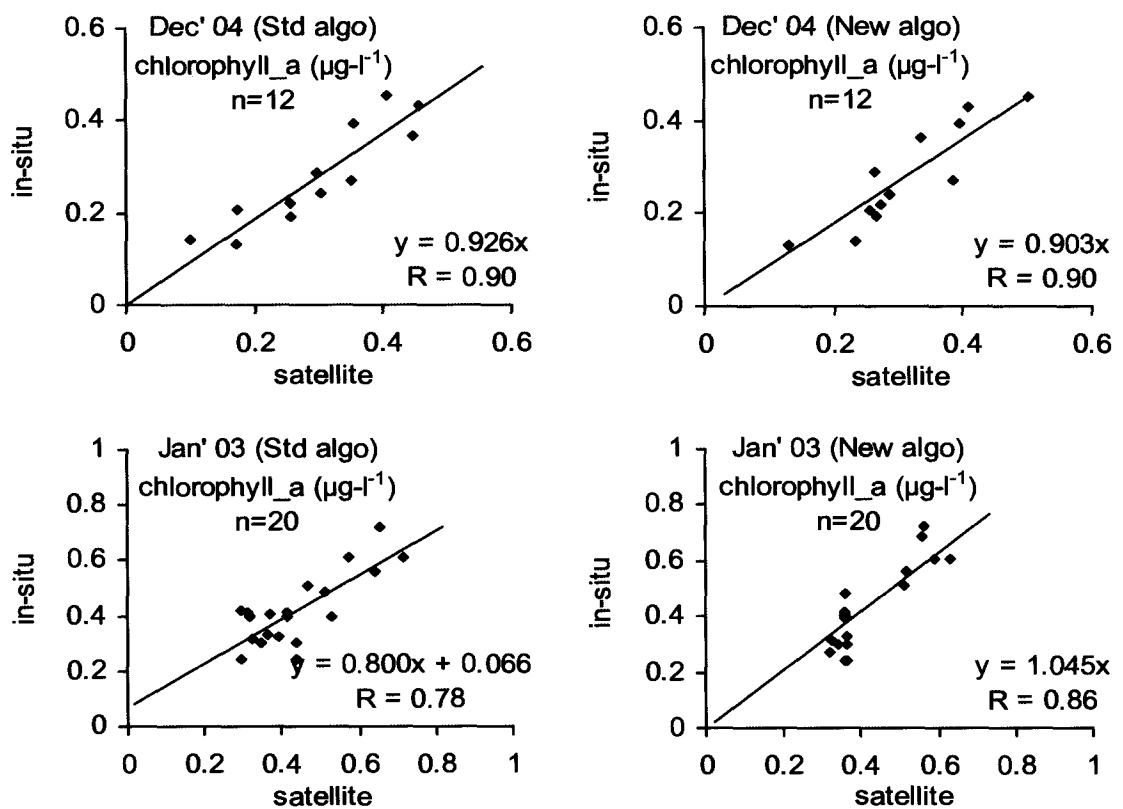


Fig. 7.3.1.1

Correlation between in situ and satellite derived chlorophyll_a using standard algorithm (O'Reilly, 1998) and new algorithm

Fig 7.3.1.1 shows the regression between in-situ and satellite derived chlorophyll_a generated using standard algorithm and new algorithm during December

2004 and January 2003. During December in-situ and satellite derived chlorophyll_a were found in good agreement for the data generated using both the algorithms. Although, satellite derived values were closer to in situ ($\text{in situ} = 0.926 \times \text{satellite}$) using standard algorithm, the new algorithm produces good result ($\text{in situ} = 0.903 \times \text{satellite}$). The regression coefficient was 0.9 in both the cases. During January, it was seen that standard algorithm produces a poor result ($R=0.78$) as compared to new algorithm ($R=0.86$). Also the satellite derived values using new algorithm tends to overestimate the chlorophyll_a values. This was due to the interference of signals form CDOM in blue region.

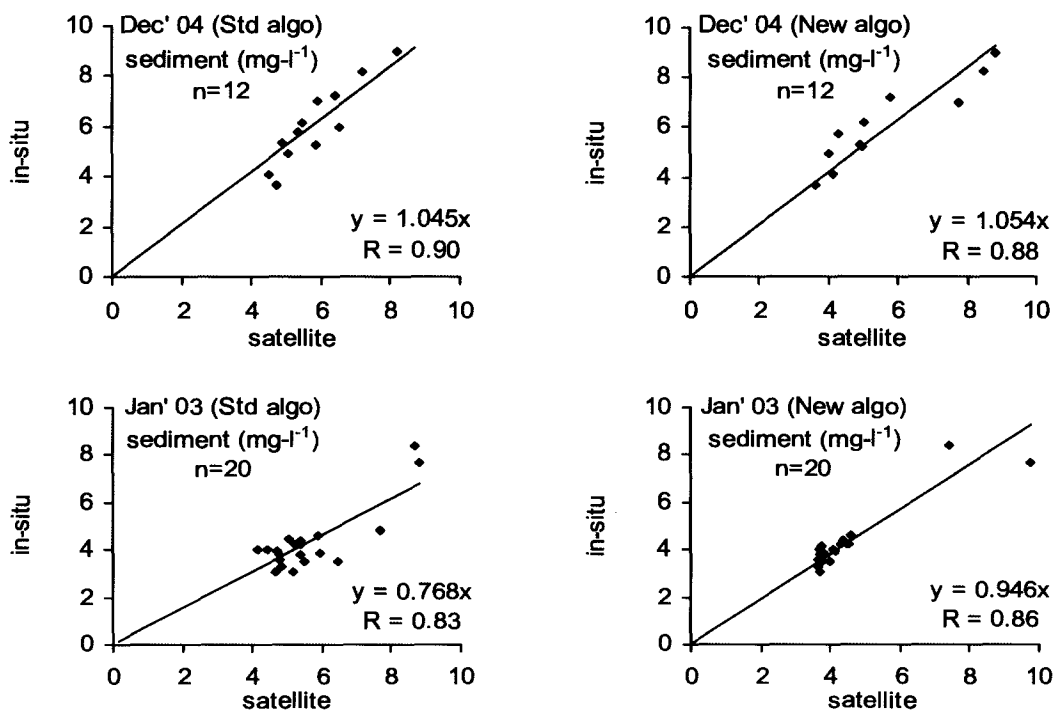


Fig. 7.3.1.2

Correlation between in situ and satellite derived TISM using standard algorithm (Tassan, 1994) and new algorithm

In the case of TISM, it was observed that (Fig. 7.3.1.2) though standard algorithm produces a better results ($R=0.9$) during December, new algorithm works well in clear waters ($R=0.88$). During January, standard algorithm tends to overestimate TISM by 23%. Where as new algorithm produces significantly better results with regression coefficient of 0.86 as compared to 0.83 achieved through standard algorithm.

The in-situ observations carried out during December showed that CDOM was negligible. Also no standard algorithms were available to retrieve CDOM from the area. Hence, the new multi-spatial algorithms were tested in waters sampled during January. The validation of in-situ $a_{\text{CDOM}440}$ with satellite derived produced very good result with regression coefficient of 0.95 (Fig. 7.3.1.3).

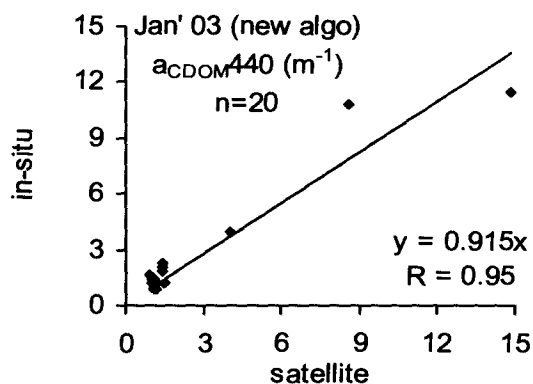


Fig. 7.3.1.3

Correlation between in situ and satellite derived $a_{\text{CDOM}440}$ using new algorithm

Chapter 8

Summary and Conclusion

8.1	Summary-----	(100)
8.2	Conclusion-----	(101)

8.1 Summary

The flowchart given in Fig. 8.1.1 explains the systematic flow of the research work. Observations were performed in oceanic waters and atmosphere above. In water radiometric measurements were carried out in seven bands for the estimation of light field within the water column along with water sample collection. AOP were derived from radiometric measurement whereas IOP were derived from water sample analysis (Menon et al., 2005). IOP were also derived from AOP using an inversion algorithm (McKee et al., 2003). Water leaving radiance was then simulated using a bio-optical and radiative transfer model using IOP (Doerffer, 1992; Menon, 2004). The simulated water leaving radiance was validated against that measured using radiometer. Further, using the water leaving radiance, band-ratio algorithms were developed for the retrieval of OAS through OCM (Menon et al., 2006a, b).

The atmospheric measurements were performed using Microtops II sunphotometer. The AOT was generated at five channels. Using AOT, Angstrom wavelength exponent (α) and turbidity factor (β) were generated (Angstrom, 1961, 1964). Subsequently, path radiance (Aerosol and Rayleigh radiance) was simulated using a radiative transfer model (Doerffer, 1992; Menon, 2004). A proper atmospheric correction technique was developed so as to eliminate all the noise received by OCM due to intermediate atmosphere. The OCM data were then processed to map OAS after applying atmospheric correction.

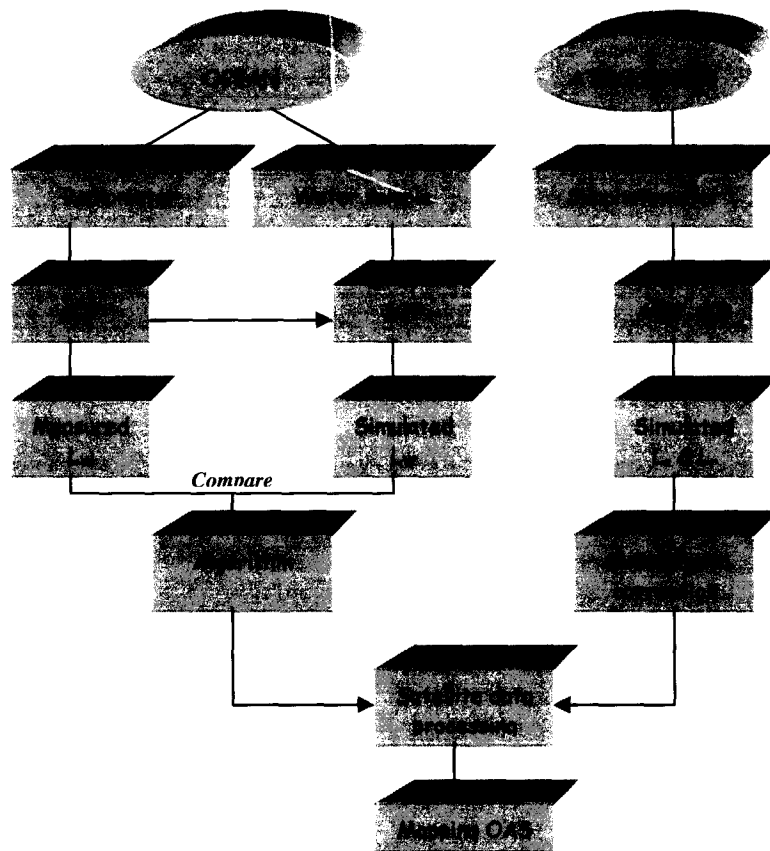


Fig. 8.1.1. Flowchart showing the summary of the thesis

8.2. Conclusion

The significant conclusions drawn from the research work were as follows.

- The optical properties of the water column varied largely with the domains and also reflected the nature of OAS present in the water column. Downwelling diffuse attenuation coefficient (k_d) was maximum in red and minimum in blue part of EMR in open ocean waters, minimum in green and maximum in blue and red part of EMR in coastal waters and maximum in blue and minimum in red part of EMR in estuarine waters.

Bibliography

- The relationship developed between k_d (490) and deep chlorophyll maxima (DCM) can very well be used for retrieval of DCM from any ocean colour sensor.

- Chlorophyll_a was found to be a major light absorbing component in open ocean waters, whereas in coastal waters it was CDOM and in estuarine waters it was TISM.

- Algorithms were derived to retrieve OAS such as chlorophyll_a, TISM and CDOM using IRS – P4 – Ocean Colour Monitor data. The wavelengths used for developing the algorithms were found to be same irrespective of the area of study. But depending on the optical complexity, algorithm can be linear or non-linear. This means it can be linear, 2nd degree or 3rd degree polynomial. It was shown that through ocean colour analysis, estuarine dynamics could be well explained. For the first time, this study revealed that it was possible to delineate an area of perennial source of CO₂ through mapping CDOM.

- The atmospheric correction procedure using Angstrom wavelength exponent approach provided good result. The satellite derived aerosol radiances were in good agreement with in-situ.

- Abbott, M. R., Zion, P. M. 1985. Satellite observations of phytoplankton variability during an upwelling event. *Continental Shelf Research*, 4, 661 – 680.
- Alberotanza, L. 1989. Marine Applications. In “Imaging Spectroscopy: Fundamentals and Prospective Applications”. Toselli, F., Bodechtel, J. (Eds.). Kluwer Academic Publishers, London, 193–213.
- Angstrom, A. 1961. Techniques of determining the turbidity of the atmosphere. *Tellus*, 13, 214 - 223.
- Angstrom, A. 1964. The parameters of atmospheric turbidity. *Tellus*, 16, 64 – 75.
- Ansari, Z. A., Sreepada, R. A., Dalal, S. G., Ingole, B. S., Chatterji, A. 2003. Environmental influence on the trawl catches in a bay – estuaries of Goa, West coast of India. *Estuarine Coastal and Shelf Science*, 56, 503 – 515.
- Babin, M., Morel, A., Fournier-Sicre, V., Fell, F., Stramski, D. 2003. Light scattering properties of marine particles in coastal and open ocean waters related to the particle mass concentration. *Limnology and Oceanography*, 48, 843 – 859.
- Babin, M., Stramski, D., Ferrari, G. M., Claustre, H., Bricaud, A., Obolensky, G., Hoepffner, N. 2003. Variations in the light absorption coefficients of phytoplankton, nonalgal particles, and dissolved organic matter in coastal waters around Europe. *Journal of Geophysical Research (C)*, 108, 7, 1 – 4.
- Barlow, R. G., Aiken, J., Holligan, P. M., Cummings, D. G., Maritorena, S., Hooker, S. 2002. Phytoplankton pigment and absorption characteristics along meridional transects in the Atlantic Ocean. *Deep Sea Research I*, 47, 637 – 660.
- Bauer, S., Hitchcock, G. L., Olson, D. B. 1991. Influence of monsoonally forced Ekman dynamics of upper layer depth and phytoplankton biomass distribution in the Arabian Sea. *Deep Sea Research*, 38, 531 – 553.

- Behrenfeld, M. J., Falkowski, P. G. 1997. A consumer's guide to phytoplankton primary productivity models. *Limnology and Oceanography*, 42, 1479 – 1491.
- Belzile, C., Vincent, W. F., Howard-Williams, C., Hawes, I., James, M. R., Kumagai, M., Roesler, C. R. 2004. Relationship between spectral optical properties and optically active substances in a clear oligotrophic lake. *Water Resources Research*, 40, W12512, doi:10.1029/2004WR003090.
- Belzile, C., Johannessen, S. C., Gosselin, M., Demers, S., Miller, W. L. 2000. Ultraviolet attenuation by dissolved and particulate constituents of first-year ice during late spring in an Arctic polynya. *Limnology and Oceanography*, 45, 1265–1273.
- Binding, C. E., Bowers, D. G., Mitchelson-Jacob, E. G., 2005. Estimating suspended sediment concentrations from ocean colour measurements in moderately turbid waters: the impact of variable particle scattering properties. *Remote Sensing of Environment*, 94, 373-383.
- Blough, N. V., Del Vecchio, R. 2002. Distribution and dynamics of chromophoric dissolved organic matter (CDOM) in coastal environment. In Hansell, D. A., Carison, C. A. (Eds). *Biogeochemistry of marine dissolved organic matter* Academic press, New York, 500.
- Blough, N. V., Green, S. A. 1995. Spectroscopic characterization and remote sensing of non-living organic matter. In *The Dahlem Workshop on the Role of Nonliving Organic Matter in the Earth's Carbon Cycle*, Berlin, 1993, eds by Zepp, R. G., Sonntag, C. 23–45, John Wiley, New York.
- Bowers, D. G., Binding, C. E. 2006. The optical properties of mineral suspended particles: A review and synthesis. *Estuarine, Coastal and Shelf Science*, 67, 219 – 230.

- Bowers, D. G., Evans, D., Thomas, D. N., Ellis, K., Williams, P. J. le. B. 2004. Interpreting the colour of an estuary. *Estuarine, Coastal and Shelf Science*, 59, 13 – 20.
- Bowers, D. G., Harker, G. E. L., Smith, P. S. D., Tett, P., 2000. Optical properties of a region of freshwater influence (the Clyde Sea). *Estuarine Coastal and Shelf Science*, 50, 717 – 726.
- Bricaud, A., Morel, A., Babin, M., Allali, K., Claustre, H. 1998. Variations of light absorption by suspended particles with the chlorophyll a concentration in oceanic (case I) waters: Analysis and implications for bio-optical models. *Journal of Geophysical Research*, 103, 31,033 – 31, 044.
- Bricaud A., Babin M., Morel A., Claustre H. 1995. Variability in the chlorophyll-specific absorption coefficients of natural phytoplankton: analysis and parameterization. *Journal of Geophysical Research*, 100, 13321–13332.
- Carder, K. L., Chen, F. R., Lee, Z. P., Hawes, S. K., Kamykowski, D. 1999. Semianalytic moderate-resolution imaging spectrometer algorithms for chlorophyll a and absorption with bio-optical domains based on nitrate depletion temperatures. *Journal of Geophysical Research*, 104, 5403-5421.
- Carder, K. L., Steward, R. G., Harvey, G. R., Ortner, P. B. 1989. Marine humic and fulvic acids: their effects on remote sensing of ocean chlorophyll. *Limnology and Oceanography*, 34, 1, 68 – 81.
- Chang, G., Mahoney, K., Whitmire, A. B., Kohler, D. D. R., Mobley, C. D., Lewis, M., Moline, M. A., Boss, E., Kim, M., Philpot, W., Dickey, T. D. 2004. The new age of hyperspectral oceanography. *Oceanography*, 17, 16 – 23.
- Chang, G.C., Dickey, T.D., 2001. Optical and physical variability on timescales from minutes to the seasonal cycle on the New England shelf: July 1996 to June 1997. *Journal of Geophysical Research*, 106, 9434-9453.

- Charlson, R. J., Schwartz, S. E., Hales, J. M., Cess, R. D., Coakley (Jr.), J. A., Hansen, J. E., Hoffman, D. J. 1992. Climate forcing by anthropogenic aerosols. *Science*, 255, 423-430.
- Charlson, R. J., Lovelock, J. E., Andreae, M. O., Warren, S. G. 1987. Oceanic phytoplankton, atmospheric sulphur, cloud albedo and climate. *Nature*, 326, 655 - 657.
- Chauhan, P., Mohan, M., Nayak, S. R., Navalgund, R. R. 2002. Comparison of ocean colour algorithms for IRS-P4-OCM sensor using in-situ data. *Journal of Indian Society of Remote Sensing*, 30, 1&2, 2002.
- Ciotti, A. M., Lewis, M. R., Cullen, J. J. 2002. Assessment of the relationships between dominant cell size in natural phytoplankton communities and the spectral shape of the absorption coefficient. *Limnology and Oceanography*, 47, 2, 404-417.
- Coble, P. G. 1996. Characterization of marine and terrestrial DOM in seawater using excitation – emission spectroscopy. *Marine Chemistry*, 51, 325 – 346.
- Stedmon, C. A., Markager, S., Bro, R. 2003. Tracing dissolved organic matter in aquatic environments using a new approach to fluorescence spectroscopy. *Marine Chemistry*, 82, 239– 254.
- Conde, D., Aubriot, L., Sommaruga, R. 2000. Changes in UV penetration in marine intrusions and freshwater discharge in a shallow coastal lagoon of the Southern Atlantic Ocean. *Marine Ecological Progressive Series*, 207, 19 – 31.
- D'sa, E. J., Miller, R. L. 2003. Bio – optical properties in water influenced by the Mississippi River during flow conditions. *Remote Sensing of Environment*, 84, 538 – 549.
- Darecki, M., Weeks, A., Sagan, S., Kowalczyk, P., Kaczmarek, S. 2003. Optical characteristics of two contrasting Case 2 waters and their influence on remote sensing algorithms. *Continental Shelf Research*, 23, 237 – 250.

- Das, I., Mohan, M., Krishnamoorthy, K. 2002. Detection of marine aerosols with IRS – P4 – Ocean Colour Monitor. Proceeding of Indian Academy of Science (Earth and Planetary Science), 111, 4, 425 – 435.
- Devassy, V. P., Goes, J. I. 1989. Seasonal patterns of phytoplankton biomass and productivity in tropical estuarine complex (west coast of India). Proceedings of Indian Academy of Science (Plant Science), 99, 485 – 501.
- Devassy, V. P., Goes, J. I., 1988. Phytoplankton Community Structure and Succession in a Tropical Estuarine Complex (Central West Coast of India). Estuarine, Coastal and Shelf Science, 27, 671-685.
- Devassy, V. P., Battathiri, P. M. A., Qasim, S. Z. 1978. Trichodesmium phenomenon. Indian Journal of Marine Sciences, 7, 168 – 186.
- Doerffer, R. 1992. Imaging Spectroscopy for Detection of Chlorophyll and Suspended Matter. In GKSS 92/E/54, 215 – 257.
- Doerffer, R., Fisher, J. 1994. Concentration of chlorophyll, suspended matter and gelbstoff in case II waters derived from satellite coastal zone colour scanner data with inverse modeling method. Journal of Geophysical Research, 99, 7457 – 7466.
- Doxaran, D., Cherukuru, N., Lavender, S. J. 2006. Apparent and inherent optical properties of turbid estuarine waters: measurements, empirical quantification relationships and modeling. Applied Optics, 45, 10, 2310 – 2324.
- Doxaran, D., Froidefond, J. M., Castang, P. 2003. Remote sensing reflectance of turbid sediment dominated waters. Reduction of sediment type variation and changing illumination conditions effects using reflectance ratios. Applied Optics, 42, 2623 – 2634.

- Doxaran, D., Froidefond, J. M., Castang, P. 2002. A reflectance band ratio used to estimate suspended matter concentrations in sediment-dominated coastal waters. *International Journal of Remote Sensing*, 23, 23, 5079 – 5085.
- Dwivedi, R. M., Raman, M., Parab, S., Matondkar, S. G. P., Nayak, S. R. 2006. Influence of northeasterly trade winds on intensity of winter bloom in Northern Arabian Sea. *Current Science*, 90, 10, 1937 – 1406.
- Eisma, D., Kalf, J. 1987. Distribution, organic content and particle size of suspended matter in the North Sea. *Netherlands Journal of Sea Research*, 21, 265–285.
- Field, C. B., Behrenfeld, M. J., Randerson, J. T., Falkowski, P. 1998. Primary production of the biosphere: integrating terrestrial and oceanic components. *Science*, 281, 237-240.
- Froidefond, J. M., Lavender, S., Laborde, P., Herbland, A., Lafon, V. 2002. SeaWiFS data interpretation in a coastal area in the Bay of Biscay. *International Journal of Remote Sensing*, 23, 5, 881 – 904.
- Fujiki, T., Taguchi, S. 2002. Variability in chlorophyll a specific absorption coefficient in marine phytoplankton as a function of cell size and irradiance. *Journal of Plankton Research*, 24, 9, 859 – 874.
- Gallegos, C.L., Neale, P.J., 2002. Partitioning spectral absorption in case 2 waters: discrimination of dissolved and particulate components. *Applied Optics* 41, 4220-4233.
- Gallie, E. A., Murtha, P. A. 1992. Specific absorption and backscattering spectra for suspended minerals and chlorophyll-a in Chilko Lake, British Columbia. *Remote Sensing of Environment*, 39, 103-118.
- Gerhardt, F. R., James, G. S., Denise, L. B. 2003. Seasonal variability in response of estuarine phytoplankton communities to stress: Linkages between toxic trace elements and nutrient enrichment. *Estuaries*, 26, 323-338.

- Gordon, H. R. 1997. Atmospheric correction of Ocean Colour Imagery in the Earth Observing System Era. *Journal of Geophysical Research*, 102D, 17081 – 17106.
- Gordon, H. R. 1989. Can the Lambert – Beer law be applied to the diffuse attenuation coefficient of ocean water? *Limnology and Oceanography*, 34, 1389 – 1409.
- Gordon, H. R. 1978. Removal of atmospheric effects from satellite imagery of the ocean. *Applied Optics*, 17, 1631 - 1636.
- Gordon, H. R., Morel, A. 1983. *Remote Assessment of Ocean Color for Interpretation of Satellite Visible Imagery: A Review*, 114, Springer, New York.
- Gordon, H. R., Clark, D. K., Muller, J. L., Hovis, W. A. 1980. Phytoplankton pigment derived from Nimbus 7 CZCS: Initial comparisons with surface measurements. *Science*, 210, 63 – 66.
- Green, R. E., Sosik, H. M. 2004. Analysis of apparent optical properties and ocean colour model using measurements of seawater constituents in New England continental shelf waters. *Journal of Geophysical Research*, 109, C03026, doi:10.1029/2003JC001977.
- Green, S., Blough, N. 1994. Optical absorption and fluorescence properties of chromophoric dissolved organic matter in the natural waters. *Limnology and Oceanography*, 39, 1903 – 1916.
- Gregg, W. W., Casey, N. W., McClain, C. R. 2005. Recent trends in global ocean chlorophyll. *Geophysical Research Letters*, 32, L03606, doi: 10.1029 / 2004 GL 021808.
- Gross, L., Thiria, S., Frouin, R. 1999. Applying artificial neural network methodology to ocean colour remote sensing. *Ecological Modeling*, 120, 237 – 246.
- Han, Q., Rossow, W. B., Lacis, A. A. 1994. Near-global survey of effective droplet radii in liquid water clouds using ISCCP data. *Journal of Climate*, 7, 465-497.

- Hoepffner, N., Sathyendranath, S. 1993. Determination of the major groups of phytoplankton pigments from the absorption spectra of total particulate matter. *Journal of Geophysical Research*, 98, 22789 – 22803.
- Hovis, W. A. 1980. Coastal Zone Color Scanner: system description and initial imagery, *Science*, 210, 60–63.
- IOCCG, 2000. Remote Sensing of Ocean Colour in Coastal, and Other Optically-Complex, Waters. In “Reports of the International Ocean-Colour Coordinating Group”. S. Sathyendranath (Ed.), No. 3, IOCCG, Dartmouth, Canada.
- IOCCG. 1999. Status and Plans for Satellite Ocean-Colour Missions: Considerations for Complementary Missions. In “Reports of the International Ocean-Colour Coordinating Group”. J. A. Yoder (Ed.), No. 2, IOCCG, Dartmouth, Canada.
- Jayaraman, A., Ramachandran, S. 2002. In situ study of aerosol characteristics over the Arabian Sea and Indian Ocean of relevance to correction of satellite remote sensed data. *Advances in Space Research*, 25, 5, 1045 – 1049.
- Jeffery, S. W., Mantoura, R. F. C. 1997. Development of pigment methods for oceanography: SCOR – supported Working Groups and objectives. In “Phytoplankton Pigments in Oceanography: Guidelines to Modern Methods”. S. E. Jeffery, R. F. C. Mantoura and S. W. Wright (Ed.), Paris: UNESCO Publishing, 19 – 36.
- Jerlov, N. G. 1976. *Optical Oceanography*, Elsevier, New York, 118 – 112.
- Karabulut, M., Ceylan, N. 2005. The spectral reflectance responses of water with different levels of suspended sediment in the presence of algae. *Turkish Journal of Engineering and Environmental Science*, 29, 351 – 360.
- Kaufman, Y. J., Tanre, D., Gordon, H. R., Nakajima, T., Lenoble, J., Frouin, R., Grassl, H., Herman, B. M., King, M. D., Teillet, P. M. 1997. Passive remote sensing of

tropospheric aerosol and atmospheric correction for the aerosol effect. *Journal of Geophysical Research*, 102, D4, 16815 – 16830.

Kibirige, I., Perissinotto, R. 2003. The zooplankton community of the Mpenjati Estuary, a South African temporarily open/closed system, *Estuarine Coastal and Shelf Science*, 58, 727–741.

Kirk, J. T. O. 1994. *Light and Photosynthesis in aquatic ecosystem*. Cambridge University Press, Cambridge, 509.

Kowalczyk, P., Darecki, M., Olszewski, J., Kaczmarek, S., 2005. Empirical relationships between Coloured Dissolved Organic Matter (CDOM) absorption and apparent optical properties in Baltic Sea waters. *International Journal of Remote Sensing* 26, 345–370.

Kowalczyk, P., Cooper, W. J., Whitehead, R., Durako, M.J., Sheldon, W.J., 2003. Characterization of CDOM in an organic-rich river and surrounding coastal ocean in the South Atlantic Bight. *Aquatic Sciences* 65, 384 - 401.

Kowalczyk, P., Kaczmarek, S. 1996. Analysis of temporal and spatial variability of Yellow Substance absorption in the southern Baltic. *Oceanologia*, 3 – 32.

Krishna Kumari, L., Bhattathiti, P. M. A., Matondkar, S. G. P., John, J. 2002. Primary productivity in Mandovi-Zuari estuaries in Goa. *Journal of Marine Biological Association of India*, 44, 1&2, 1 – 13.

Krishnamurthi, T., Jha, B., Rasch, P., Ramnathan, V. 1997. A high resolution global reanalysis highlighting the winter monsoon, Part I, Reanalysis fields, *Meteorology and Atmospheric Physics*, 64, 123 – 150.

Leon, J. F., Chazette, P., Dulac, F., Pelon, J., Flamant, C., Bonazzola, M., Foret, G., Alfaro, S. C., Cachier, H., Cautenet, S., Hamonou, E., Gaudichet, A., Gomes, L., Rajot, J. L., Lavenu, F., Inamdar, S. R., Sarode, P. R., Kadadevarmath, J. S. 2001.

- Large – scale advection of continental aerosols during INDOEX. *Journal of Geophysical Research*, 106, D22, 28427 – 28439.
- Lewis, M. R., Carr, M. E., Feldman, G. C., Esaias, W., McClain, C. 1990. Influence of penetrating solar radiation on the heat budget of the equatorial Pacific Ocean. *Nature*, 347, 543 – 545.
- Liu, C. C., Carder, K. L., Miller, R. L., Ivey, J. E. 2002. Fast and accurate model of underwater scalar irradiance. *Applied Optics*, 41, 4962 – 4974.
- Lorenz, S. E., Cai, W. 2006. Satellite ocean colour assessment of air-sea fluxes of CO₂ in a river-dominated margin. *Geophysical Research Letters*, 33, L01601, doi: 10.1029 / 2005 GL023942.
- Madhupratap, M., Sawant, S. and Gauns, M. 2000. A first report on a bloom of the marine prymnesiophycean, *Phaeocystis globosa* from Arabian Sea. *Oceanologica Acta*, 23, 1, 83 – 90.
- Magnuson, A., Harding (Jr), L. W., Mallonee, M. E., Adolf, J. E. 2004. Bio-optical model for Chesapeake Bay and the Middle Atlantic Bight. *Estuarine, Coastal and Shelf Science*, 61, 403-424.
- Masmoudi, M., Chaabane, M., Tanre, D., Gouloup, P., Blarel, L., Elleuch, F. 2003. Spatial and temporal variability of aerosol: size distribution and optical properties. *Atmospheric Research*, 66, 1– 19.
- McKee, D., Cunning, A., Slater, J., Jones, K. J., Griffiths, C .R. 2003. Inherent and apparent optical properties in coastal waters: a study of the Clyde Sea in early summer. *Estuarine, Coastal and Shelf Science*, 56, 369 – 376.
- Menon, H. B. 2004. Calibration of an optical equation to analyze the atmospheric turbidity and water quality of an estuarine environment. *Photonirvachak, Journal of Indian Society of Remote Sensing*, 32, 287 - 300.

- Menon, H. B., Lotliker, A., Nayak, S. R. 2005. Pre-monsoon bio-optical properties in estuarine, coastal and Lakshadweep waters. *Estuarine, Coastal and Shelf Science*, 63, 211-223.
- Menon, H. B., Lotliker, A. A., Nayak, S. R. 2006a. Analysis of estuarine colour components during non-monsoon period through Ocean Colour Monitor. *Estuarine, Coastal and Shelf Science*, 66, 523 – 531.
- Menon, H. B., Lotliker, A. A., Krishna Moorthy, K., Nayak, S.R. 2006b. Variability of Remote sensing reflectance and implications for optical remote sensing – A study along the eastern and north eastern waters of Arabian Sea. *Geophysical Research letters*, 33, L15602, doi:10.1029/2006GL026026.
- Mishra, D. R., Narumalani, S., Rundquist, D., Lawson, M. 2005. Characterizing the vertical diffuse attenuation coefficient for downwelling irradiance in coastal waters: Implications for water penetration by high resolution satellite data. *Photogrammetry and Remote Sensing*, 60, 48 – 64.
- Mobley, C. D. 1994. *Light and Water; Radiative transfer in natural waters*. San Diego: Academic Press.
- Morel, A. 1991. Light and marine photosynthesis: a spectral mode with geochemical and climatological implications. *Progresses in Oceanography*, 26, 263.
- Morel, A. 1988. Optical modeling of the upper ocean in relation to its biogenous matter content (case I waters). *Journal of Geophysical Research*, 93, C9, 10749 – 10768.
- Morel, A. 1974. Optical properties of pure water and sea water. In Jerlov, N. G., Nielsen, E. S. (Eds). *Optical aspects of oceanography*. Academic press, 1 – 24.
- Morel, A., Prieur, L. 1977. Analysis of variation in ocean colour. *Limnology and Oceanography*, 22, 709 – 722.

- Moulin, C., Gordon, H. R., Banzon, V. F., Evans, R. H. 2001. Assessment of Saharan dust absorption in the visible Sea WiFS imagery. *Journal of Geophysical Research*, 106, D16, 18239 – 18249.
- Mukai, S., Sano, I., Okado, Y. 2000. Inverse problems in the atmosphere – ocean system: estimation of aerosol characteristics and phytoplankton distribution. *Applied Mathematics and Computation*, 116, 93 – 101.
- Muller, J. L., Austin, R.W. 1995. Ocean Optics protocols for Sea WiFs validation, Revision 1. NASA technical Memorandum 104566, 25, eds by Hooker, S. B., Firestone E. R., Acker J. G. (Greenbelt, MD: NASA), 1 – 67.
- Murthy C. S., Das, P. K., Nair, R. R., Veerayya, M., Varadachari, V. V. R. 1976. Circulation and sedimentation process in and around the Aguada bar. *Indian Journal of Marine Science*, 5, 9 – 17.
- Murthy, C. S., Das, P. K. 1972. Pre – monsoon tidal flow characteristics of Mandovi estuary. *Indian Journal of Marine Science*, 1, 220 – 225.
- Navalgund, R. R., Kiran Kumar, A. S. 2001. Ocean Colour Monitor (OCM) on Indian Remote Sensing Satellite IRS-P4. <http://www.ioccg.org/general/ocm/ocm.html>
- Nayak, G. N., Bukhari, S. S. 1992. Spatial and temporal distribution of total suspended matter and other associated parameters in the Zuari estuary, Goa. *Journal of Indian association of Sedimentologists*, 11, 55 – 69.
- Nayak, S. R., Sahay, B. 1985. Coastal Morphology: A case study of the Gulf of Kambhat (Cambay). *International Journal of Remote Sensing*, 6, 559 – 567.
- Neale, P. J., Kieber, D. J. 2000. Assessing biological and chemical effects of UV in the marine environment: Spectral weighting functions. In “Causes and Environmental Implications of Increased UV-B Radiation”. R. E. Hester and R. M. Harrison (Ed.), *Issues in Environmental Science and Technology*. The Royal Society of Chemistry. Cambridge, UK, 14, 61 – 83.

- Neill, M. 2005. A method to determine which nutrient is limiting for plant growth in estuarine waters at any salinity. *Marine Pollution Bulletin* 50, 945-955.
- Nickel, H., Labs, D. 1984. The solar radiation between 3300 and 12500 Å. *Solar Physics*, 90, 202 – 258.
- O'Reilly, J. E., Maritorena, S., Mitchell, G., Siegel, D. A., Carder, K. L., Garver, S. A., Kahru, M., McClain, C. 1998. Ocean Colour chlorophyll_a algorithms for SeaWiFS. *Journal of Geophysical Research*, 103, C11, 24,937 – 24,953.
- O'Neill, N., Royer, A., 1993. Extraction of bimodal aerosol-size distribution radii from spectral and angular slope (Angstrom) coefficients. *Applied Optics*, 32, 1642-1654.
- Platt, T., Sathyendranath, S. 1988. Oceanic primary production: estimation by remote at local and regional scales. *Science*, 241, 1613-1617.
- Pope, R. M., Fry, E. S. 1997. Absorption spectrum (380 - 700 nm) of pure water II integrated cavity measurement. *Applied Optics*, 36, 8710 - 8723.
- Prasanna Kumar, S., Ramaiah, N., Gauns, M., Sarma, V. V. S. S., Muralidharan, P. M., Raghukumar, S., Dileep Kumar, M., Madhupratap, M. 2001. Physical forcing of biological productivity in the Northern Arabian Sea during the Northeast Monsoon, *Deep-Sea Research II*, 48, 1115 – 1126.
- Preisendorfer, R. W. 1965. *Radiative Transfer on discrete space*. Pergamen, Tarrytown, N.Y., 1 - 462.
- Prieur, L., Sathyendranath, S. 1981. An optical classification of coastal and oceanic waters based on specific absorption curves of phytoplankton pigments, dissolved organic matter and other particulate matter. *Limnology and Oceanography*, 26, 4, 671 – 689.

- Pundare, U. V. 1989. Studies for improvement of navigation in Aguada bay at Goa. 3rd National conference on Dock and Harbor engineering, Surathkal, 589 – 595.
- Qasim, S. Z. 2003. Indian Estuaries. New Delhi: Allied Publishers Pvt. Ltd., 280-282.
- Qasim, S. Z., Sen Gupta, R. 1981. Environmental Characteristics of the Mandovi – Zuari Estuarine system of Goa. *Estuarine Coastal and Shelf Science*, 13, 557 – 578.
- Ramachandran, S. 2004a. Spectral aerosol optical characteristics during the northeast monsoon over the Arabian Sea and the tropical Indian Ocean: 1. Aerosol optical depths and their variabilities. *Journal of Geophysical Research*, 19, D19207, doi: 10.1029/2003JD004476.
- Ramachandran, S. 2004b. Spectral aerosol optical characteristics during the northeast monsoon over the Arabian Sea and the tropical Indian Ocean: 2. Angstrom parameters and anthropogenic influence. *Journal of Geophysical Research*, 109, D19208, doi: 10.1029/2003JD004483.
- Rao, G. D., Rao, T. C. S. 1974. Textural characteristics of sediments of Marmagao bay, Central West Coast of India. *Indian Journal of Marine Science*, 3, 93 – 98.
- Raymont, J. E. G. 1980. Plankton and productivity in ocean. Permagon Press, 65 – 126.
- Roesler, C. S., Perry, M. J. 1995. In situ phytoplankton absorption fluorescence emission and particulate backscattering spectra determined from reflectance. *Journal of Geophysical Research*, 100, C7, 13279 – 13294.
- Ross, A. H., Gurney, W. S. C., Heath, M. R. 1994. A comparative study of the ecosystem dynamics of four Fjords. *Limnology and Oceanography*, 39, 318 – 343.
- Sarma, V. V. S. S., Kumar, M. D., George, M. D. 1998. The central and eastern Arabian Sea as a perennial source to atmospheric carbon dioxide. *Tellus*, 50B, 179 – 18.

- Sathyendranath, S., Stuart, V., Platt, T., Bouman, H., Ullao, O., Maass, H. 2005. Remote sensing of ocean colour: Towards algorithms for retrieval of pigment composition. *Indian Journal of Marine Science*, 34, 4, 333 – 340.
- Sathyendranath, S., Gouveia, A. D., Shetye, S. R., Ravindran, P., Platt, T. 1991. Biological control of surface temperature in the Arabian Sea. *Nature*, 349: 54-56.
- Sathyendranath, S., Platt, T., Caverhill, C. M., Warnock, R. E., Lewis, M. R. 1989. Remote sensing of oceanic primary production: comparison using a spectral model. *Deep Sea Research*, 36, 431 – 453.
- Schott, F. A., Dengler, M., Schoenefeldt, R. 2002. The shallow overturning circulation of the Indian Ocean. *Progresses in Oceanography*, 53, 57–103.
- Sheridan, P. J., Delene, D. J., Ogren, J. A. 2001. Four years of continuous surface aerosol measurement from the Department of energy's atmospheric Radiation Measurement Program southern Great Plains Cloud and Radiation Tested sites. *Journal of Geophysical Research*, 106, D18, 20735-20747.
- Shetye, S. R., Gouveia, A. D., Singbal, S. Y. S., Nampoothiri, G. 1995. Propagation of tides in the Mandovi – Zuari estuarine network. *Proceedings in Indian Academy of Science (Earth and Planetary Science)*, 104, 667 – 682.
- Smith, R. C. 1981. Remote Sensing and depth distribution of ocean chlorophyll. *Marine Ecological Progressive Series*, 5, 359 – 361.
- Stabenau, E. R., Zika, R. G. 2004. Correlation of the absorption coefficient with a reduction in mean mass for dissolved organic matter in southwest Florida river plumes. *Marine Chemistry*, 89, 55– 67.
- Stedmon, C. A., Markager, S. 2003. Behaviour of the optical properties of coloured dissolved organic matter under conservative mixing. *Estuarine, Coastal and Shelf Science*, 57, 1 – 7.

- Stedmon, C. A., Markanger, S., 2001. The optics of chromophoric dissolved organic matter (CDOM) in the Greenland sea: an algorithm for differentiation between marine and terrestrially-derived organic matter. *Limnology and Oceanography* 46, 8, 2087–2093.
- Stedmon, C. A., Markanger, S., Kaas, H. 2000. Optical properties and signatures of chromophoric dissolved organic matter (CDOM) in Danish coastal waters. *Estuarine, Coastal and Shelf Science*, 51, 267 – 278.
- Stramaska, M., Stramaski, D. 2005. Effects of a non uniform vertical profile of chlorophyll concentration on remote-sensing reflectance of the ocean. *Applied Optics*, 44, 9, 1735 – 1747.
- Strickland, J. D., Parson, T. R. 1972. A Practical handbook of Seawater Analysis. *Bulletin of Fishery Research Board, Canada*, 167 – 310.
- Sturm, B. 1980. The atmospheric corrections of the remotely sensed data and the qualitative determination of suspended matter in marine water surface layers. In: *Remote Sensing in Meteorology, Oceanography and Hydrology* (Ed) A. P. Cracknell, Ellis Horwood Ltd., Chichester, 163 – 197.
- Suresh, T., Desa, E. 2005. Seasonal variations of aerosol over Dona Paula, a coastal site on the west coast of India. *Atmospheric Environment*, 39, 3471–3480.
- Suzuki, K., Kishini, M., Sasaoka, K., Satob, S., Saino, T. 1998. Chlorophyll-Specific Absorption Coefficients and Pigments of Phytoplankton off Sanriku, Northwestern North Pacific. *Journal of Oceanography*, 54, 517 – 526.
- Szekielda, K. H. 2005. Use of the first and second chlorophyll absorption bands for marine biogeochemical path recognition. *Indian Journal of Marine Sciences*, 34, 4, 387 – 395.

- Tassan, S. 1994. Local algorithms using SeaWiFS data for the retrieval of phytoplankton, pigments, suspended sediment, and yellow substance in coastal waters. *Applied Optics*, 33, 2369-2377.
- Twardowski, M. S., Boss, E., Sullivan, J. M., Donaghay, P. L. 2004. Modeling the spectral shape of absorption by chromophoric dissolved organic matter. *Marine Chemistry*, 89, 69– 88.
- Verma, K. K., Rao, L. V. G., Cherian, T. 1975. Temporal and spatial variations in hydrographic conditions of Mandovi estuary. *Indian Journal of Marine Science*, 4, 11 – 17.
- Vinoj, V., Babu, S. S., Sathesh, S. K., Moorthy, K. K., Kaufman, Y. J. 2004. Radiative forcing by aerosols over the Bay of Bengal region derived from ship borne, island-based and satellite (Moderate-Resolution Imaging Spectroradiometer) observations. *Journal of Geophysical research*, 109, D05203.
- Vodacek, A., Blough, N. V., DeGrandpre, M. D., Peltzer, E. T., Nelson, R. K. 1997. Seasonal variation of CDOM and DOC in the Middle Atlantic Bight: terrestrial inputs and photo oxidation. *Limnology and Oceanography*, 42, 674 – 686.
- Vodacek, A., Hoge, F., Swift, R. N., Yungel, J. K., Peltzer, E. T., Blough, N. V. 1995. The use of in situ and airborne fluorescence measurements to determine UV absorption coefficients and DOC concentrations in surface waters. *Limnology and Oceanography*, 40, 411 – 415.
- Wang, M. 1999. Atmospheric correction of ocean colour sensors: computing atmospheric transmittance. *Applied Optics*, 38, 451 – 455.
- Watts, C. D., Naden, P. S., Cooper, D. M., Gannon, B. 2003. Application of a regional procedure to assess the risk to fish from high sediment concentrations. *The Science of the Total Environment*, 314, 551 – 565.

- Williamson, C. E., Stemberger, R. S., Morris, D. P., Frost, T. M., Pauslen, S. G. 1996. Ultra-violet radiation in North American lakes: Attenuation estimates from DOC measurements and implications for plankton communities. *Limnology and Oceanography*, 41, 1024 – 1034.
- Yan, B., Stamnes, K., Toratani, M., Li, W., Stamnes, J. 2002. Evaluation of a reflectance model used in the Sea WiFS ocean color algorithm: implications for chlorophyll concentration retrievals. *Applied Optics*, 41, 30, 6243 – 6259.
- Yang, H., Gordon, H. R. 1997. Remote Sensing of Ocean Colour: Assessment of water-leaving radiance, bi-directional effects on atmospheric diffuse transmittance. *Applied Optics*, 36, 7887 – 7897.
- Zaneveld, J. R. V. 1982. Remotely sensed reflectance and its dependence on vertical structure: a theoretical derivation. *Applied Optics*, 21, 4146 – 4150.
- Zepp, R. G., Callaghan, T. V., Erickson, D. J. 1998. Effects of enhanced solar ultraviolet radiation on biogeochemical cycles. *Journal of Photochemistry and Photobiology*, 46, 69 – 82.

Annexure I Papers published



Available online at www.sciencedirect.com

SCIENCE @ DIRECT®

Estuarine, Coastal and Shelf Science 63 (2005) 211–223

ESTUARINE
COASTAL
AND
SHELF SCIENCE
www.elsevier.com/locate/ECSS

Pre-monsoon bio-optical properties in estuarine, coastal and Lakshadweep waters

H.B. Menon^{a,*}, A. Lotliker^a, S.R. Nayak^b

^aDepartment of Marine Science, Goa University, University P.O. 403 206 Goa, India

^bMarine Water and Resource Division, Space Application Centre, Indian Space Research Organization, Ahmedabad, 380 015, India

Received 9 January 2004; accepted 24 November 2004

Abstract

Spatial patterns of bio-optical properties were studied in coastal, estuarine and Lakshadweep waters during the pre-monsoon period. This was carried out by analysing the profiles of downward irradiance, upward radiance and water samples collected from 26 stations. The apparent optical properties such as subsurface reflectance (R) and diffuse attenuation coefficient (k) derived from these profiles were processed to generate inherent optical properties, a (total absorption coefficient) and b_b (total backscattering coefficient). Highly variable surface-coloured dissolved organic matter (CDOM) absorption ($1.8\text{--}21.6\text{ m}^{-1}$ at 440 nm) was observed in the coastal waters. The distribution of optical properties a and b_b reflected the distribution of optically active constituents with CDOM contributing to most of the variation in coastal waters, sediment in estuarine waters, and chlorophyll a and water molecules in Lakshadweep waters. The spectral remote sensing reflectance ($R_{rs}(\lambda)$) is a linear function of a and b_b , k was lowest and R was at maximum in the green part of the electromagnetic spectrum (EMR) in estuarine and coastal waters while this is true in the blue region of EMR in Lakshadweep waters. A linear relationship was seen between downwelling diffuse attenuation coefficient (k_d) at 490 nm and attenuation of photosynthetically available radiation (k_{PAR}). Examination of the light field revealed maximum chlorophyll at greater depth in Lakshadweep waters and at shallow depth in coastal waters, with no well-defined maxima in the estuarine waters. An exponential inverse relation is evident between k_d (490) and depth of chlorophyll maxima. Through a radiative transfer computation, a ratio between water-leaving radiance at 400 and 670 nm is found to be an index of CDOM and hence could be used to retrieve it through an optical sensor.

© 2004 Elsevier Ltd. All rights reserved.

Keywords: coloured dissolved organic matter; diffuse attenuation coefficient; photosynthetically available radiation; water leaving radiance



Available online at www.sciencedirect.com

SCIENCE @ DIRECT®

Estuarine, Coastal and Shelf Science 66 (2006) 523–531

ESTUARINE
COASTAL
AND
SHELF SCIENCE
www.elsevier.com/locate/eess

Analysis of estuarine colour components during non-monsoon period through Ocean Colour Monitor

H.B. Menon^{a,*}, A.A. Lotliker^a, S.R. Nayak^b

^a Department of Marine Science, Goa University, University P.O., 403 206, Goa State, India

^b Marine Water and Resource Division, Space Application Center, Indian Space Research Organization, Ahmedabad 380 015, India

Received 6 July 2005; accepted 21 October 2005
Available online 13 December 2005

Abstract

Simultaneous acquisition of water samples, radiance and irradiance measurements were carried out from 40 stations in the Mandovi–Zuari estuaries during February to May 2002. From the samples collected, inherent and apparent optical properties (IOP and AOP) such as absorption coefficient (a), upwelling diffuse attenuation coefficient (k_u) and subsurface reflectance (R) were derived. Using these optical properties, radiative transfer at each water column is examined. On the basis of the radiative transfer outcome, band-ratio algorithms are derived for three optically active substances (OAS), viz. chlorophyll- a , suspended sediment and coloured dissolved organic matter (CDOM). The respective algorithms are 670/555, 490/670 and 412/670 nm for chlorophyll- a , suspended sediment and CDOM. These algorithms are applied to Ocean Colour Monitor (OCM), onboard Indian Remote Sensing Satellite (IRS)-Polar Satellite Launch Vehicle (P4), scenes (digital data), to synoptically analyze these OAS. The synoptic analysis of OAS revealed different hydrodynamic characteristics of the estuaries during non-monsoon seasons.

© 2005 Elsevier Ltd. All rights reserved.

Keywords: algorithm; IRS-P4-OCM; band ratio; CDOM; chlorophyll- a ; suspended sediment; hydrodynamics; non-monsoon

Click
Here
for
Full
Article

Variability of remote sensing reflectance and implications for optical remote sensing—A study along the eastern and northeastern waters of Arabian Sea

Harilal B. Menon,¹ Aneesh A. Lotliker,¹ K. Krishna Moorthy,² and Shailesh R. Nayak³

Received 11 February 2006; revised 12 May 2006; accepted 6 June 2006; published 2 August 2006.

[1] Situated in the eastern and northeastern regions and subjected to similar oceanic processes, the inshore waters north of 20°N and east of 65°E are more optically complex than the offshore waters and waters south of 20°N and east of 65°E. This has been observed through the analysis of variations of the remote sensing reflectance ($R_{rs}(\lambda)$) in the optical spectrum of Electromagnetic radiation. The optical complexity has further been studied through the examination of optically active substances (OAS) such as chlorophyll_a, suspended sediment and coloured dissolved organic matter (CDOM). It is found that CDOM is the significant component in making the area optically non-linear. For the first time multi-spatial/temporal band-ratio algorithms are developed to map OAS from these waters through Ocean Colour Monitor flown on IRS – P4 satellite.

Citation: Menon, H. B., A. A. Lotliker, K. K. Moorthy, and S. R. Nayak (2006), Variability of remote sensing reflectance and implications for optical remote sensing—A study along the eastern and northeastern waters of Arabian Sea, *Geophys. Res. Lett.*, 33, L15602, doi:10.1029/2006GL026026.